Characterization of Mitochondrial DNA Mutations in *Drosophila melanogaster*

Leslie Itsara

A dissertation
submitted in partial fulfillment of the
requirement for the degree of

Doctor of Philosophy

2014

Reading Committee:
Leo Pallanck, Chair
David Hockenbery
Margaret Sedensky

Program Authorized to Offer Degree:
Molecular and Cellular Biology

University of Washington

Abstract

Characterization of Mitochondrial DNA Mutations in *Drosophila melanogaster*

Leslie Itsara

Chair of the Supervisory Committee:
Professor Leo J. Pallanck
Department of Genome Sciences

Mitochondria are vital organelles as they produce the majority of cellular energy in the form of ATP through oxidative phosphorylation (OXPHOS). Mitochondria contain their own genome (mtDNA), which encodes essential respiratory chain proteins that function in OXPHOS along with RNAs that are necessary for the translation of the OXPHOS genes. Mutations in mtDNA cause maternally inherited mitochondrial diseases and somatic mutations are implicated in aging and age-related diseases, such as Parkinson's disease. To explore the pathogenesis of mitochondrial disease due to an mtDNA mutation, we characterized a mutation in NADH dehydrogenase subunit 2 (*mt:ND2*). We found that *ND2* mutants model mitochondrial disease as they exhibit a shortened lifespan, neurodegeneration, and seizures. Additionally, *ND2* mutants display complex I specific defects along with decreased mitochondrial membrane potential and ATP levels. Importantly, we show that the *ND2* mutation uncouples complex I dependent proton pumping from electron transport and demonstrate a role for ND2 in proton pumping. These studies support the use of *Drosophila* as a model to study complex I disease and potential complex I therapeutics. In addition to studying mitochondrial disease pathogenesis, I adapted techniques to measure mtDNA mutations in *Drosophila*,

including the Random Mutation Capture Assay and Duplex Sequencing. Utilizing the Random Mutation Capture Assay, I found that the somatic mtDNA mutation patterns in flies are conserved with vertebrates, including the mutation frequency ($\sim 10^{-5}$) and the age-dependent accumulation of mutations. I also explored factors that influence somatic mtDNA mutations, including reactive oxygen species (ROS), which are thought to be an important contributor to mtDNA mutations. Using the distribution of mutations along with loss of function studies in oxidative stress defense factors, I concluded that oxidative stress is only a minor contributor to the mutation frequency. Instead, errors created during replication of mtDNA are the primary source of somatic mtDNA mutations. After completing these studies, I established the Duplex Sequencing method in flies, which is a next-generation sequencing approach as a more comprehensive and high-throughput technique to measure mtDNA mutations. These studies extend our knowledge of sources that contribute to the mtDNA mutation frequency and support *Drosophila* as a model to study genetic factors that influence mtDNA mutations.

TABLE OF CONTENTS

Page

1 Introduction to Mitochondrial DNA Mutations 1
1.1 Mitochondria and the Mitochondrial Genome 1
1.2 Inherited Mitochondrial DNA Mutations 3
1.3 Complex I Disease 5
1.4 Somatic Mitochondrial DNA Mutations 8
1.5 Factors that Influence the Frequency of mtDNA Mutations 10
1.6 Mitochondrial Quality Control 13

2 A *Drosophila* Model of Mitochondrial Disease Caused by a Complex I Mutation that Uncouples Proton Pumping from Electron Transfer 18
2.1 Summary 18
2.2 Introduction 19
2.3 Results 20
2.3.1 Structural analysis of ND2 20
2.3.2 Behavioral analysis of ND2 mutants 22
2.3.3 Tissue integrity of ND2 mutants 24
2.3.4 Functional analysis of mitochondria isolated from ND2 mutants 26
2.4 Discussion 32
2.5 Materials and Methods 33
2.6 Notes 39

3 Oxidative Stress is Not a Major Contributor to Somatic Mitochondrial DNA Mutations 41
3.1 Summary 41
3.2 Introduction 42
3.3 Results 44
3.3.1 mtDNA replication occurs in somatic tissues of *Drosophila* 44
3.3.2 Multiple *TaqI* sites are suitable for detecting mutations in *Drosophila* mtDNA 46
3.3.3 Somatic mtDNA mutations accumulate with age in *Drosophila* 47
3.3.4 Oxidative stress is only a minor contributor to somatic mtDNA mutations 52
3.4 Discussion 59
3.5 Materials and Methods 63
3.6 Notes 71

4 Using Duplex Sequencing to Detect and Measure Mitochondrial DNA Mutations 72
4.1 Summary 72
4.2 Introduction 72
4.2.1 Using *Drosophila* as a model 72
4.2.2 Methods to measure the frequency of mtDNA mutations 73
4.3 Results 75
4.4 Discussion 78

4.5 Materials and Methods 81
5 Summary and Future Directions 88
5.1 A *Drosophila* Model of Complex I Disease 88
5.2 The Study of Somatic Mitochondrial DNA Mutations in *Drosophila* 92

Appendix A Supplemental Material for Chapter 3 97

6 References 110

LIST OF FIGURES

Figure 1.1 Depiction of the *Drosophila* mitochondrial genome 2
Figure 1.2 Cells with mtDNA mutations above a threshold exhibit respiratory chain dysfunction 5
Figure 1.3 The mitochondrial reactive oxygen species vicious cycle theory 12
Figure 2.1 ND2 sequence alignment and secondary structure prediction 21
Figure 2.2 *ND2* mutants exhibit behavioral abnormalities and shortened lifespan 23
Figure 2.3 *ND2* mutants exhibit progressive neurodegeneration, but lack muscle pathology 25
Figure 2.4 *ND2* mutants exhibit decreased mitochondrial function 28
Figure 3.1 The locations of *TaqI* sites in *Drosophila* mtDNA 48
Figure 3.2 Mitochondrial DNA mutation frequency increases with age and is greater in thoraces than in heads 50
Figure 3.3 GC:TA transversions account for only a small percentage of mtDNA mutations 53
Figure 3.4 Oxidative stress response pathway mutants do not have an increased mtDNA mutation frequency 55
Figure 3.5 An *Ogg1* mutation diminishes Ogg1 activity and interacts genetically with *Sod2* 57

LIST OF TABLES

Table 1.1 Mitochondrial DNA mutations cause disease and are usually heteroplasmic.....4
Table 2.1 Oxygen consumption rates and respiratory ratios 30
Table 4.1 Number of sequenced mtDNA nucleotides.....77
Table 4.2 mtDNA point mutation counts and frequencies 77
Table 4.3 Insertion and deletion counts and frequencies.....77
Table 4.4 Mutation spectra obtained using DS and RMC.....78

ACKNOWLEDGEMENTS

I sincerely thank my parents, In Bae Kim and Pun Sun Kim for their passion to provide educational opportunities to their children and for their constant love and support. I thank my three older sisters, Dorothy, Carol, and Eleasa for being great role models and wonderful friends. I thank my husband, Andy Itsara for providing an example of true dedication, an important quality to have in graduate school. I thank my cat, Rocky Eugene Itsara for being a great companion and friend. I thank my graduate school classmates for their support, love, and great memories.

I thank my high school teachers and college professors who have helped shape my interests in research and/or love for science. At Opelika, AL High School, I thank my senior English teacher, Dr. Charles Hannah and my newspaper staff advisor Mrs. Williamson. At Vanderbilt University, I thank my college research advisor, Dr. Todd Graham, my genetics professor and unofficial advisor, Dr. Katherine Friedman, my organic chemistry professor, Dr. Michelle Sulikowski, and my biochemistry professor, Dr. Andrzej Krezel.

I thank my collaborators at the University of Washington that have made this work possible. I thank the members of the Lawrence Loeb laboratory for a providing a welcoming research environment. In particular I thank Dr. Scott Kennedy for his assistance setting up the Random Mutation Capture Assay and Duplex Sequencing in *Drosophila*. I also thank Dr. Edward Fox for his assistance troubleshooting aspects of the Random Mutation Capture Assay. I thank the members of the Philip Morgan and Margaret Sedensky laboratories for providing a welcoming and helpful research

environment. In particular I thank Ernst-Bernhard Kayser for his assistance with respiration assays and for providing thorough and thoughtful explanations.

I thank the Molecular and Cellular Biology Program for allowing me the opportunity to receive training and to conduct research at the University of Washington. I also thank my funding sources, the National Institute of Neurological Disorders and Stroke, and the Genetic Approaches to Aging Training Grant.

I thank my committee members Sandra Bajjalieh, Dan Gottschling, Dave Hockenbery, Matt Kaeberlein, and Margaret Sedensky for their time, guidance, and feedback. I appreciate both their support and challenges.

I thank the wonderful members of the Pallanck Lab for providing a great environment for the learning and growth of graduate students. In particular, I thank Kien Trinh, Angela Poole, Ruth Thomas, Evelyn Vincow, and Pranali Pathare. I also thank the undergraduates, Selina Yu and Alice Chu for their contributions to the entire lab and for their assistance on personal research projects.

Finally, I thank my research advisor, Leo Pallanck for his immeasurable contribution to my scientific development, especially in the areas of writing and presenting. I thank him for his patience and encouragement with my graduate school research. I am grateful for his availability to help and guide me on my research endeavors and also on my future career prospects.

Introduction to Mitochondrial DNA Mutations

1.1 Mitochondria and the Mitochondrial Genome

The presence of mitochondria in eukaryotic cells is the result of a ~1.5-billion-year old endosymbiotic event between a relative of α-proteobacteria and a non-respiring eukaryotic ancestor[1]. The acquisition of respiring mechanisms enabled eukaryotes to produce up to 90% of cellular adenosine triphosphate (ATP) through oxidative phosphorylation (OXPHOS). Mitochondria are comprised of an outer and inner mitochondrial membrane, and the OXPHOS machinery resides in the inner membrane. In addition to energy production, mitochondria perform many other functions, including metabolite regulation, Ca^{2+} buffering, and apoptosis[2–4]. In order to carry out these functions in different parts of the cell, the distribution and structural organization of mitochondria is dynamic. For example, the mitochondrial network may undergo fusion or division, and trafficking mechanisms direct mitochondria on cytoskeleton networks where they are needed[5].

The mitochondrion contains its own circular genome due to its bacterial origin, and depending on the species, usually encodes 37 genes (Figure 1.1). Thirteen of these genes encode proteins that function in OXPHOS, and mitochondrially-encoded proteins comprise only a small portion of total OXPHOS machinery as the majority of OXPHOS proteins are encoded by the nuclear genome (~100 genes). The remaining 24 genes in the mitochondrial genome encode RNAs (22 tRNAs and 2 rRNAs) that function in intramitochondrial protein synthesis.

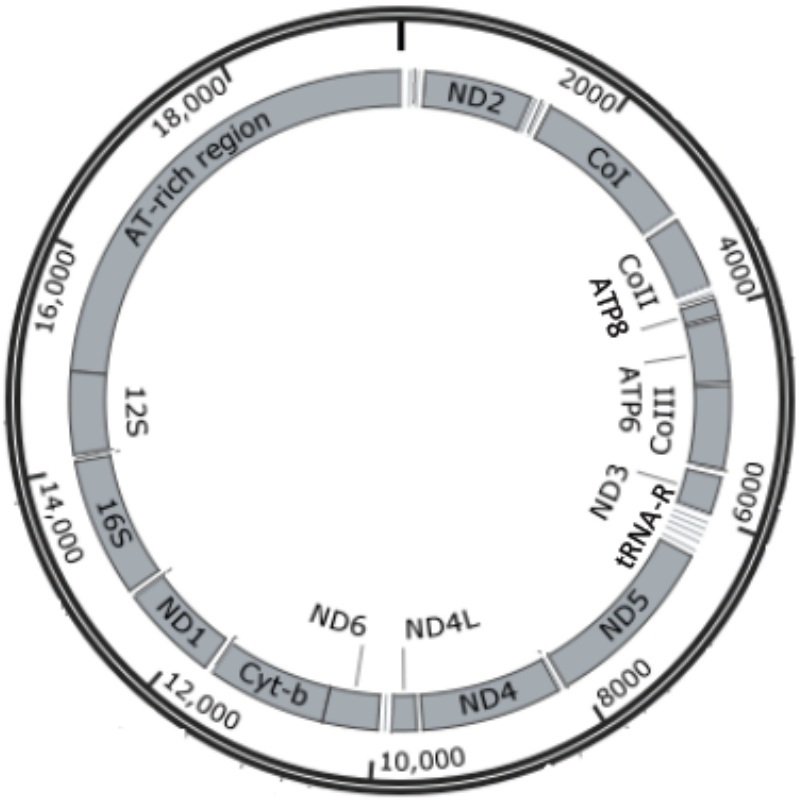

Figure 1.1 Depiction of the *Drosophila* mitochondrial genome. The *Drosophila* mtDNA contains 19,517 base pairs and encodes proteins that function in OXPHOS and rRNAs (12S and 16S rRNAs) and 22 tRNAs (indicated by the horizontal lines adjacent to mitochondrial genes) that translate the protein-encoding genes. The AT-rich region does not contain any genes, but harbors the origin of replication for the minor strand (leading strand). The location for the major strand origin of replication is unknown. The fly mitochondrial genome contains the same genes as the human mitochondrial genome, but the genes differ in arrangement.

Properties of mitochondrial DNA (mtDNA) are unique compared to nuclear DNA in several ways. mtDNA is maternally transmitted and mtDNA lacks many of the DNA repair pathways found in the nucleus, including nucleotide excision repair and translesion synthesis[6]. Additionally, mtDNA is polyploid and multiples copies (between 2-8 genomes) are packaged with protein into structures called nucleoids[7], and mtDNA copy number varies depending on the bioenergetic needs of the tissue[8]. Due to the multi-copy

nature of mtDNA, different mitochondrial genotypes may be present within a single cell, and this state is termed heteroplasmy.

Several differences between the mitochondrial and nuclear genome likely contribute to a ~100x higher mutation rate in the mitochondrial genome. For example, the mitochondrial genome lacks protective histones and the aforementioned DNA repair pathways present in the nuclear genome. Additionally, because mtDNA replicates post-mitotically, it may incur replication-induced errors. Finally, the proximity of mtDNA to reactive oxygen species, which are produced as byproducts of normal respiration and damage DNA may contribute to the higher mutation frequency in mtDNA. If present at high enough levels, mutant genomes can lead to mitochondrial diseease.

1.2 Inherited Mitochondrial DNA Mutations

Pathogenic mtDNA mutations were first reported in 1988[9–11], and to date nearly 200 different disease-causing mutations have been reported[12]. Pathogenic mtDNA mutations represent the most common class of genetic disorders as they affect ~1/5000 adults[13]. Mitochondrial diseases often affect energetically demanding tissues, such as muscle and/or brain. These diseases are heterogeneous as they may either be multi-systemic or tissue-specific causing an array of symptoms that may include lactic acidosis, diabetes, deafness, stroke, or death. Mitochondrial disease pathogenesis has been attributed to various factors including but not limited to OXPHOS impairment, increased reactive oxygen species (ROS), deficient ATP levels, and an imbalance in $NADH/NAD^+$ ratios and Ca^{2+} homeostasis[14].

Disorder	Phenotype	Mutation Status	Inheritance
Kearns-Sayre syndrome	Progressive myopathy, opthalmoplegia, cardiomyopathy	Heteroplasmic	Usually sporadic
CPEO	Opthalmoplegia	Heteroplasmic	Usually sporadic
Pearson Syndrome	Pancytopoenia, lactic acidosis	Heteroplasmic	Usually sporadic
MELAS	Myopathy, encephalomyopathy, lactic acidosis, stroke-like episodes	Heteroplasmic	Maternal
MERRF	Myoclonic epilepsy	Heteroplasmic	Maternal
NARP	Neuropathy, ataxia, retinitis pigmentosa	Heteroplasmic	Maternal
MIDD	Diabetes, deafness	Heteroplasmic	Maternal
LHON	Optic neuropathy	Hetero or homoplasmic	Maternal
Myopathy and Diabetes	Myopathy, weakness	Hetero or homoplasmic	Maternal
Sensorineural hearing loss	Deafness	Hetero or homoplasmic	Maternal
Exercise Intolerance	Fatigue, muscle weakness	Heteroplasmic	Sporadic
Fatal infantile encephalopathy Leigh like Syndrome	Encephalopathy, lactic acidosis	Heteroplasmic	Sporadic

Table 1.1. Mitochondrial DNA mutations cause disease and are usually heteroplasmic. CPEO, chronic progressive external ophthalmoplegia; LHON, Leber hereditary optic neuropathy; MELAS, mitochondrial myopathy, encephalopathy, lactic acidosis and stroke-like episodes; MERRF, myoclonic epilepsy and ragged-red fibres; MIDD, maternally-inherited diabetes and deafness; NARP, neurogenic weakness, ataxia and retinitis pigmentosa. Table modified from reference[15].

The majority of mitochondrial disease-causing mutations are heteroplasmic[15] (Table 1.1). Heteroplasmy levels can vary between siblings or even between tissues or cells within the same individual due to segregation of mtDNA variants during transmission in primordial germ cells or during cell division[16]. A cellular threshold for mutations must be reached before respiratory chain deficiency is observed, which is normally measured by complex IV activity[15]. In particular, the mutation frequency

threshold can be as low as ~60% for certain mtDNA deletions[17] or up to ~95% for tRNA point mutations[18]. A threshold likely exists because WT mtDNA genomes complement their mutant counterparts (Figure 1.2). Interestingly, varying degrees of the same mutation can result in different mitochondrial diseases, and higher levels of heteroplasmy generally exhibit a more deleterious effect[13].

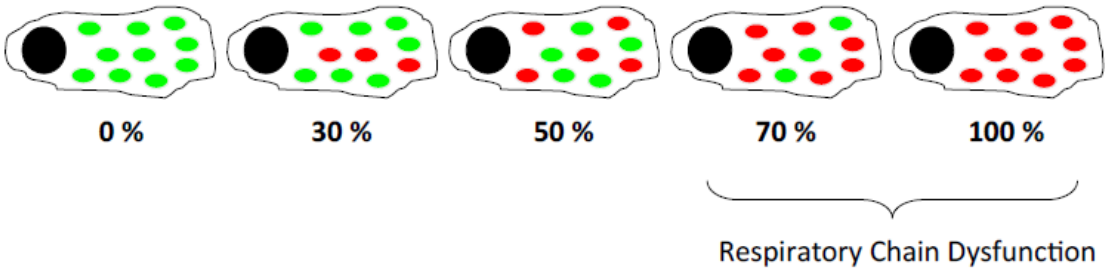

Figure 1.2. Cells with mtDNA mutations above a threshold exhibit respiratory chain dysfunction. The threshold effect is a phenomenon whereby the biochemical effect and clinical presentation of an mtDNA mutation are exhibited only when heteroplasmy levels reach a certain degree. Mitochondria with wild-type mtDNAs are depicted in green and mutant in red. Figure modified from reference [19].

1.3 Complex I disease

Mitochondrial complex I is the first enzyme of the mitochondrial respiratory chain (MRC), which functions to create an electrochemical gradient across the inner mitochondrial membrane that is used to produce ATP. Complex I is the largest respiratory chain complex consisting of ~45 subunits[20], seven of which are encoded by the mitochondrial genome and the remaining by the nuclear genome. The subunits of complex I form an L shape with a hydrophilic arm that extends into the mitochondrial matrix mediating redox reactions and electron transfer and a hydrophobic arm that is embedded in the inner mitochondrial membrane[21]. The catalytic core is located within the membrane arm and consists of 14 evolutionarily conserved proteins, which likely have roles in proton pumping[20,22]. All seven of the mitochondrially-encoded complex I

proteins function in the core, and mutations in these genes along with other components of complex I result in dysfunctional complex I.

Complex I dysfunction leads to defects in OXPHOS and causes numerous encephalomyopathies. Brain and muscle are likely affected because of the high energetic demand of these tissues[23], and neurons in particular because they rely almost exclusively on OXPHOS for ATP. In addition to decreased in energy, a defect in OXPHOS may lead to depolarization of the mitochondrial membrane potential, which supports other functions, including the transport of molecules across the inner mitochondrial membrane, mitochondrial integrity, apoptosis, calcium homeostasis, and anabolic processes[4,24–26].

Complex I diseases, like other types of mitochondrial disorders are considered heterogeneous as they can differ in the tissues they affect, disease severity, and age of onset. For example, in addition to affecting brain and muscle, defects in complex I may also affect the liver, kidneys, and lungs. However, clinical phenotypes of nuclear complex I mutations are relatively more consistent while mtDNA mutations are more variable due to the threshold effect of heteroplasmic mtDNA mutations [23].

Mutations specifically in the mitochondrially-encoded ND2 subunit may result in Leber's Hereditary Optic Neuropathy (LHON)[27], exercise intolerance[28], or Leigh syndrome[29,30]. While differences in mutation residues is the most likely explanation for individuals with *mt:ND2* mutations exhibiting dissimilar disorders, other possible explanations include varying heteroplasmy levels (which were not measured in these studies), and/or in genetic backgrounds of the individuals, either nuclear or mitochondrial. LHON is characterized by central vision loss due to degeneration of retinal ganglion layer of the optic nerve[31]. Exercise intolerance primarily affects skeletal

muscle resulting in decreased duration or level of exercise[32]. Leigh syndrome or subacute necrotizing encephalopathy is a fatal neurological condition and the most common respiratory chain deficiency. Leigh syndrome is most frequently caused by mutations in complex I genes, and all 14 genes that comprise the core conserved subunits of complex I have reports of Leigh syndrome-causing mutations[33]. The disorder is characterized by bilateral necrotic lesions in the thalamus, basal ganglia, spinal cord, and brainstem[34]. Some of the symptoms include movement disorders, loss of motor control, seizures, kidney failure, and heart defects. While complex I mutations are the most common cause of mitochondrial disease, few animal models of complex I disease are available.

Primary skin fibroblasts from patients with complex I disease are commonly used to study the biochemical expression of complex I mutations rather than the more relevant tissues, neural or muscle because these tissues are impractical to biopsy in large amounts[23]. While biochemical effects of mutations can be studied using fibroblasts, tissue culture has obvious limitations compared to whole organisms. The first genetic models of complex I disease were in mice carrying mutations indirectly affecting complex I function. For example, apoptosis inducing factor (AIF), a cell death effector located in the intermembrane space has a role in complex I assembly[35], and mutations in AIF cause decreased complex I levels and activity, neurodegeneration and cardiomyopathy[36,37]. At the time we began our studies, there was a single mouse model with a mutation in a complex I subunit Ndufs4, which is a nuclear-encoded subunit[38]. The Ndufs4 knock-out mice develop a fatal encephalomyopathy and model Leigh Syndrome[38,39]. Moreover, *Ndufs4* mutants show reduced levels of complex I accompanied with reduced complex I activity, and the authors conclude that Ndufs4 is likely is involved in assembly and/or

stability of complex I. In the last year another mouse model with a homoplasmic mtDNA mutation in *ND6* was developed[40]. The *ND6* mutant exhibits reduced complex I activity and models LHON[40]. While other models of complex I disease exist, we contributed a unique fly model of complex I disease as described in **Chapter 2**.

Research goal

Mitochondrial disease affects 1/5,000 adults, and complex I mutations are the most common cause of mitochondrial disease. Therefore, one of my research goals was to study the pathogenesis of mitochondrial complex I disease caused by an mtDNA mutation. A *Drosophila* model of complex I deficiency would prove valuable because basic aspects of complex I and mitochondrial respiratory chain function are conserved between flies and humans. Also flies are a genetically tractable model for use in identifying and studying potential therapeutics for complex I disease, for which there are currently no effective treatments. Our *Drosophila* model represents the first fly model of complex I disease caused by a mutation in a mitochondrially-encoded subunit. We describe an *mt:ND2* mutation, which uncouples proton pumping from electron transfer and models mitochondrial complex I disease (**Chapter 2**).

1.4 Somatic mtDNA Mutations

In addition to mitochondrial disease, mtDNA mutations are implicated in age-related diseases, including cancer, diabetes, and neurodegeneration[13,41–44]. It is thought that aging may be due to an accumulation of many different mutations or single mutations that have undergone clonal expansion as described in the following section.

Several lines of evidence support a role for mtDNA mutations in aging. For example, the frequency of mtDNA mutations increases with age in several species including mice[45,46], rats[45,47], and humans[48,49], and cells from aged individuals contain a high degree of mutations that exhibit decreased respiratory chain activity[50].

While these data are correlative, greater support for a causative role for mtDNA mutations in aging derives from studies of the mtDNA polymerase-γ (pol-γ) mutator mouse, which is deficient in proofreading during mtDNA replication[51,52]. The pol-γ mutator mouse exhibits an increase in mtDNA mutations and pre-mature aging phenotypes including shorted lifespan, weight and hair loss, spine curvature, and osteoporosis[51,52]. Because different forms of mtDNA mutations, including point mutations and several types of deletions have been detected with differing methods, there is debate about which mutations are actually responsible for the aging phenotypes[46,51–55]. Moreover uncertainty exists about whether premature aging in pol-γ mutator resembles natural aging because the level of point mutations in the mutator mice is more than one order of magnitude greater than in aged humans[51,52,56–58]. While these studies implicate somatic mtDNA mutations in aging, models that could more accurately recapitulate mutation accumulation as in natural aging would serve as more appropriate models to test the causative role of somatic mtDNA mutations in aging.

There is also support for a role of mtDNA mutations in Parkinson's disease (PD), the second most common neurodegenerative disorder. PD is caused by the loss of dopamine-producing neurons in the substantia nigra of the midbrain, and results in motor impairment, including resting tremors, rigidity, and altered gait. Studies show that PD patients have an increased degree of mtDNA deletions in dopamine neurons, which

results in respiratory chain dysfunction[59,60]. Moreover, support for a causative role for mtDNA deficiency in PD derives from a separate study in mice deficient for (*Tfam)*, the mtDNA transcriptional activator. *Tfam* deficiency causes reduced mtDNA expression, respiratory chain deficiency in dopamine neurons, and results in a parkinsonism phenotype[61]. While there is strong evidence for somatic mtDNA mutations in aging and age-related diseases, the mechanisms that cause mutations and influence heteroplasmy levels are not well understood.

1.5 Factors that Influence the Frequency of mtDNA Mutations

Mitochondrial DNA mutations may be inherited or can occur somatically, and both point mutations and deletions accumulate with age in several post-mitotic tissues[49,58–60,62–66]. Age-dependent accumulation of a 4977 bp "common deletion" has been identified along with many other mtDNA deletions[67–69]. Deletions frequently reside between two direct repeats that are thought to mediate the deletion process either during replication or repair of mtDNA[67–69]. While mtDNA deletions are of great interest in aging and disease, the focus of this thesis is on studying somatic mtDNA point mutations, which occur after mtDNA replication and may be caused either by a replicating pol-γ error or by translesion mtDNA synthesis across damaged mtDNA.

Long-believed contributors to mtDNA damage are reactive oxygen species (ROS) because mitochondria have a high concentration of ROS, which are produced as normal by-products of respiration. Oxygen undergoes single electron transfer to produce superoxide anion during respiration and initial studies from 1979 proposed this occurred to approximately 1% of oxygen[70]; however, a more recent study estimates only 0.02-

0.03% [71]. Once formed, superoxide may be dismutated or undergo subsequent reactions to produce derivative reactive species, including hydroxyl radical and peroxynitrite, which are both more reactive than superoxide anion[72,73]. There are many types of mutations that can occur due to DNA damage by ROS, and the reactivity of particular ROS with DNA, the resulting base adducts, and the incorporated bases following translesion synthesis are reviewed elsewhere[74,75]. ROS may also damage other mitochondrial components, including lipids and proteins. Due to the high concentrations of ROS in mitochondria, Denham Harman posited a mitochondrial theory of aging in the 1970s[76]. A vicious cycle theory was later included, which states that ROS damage to mtDNA leads to impaired protein products that produce additional ROS, leading to increased damage of mtDNA[77] (Figure 1.3**)**.

The free-radical theory of aging is a topic of intense debate as data exists to support both sides. Studies targeting catalase to mitochondria in mice validates the theory[78]; catalase mediates the breakdown of H_2O_2, preventing the formation of the reactive hydroxyl radical. Aged mice with mitochondrially-targeted catalase have fewer mtDNA mutations and an extended lifespan[78]. The mitochondrial theory of aging is also supported by the findings that both ROS and mtDNA mutations are correlated with aging[79]. On the other hand, studies exist to refute the free-radical theory of aging. In particular, many recent studies that analyze the mutation spectra of mtDNA in aging mice and humans provide evidence for a lack of ROS induced mutations, therefore, arguing against the importance of ROS on somatic mutations with age[49,80,81].

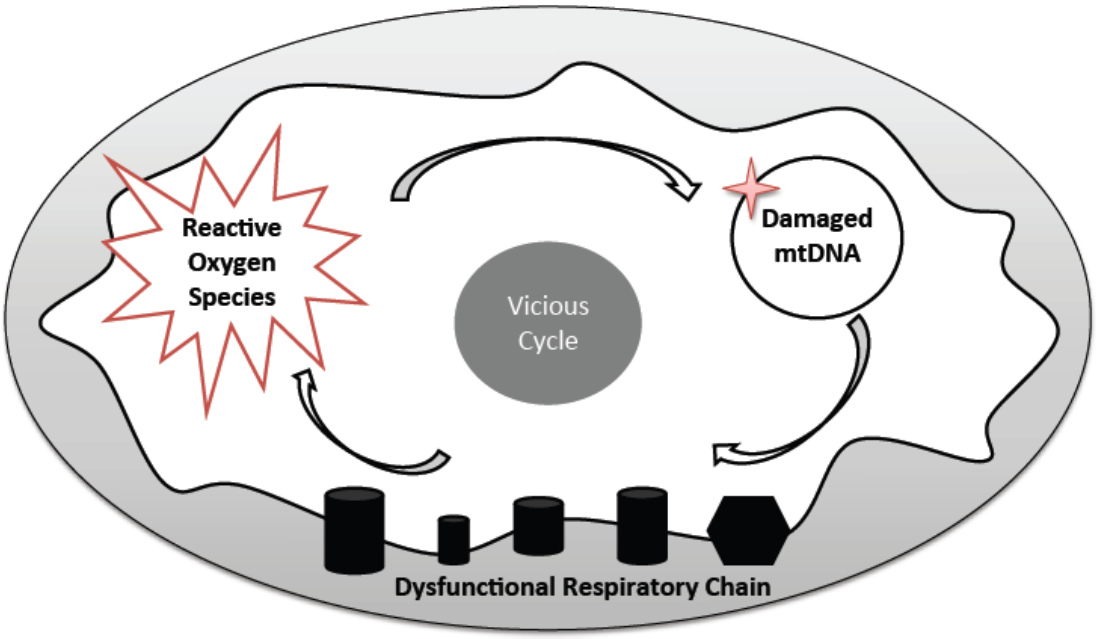

Figure 1.3. The mitochondrial reactive oxygen species vicious cycle theory. During the vicious cycle, reactive oxygen species are produced during respiration. ROS damages mtDNA resulting in dysfunctional OXPHOS subunits, which then produce greater amounts of ROS.

While the influence of ROS on mutations is under debate, it is clear that clonal expansion of mutant mtDNA molecules increases the mtDNA mutation frequency, and may even cause mutant mtDNA to represent the majority of mtDNA in a cell[60,82]. There is evidence for clonally expanded mutations in both mitotic (buccal and colonic crypt stem cells)[82–84] and post-mitotic cells (myocytes and neurons)[59,60,64,83]. Clonal expansion can occur because mtDNA turnover and replication is not linked to the cell cycle (relaxed replication) and because one mitochondrial genome may be replicated many times or not at all[85]. Several theories try to resolve how the cell would replicate a mutant mitochondrial molecule over a WT genome. For example, clonal expansion may occur because the mutation offers a selective replicative advantage to the molecule: a mutation could occur in the origin of replication, which influences how frequently it is replicated[86]. It has also been proposed that mtDNA deletions expand because the smaller molecules

can replicate faster[87]. However, because the time between replication of mtDNA molecules exceeds the time required for mtDNA replication to occur[88], this is an unlikely explanation. Alternatively, the mutation could enable the mitochondrion that harbors it to escape from mitochondrial turnover by decreasing its respiratory capacity and ROS production[89]. Another theory uses computational modeling to argue that clonal expansion occurs by random genetic drift alone[90]. Because of the relaxed nature of mtDNA replication and degradation, an mtDNA molecule that acquired a mutation during development can replicate many times over an individual's lifetime without selection acting. Regardless of whether or not selection plays a role, clonal expansion occurs and contributes to the somatic mtDNA mutation burden.

Alternative fates for pre-existing mtDNA mutations other than to undergo clonal expansion are to be repaired or removed. While there is evidence for base-excision repair in the mitochondrial genome, nucleotide excision repair and translesion synthesis, which are present in the nucleus are thought to be absent in the mitochondrion[6]. Another cellular process that could reduce mtDNA mutations is turnover of mitochondria that harbor mutant mtDNA through autophagic mechanisms.

1.6 Mitochondrial Quality Control

The first evidence for degradation of mitochondria derives from studies performed in the 1960s on macroautophagy, a form of autophagy that recycles cellular components non-selectively[91]. This classical view of autophagy is one of a response to nutrient deprivation or stress and begins with formation of an autophagosome, a double membrane bound structure that sequesters cytosolic proteins and organelles for recycling.

Autophagosomes eventually fuse with the lysosome where hydrolytic enzymes degrade its components.

More recent studies show that autophagy can act selectively to degrade damaged or excess organelles, including mitochondria, a process termed mitophagy[92]. For example, autophagy proteins remove sperm-derived mitochondria during early embryonic development to ensure maternal mitochondrial inheritance[93,94], and Nix, a mammalian-specific protein degrades mitochondria during erythrocyte development[95]. Additional mitophagy specific factors were identified from genetic screens in yeast under starvation conditions, including Atg 32, which recruits autophagic machinery to mitochondria[96], and Uth1[97] and Atg11[98], which are both required for mitochondrial removal. While the process of macroautophagy is conserved from yeast to mammals, mammalian homologues for the yeast mitophagy proteins have not been identified. Finally, in metazoans PINK1 (phosphatase and tensin homolog induced putative kinase 1) and Parkin have been shown to mediate the selective elimination of damaged mitochondria[99,100].

Parkin is a ubiquitin ligase, and PINK1 is a mitochondrial protein kinase; recessive mutations in either of these genes result in autosomal forms of PD[101,102]. Studies from our lab and others show that Parkin acts downstream of PINK1 in a pathway to promote mitochondrial fragmentation by targeting a mitochondrial fusion factor, mitofusin for degradation[103–106]. Additional studies revealed that Parkin is recruited to dysfunctional mitochondria and promotes their turnover via autophagy, a process dependent on PINK1[99,100]. Because cells with a high degree of mtDNA mutations exhibit respiratory dysfunction and because there is a mitochondrial quality control (mtQC)

system capable of detecting and degrading damaged mitochondria, this system may also detect mitochondria with a high degree of mtDNA mutations and target them for autophagy. However, because many pathogenic mutations are heteroplasmic, there is likely a threshold that must be reached to allow recognition by the mtQC system. Additional studies support a role for the mtQC in heteroplasmy, which show evidence for purifying selection against mtDNA mutations in the mouse germline[107,108]. Finally, during the course of my dissertation, a study was published using cell culture approaches supporting a role for Parkin in heteroplasmy. In particular, overexpression of Parkin in cybrid cells containing an mtDNA deletion results in a decrease in heteroplasmy[109]. Together these findings support the existence of selective mechanisms that remove pathogenic mtDNA mutations.

Research Goal

Somatic mitochondrial DNA mutations are associated with aging and age-related diseases, and severity of diseases caused by mtDNA mutations is correlated with heteroplasmy levels. Because we are largely unaware of the factors that influence the frequency of mutations, another goal of my thesis project was to establish *Drosophila* as an *in vivo* model to study factors that influence heteroplasmy. In particular, I studied the effects of age, oxidative stress, and mtDNA replication on somatic mtDNA mutations and future studies include studying the role of the mtQC on heteroplasmy.

I developed the Random Mutation Capture (RMC) assay[110] to study mutation frequencies in *Drosophila*. The RMC assay measures the frequency that a restriction enzyme site is lost due to mutation. At the time we initiated these studies, the RMC assay

was the most sensitive method available because it does not rely on PCR to identify mutations and can detect mutations as rare as 1 in 10^8 bases. PCR limits sensitivity because polymerases have an intrinsic error rate of ~$2x10^{-5}$ [111,112], so mutations that are present below or near 10^{-5} cannot be distinguished from background. Additionally, artefactual fixation of base adducts into mutations by PCR increases the apparent mutation frequency. Additional benefits of the RMC assay are that it is high-throughput, cost effective, and uses DNA from tissue homogenate, which is easier to obtain than single cells. PCR may be used to detect mutations in single cells if they undergo clonal expansion. However, if the mtDNA mutation frequency is measured within a whole tissue, clonally-expanded mutations within a single cell of the tissue may be diluted by wild-type molecules in the remaining tissue and would thus be undetectable by PCR-based methods. The mtDNA mutation frequency measured in whole tissue of several vertebrates is ~10^{-6} [46,49]. Therefore, methods that rely on PCR alone are below the detection limit to measure mtDNA mutations in whole tissues of vertebrates. Because point mutations in *Drosophila* mtDNA had not previously been measured, we utilized the most sensitive method available at the time, the RMC assay.

In my initial studies I characterized the age-dependent frequency and distribution of somatic mtDNA mutations in flies, which was previously unknown. Using this assay, I studied the relationship between age and somatic mtDNA mutations and the role of oxidative stress. I found that many of the features associated with mtDNA mutations in vertebrates are also conserved in *Drosophila*, including the mtDNA mutation frequency, the finding that their frequency increases with age, and that there is a prevalence of transition mutations. I further demonstrated that the types of mutations that accumulate

with age do not correspond to those associated with oxidative stress but rather to errors that occur during mtDNA replication. Additionally, this work supports *Drosophila* as a model to study somatic mtDNA mutations and to explore the factors that influence heteroplasmy (**Chapter 3)**.

Since our initial studies using the RMC assay to measure mtDNA mutations, a new technique, Duplex Sequencing (DS), was developed with an unprecedented sensitivity. DS uses molecular tagging of individual duplex DNA molecules and post-sequencing analysis to increase the mutation detection sensitivity of standard next-generation from ~10^{-3} to ~10^{-10} [113,114]. We transitioned from RMC to DS to measure mtDNA mutations because DS provides more data for each sample preparation as DS can potentially interrogate the entire mitochondrial genome for mutations compared to RMC, which is limited to detecting mutations at a 4 base pair restriction enzyme site. Additionally, DS can detect mutations at a greater sensitivity than RMC because restriction enzymes are not completely successful. The progress of these studies in *Drosophila* is not yet published and is described in **Chapter 4**.

2 A *Drosophila* Model of Mitochondrial Disease Caused by a Complex I Mutation that Uncouples Proton Pumping from Electron Transfer

This chapter is a manuscript in preparation for submission: Jonathon L. Burman[1], Leslie S. Itsara[1], Ernst-Bernhard Kayser, Wichit Suthammarak, Margaret M. Sedensky, Philip G. Morgan, Leo J. Pallanck

[1]These authors contributed equally to this work.

2.1 Summary

Mutations affecting mitochondrial complex I, a multi-subunit assembly that couples electron transfer to proton pumping, are the most frequent cause of heritable mitochondrial disease. However, the mechanisms underlying diseases associated with complex I dysfunction remain unclear. Here, we describe a *Drosophila* model of complex I dysfunction caused by a homoplasmic mutation in the mitochondrial-encoded *NADH dehydrogenase subunit 2* (*ND2)* gene. We show that *ND2* mutants exhibit phenotypes that parallel the features of mitochondrial disease, including shortened lifespan, progressive neurodegeneration and decreased complex I abundance. Our findings support a role for the ND2 subunit in proton pumping and indicate that the disease phenotypes we observe are due to diminished respiratory chain activity and consequent energy deficiency.

2.2 Introduction

Mitochondria perform numerous vital cellular functions, including producing the majority of adenosine triphosphate (ATP) in cells through oxidative phosphorylation via mitochondrial respiratory chain complexes. NADH ubiquinone oxidoreductase, or complex I, is the largest complex of the mitochondrial respiratory chain. It consists of ~45 subunits, including 7 that are encoded by the mitochondrial genome: (*ND1-6* and *ND4L*)[115]. All mitochondrial DNA (mtDNA) encoded subunits of complex I span the mitochondrial inner membrane, where a subset of them may function in proton pumping given their homology to characterized bacterial complex I subunits[115–118].

Mutations in genes encoding complex I subunits are a common cause of early-onset mitochondrial diseases such as Leigh syndrome and mitochondrial myopathy, encephalomyopathy, lactic acidosis, stroke-like symptoms (MELAS)[119]. These diseases are highly debilitating, and are typically characterized by progressive neurodegeneration, seizures and shortened lifespan[34].

Recently, Xu and colleagues developed a novel technology for creating targeted mtDNA mutations in *Drosophila melanogaster*, and used this technology to generate strains harboring homoplasmic mtDNA mutations, including a 9-nucleotide deletion in the *ND2* gene[120]. This deletion ($ND2^{del1}$) results in the removal of three amino acids at sequence positions 186-188 of the ND2 protein[120]. As mutations in human *ND2* have been demonstrated to cause Leigh syndrome[29,30], Leber's hereditary optic neuropathy[121], and exercise intolerance[28], we hypothesized that this *Drosophila ND2* mutant might serve as an animal model of complex I disease. Here we show that *ND2* mutants exhibit a variety of behavioral phenotypes that parallel symptoms of complex I deficiency in

humans. These phenotypes include stress-induced seizures, progressive neurodegeneration and shortened lifespan. Furthermore, our biochemical characterization of *Drosophila ND2* mutants reveals decreased complex I activity and energy production in mutants, as well as a role for the ND2 subunit in the proton pumping activity of complex I. Our findings support a model in which the $ND2^{del1}$ mutation uncouples electron transport through complex I from proton pumping, leading to energy deficits and the neurodegenerative phenotypes associated with this model of complex I deficiency.

2.3 Results

2.3.1 Structural analysis of ND2

Primary amino acid sequence comparison of *Drosophila* ND2 relative to human revealed a high degree of homology, including the region encompassing the $ND2^{del1}$ mutation (Fig. 2.1). Specifically, *Drosophila* ND2 exhibits 41% identity and 61% similarity to human ND2 and 26% identity and 46% similarity to the *E. coli* complex I NADH-quinone oxidoreductase chain N (NuoN) subunit (Fig. 2.1), which has a role in the proton pumping activity of bacterial complex I[115,118]. Secondary structural analysis predicted the existence of 10 transmembrane helices within ND2. The $ND2^{del1}$ mutation removes three conserved amino acids from the sixth predicted transmembrane helix of ND2 (Fig. 2.1, B). Because a previously characterized human Leigh syndrome mutation (L71P)[29] is found within the third transmembrane helix of ND2 (Fig. 2.1, A) we proceeded to test whether *Drosophila* $ND2^{del1}$ mutants could serve as a model of mitochondrial disease.

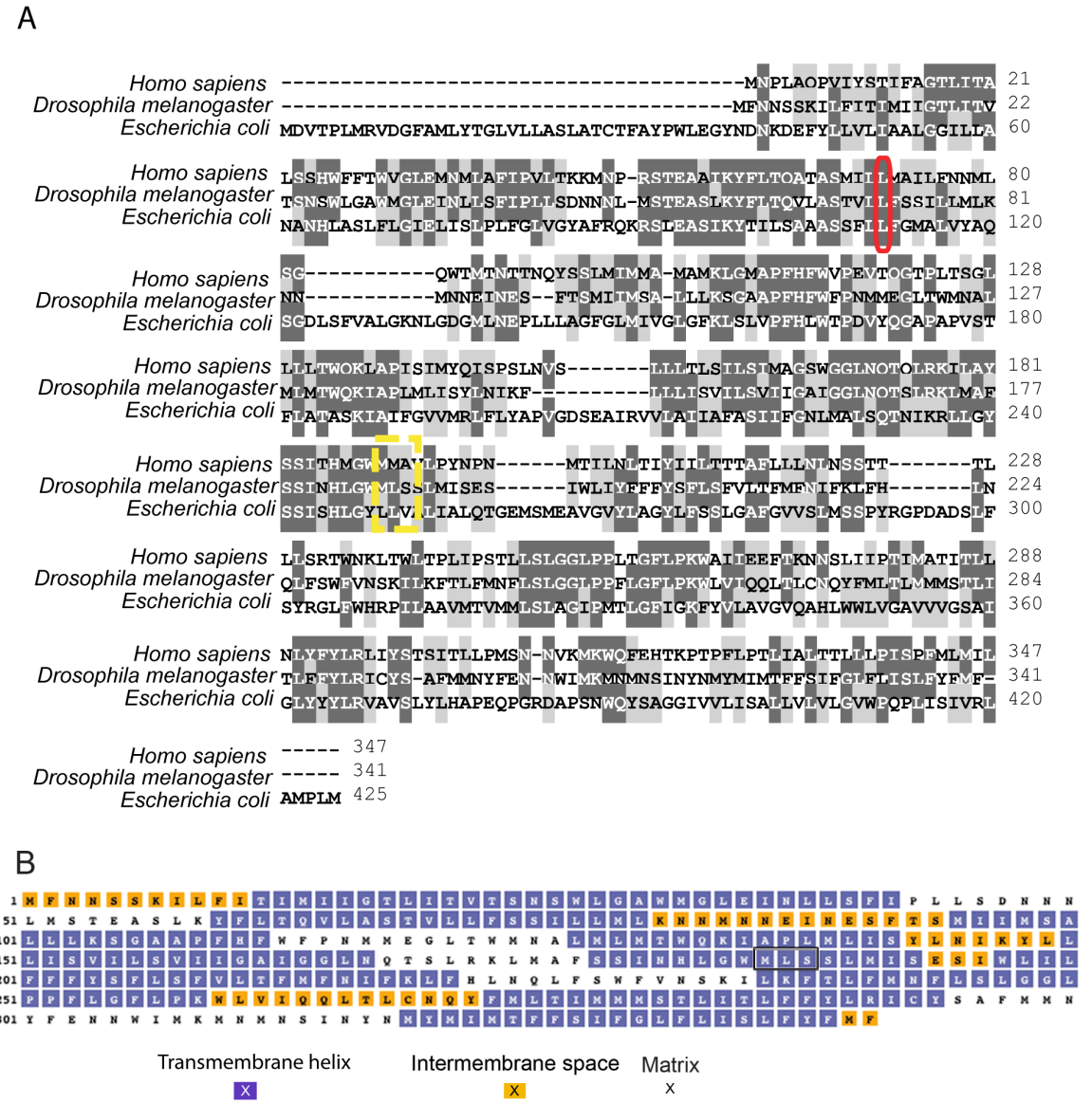

Figure 2.1. ND2 sequence alignment and secondary structure prediction. (A) Primary sequence alignment of ND2 from *Homo sapiens*, *Drosophila melanogaster, and Escherichia coli* is depicted. Identical residues are shaded dark grey with white font, and similar residues shaded light grey with black font. The three amino acid deletion caused by the *ND2*^{del1} mutation is indicated with a yellow dashed box. The L71P missense mutation found in a human Leigh syndrome patient is indicated with a red oval. (B) *Drosophila* ND2 amino acid sequence and secondary structural prediction depicting residues found within the mitochondrial intermembrane space (orange), transmembrane helices of the inner membrane (purple) or the matrix (no color). The three amino acid *ND2*^{del1} deletion occurs within the sixth transmembrane helix, and is indicated with a box.

2.3.2 Behavioral analyses of ND2 mutants

Complex I-associated mitochondrial diseases are often associated with dramatically shortened lifespan[23,29], so we tested whether *ND2* mutants were also short-

lived. We found that the median lifespan of a mixed population of *ND2* mutant male and female flies (39 days) was reduced compared to wild-type controls (49 days), while the maximum lifespan remained unchanged between experimental and control groups (Fig.2, A). A gender-separated experiment (Fig.2, B) showed that the decreased median lifespan observed in mixed populations of *ND2* mutants arises primarily from increased early mortality of females.

Mitochondrial encephalopathies are typically characterized by neurological symptoms such as seizures and heat intolerance[122]. Similarly, Drosophila strains with mutations affecting mitochondrial function often show analogous phenomena including mechanical-stress induced paralytic seizures termed "bang sensitivity" and heat-induced paralysis[123–125]. We therefore tested whether *ND2* mutants exhibited bang-sensitive and heat-induced paralytic phenotypes. Both male and female *ND2* mutants displayed a bang-sensitive phenotype that progressively worsened with age. The bang-sensitive phenotype was more severe in females than males: *ND2* mutant females displayed substantial bang-sensitive paralysis by 10-days of age, whereas *ND2* mutant males did not exhibit significant bang-sensitive paralysis until 26-days of age (Fig. 2.2, C). We next tested whether *ND2* mutants displayed heat-induced paralysis. Because female *ND2* mutants exhibited more severe lifespan and bang-sensitive phenotypes than males, only females were used in our subsequent experiments. We found that *ND2* mutants fully paralyzed following exposure to 39^{o}C, and required a prolonged recovery period after being returned to room temperature. In contrast, age-matched control animals failed to undergo heat-induced paralysis under these conditions (Fig. 2.2, D). These results demonstrate that *ND2* mutants display phenotypes that parallel those found in mitochondrial diseases.

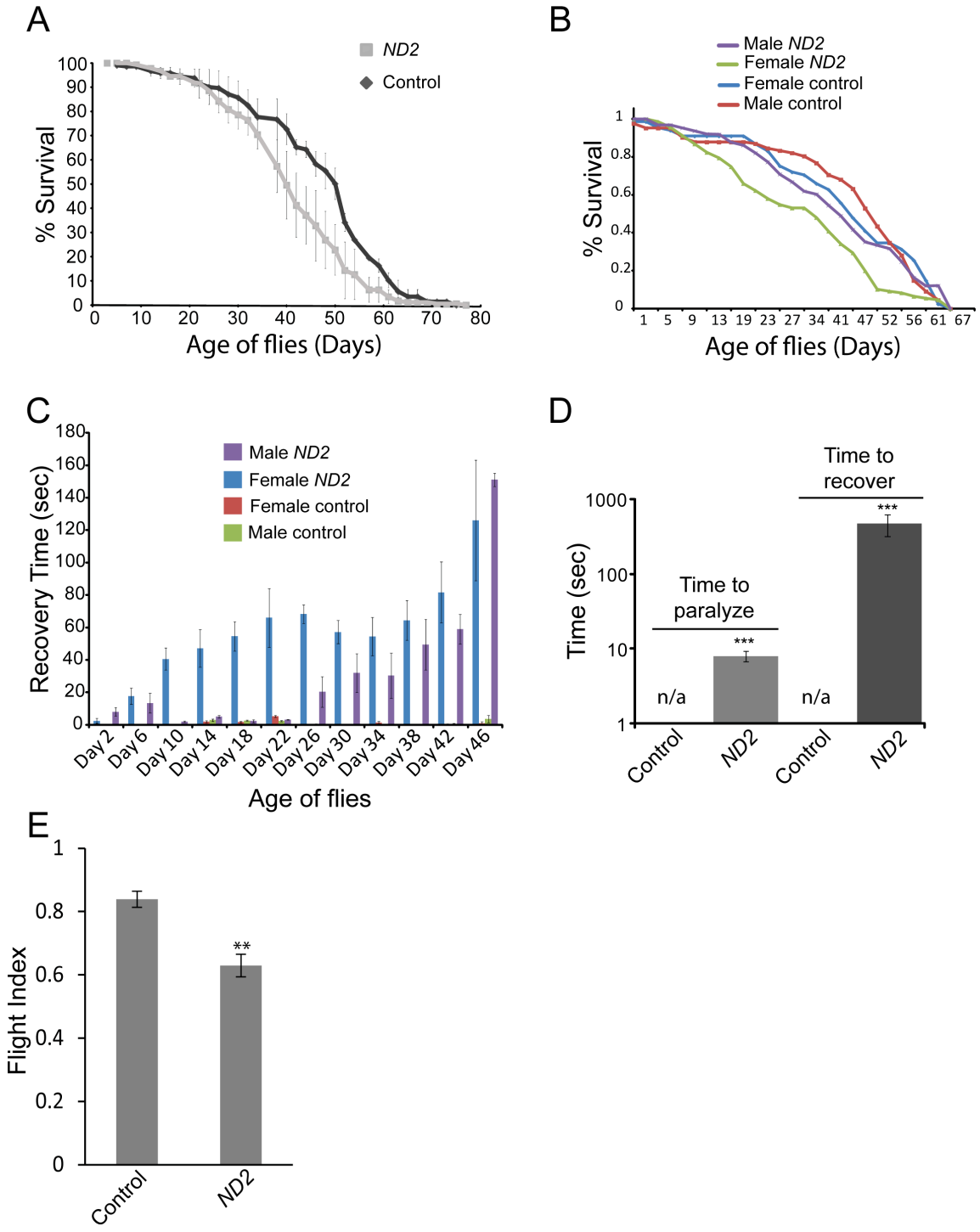

Figure 2.2. *ND2* mutants exhibit behavioral abnormalities and shortened lifespan. (A) A gender combined lifespan analysis depicting a decrease in the median lifespan of *ND2* mutants, while the maximum lifespan of *ND2* mutants is indistinguishable from controls. Error bars represent standard error of the mean; n=10 independent groups of 12-20 animals. (B) A gender separated lifespan analysis depicting a shortened average lifespan of *ND2* mutant females compared to controls or *ND2* mutant males; n=7 independent groups of 13-22 animals. (C) *ND2* mutants exhibit stress-induced paralysis. Both male and female *ND2* mutant and control animals were assayed for the length of time that flies remained paralyzed

following mechanical stress. Error bars represent standard error of the mean; n=3 independent groups of 6-12 individual animals. (D) *ND2* mutants exhibit heat-induced paralysis. Middle-aged *ND2* mutants were incubated at 39^{o}C, and the time for each individual flies to paralyze measured in seconds. After 6 minutes the flies were then placed in room temperature vials, and the time to recover from paralysis recorded in seconds. Control animals did not exhibit heat-sensitive paralysis over the time course of the assay (n/a). Histograms depict the median time animals took to completely paralyze and recover from paralysis (n=3 independent groups of 7-9 animals); $p=4.37x10^{-17}$ and $p=8.7x10^{-11}$ for paralysis and recovery, respectively; ***=$p<0.001$; Error bars represent standard error of the mean. (E) *ND2* mutants have reduced flight ability. *ND2* mutants and control animals were tested for their flying ability by measuring the distance that flies alighted when dispensed into a cylinder ($p=0.001$). Histograms represent the average flight index of the indicated genotypes and error bars represent the standard error of the mean; n=6 independent groups of 11-20 animals; *=$p<0.01$.

Mitochondrial disease preferentially affects tissues with high energetic demands, such as muscle and brain[126]. To test for impaired function in muscle and/or neural tissue, we measured the flight performance of young (7-day-old) *ND2* mutants using a well-established flight assay[127,128]. *ND2* mutants displayed significantly reduced flying ability compared to age-matched control flies (Fig. 2.2, E). In total our behavioral results support the hypothesis that the $ND2^{del1}$ mutation affects energy demanding muscle and/or brain tissue(s), mirroring deficits frequently seen in human mitochondrial disease.

2.3.3 *Tissue integrity of ND2 mutants*

A hallmark of mitochondrial disease is the progressive degeneration of neural and/or muscle tissue(s)[33]. We therefore analyzed muscle and brain integrity by hematoxylin and eosin staining of tissue from middle-aged (26-day-old) and old (42-day-old) *ND2* mutants. We detected no abnormalities in the flight muscles of middle-aged or old *ND2* mutants (Fig. 2.3, A). Similarly, the brains of middle-aged *ND2* mutants were indistinguishable from age-matched control animals (Fig. 2.3, B). However,

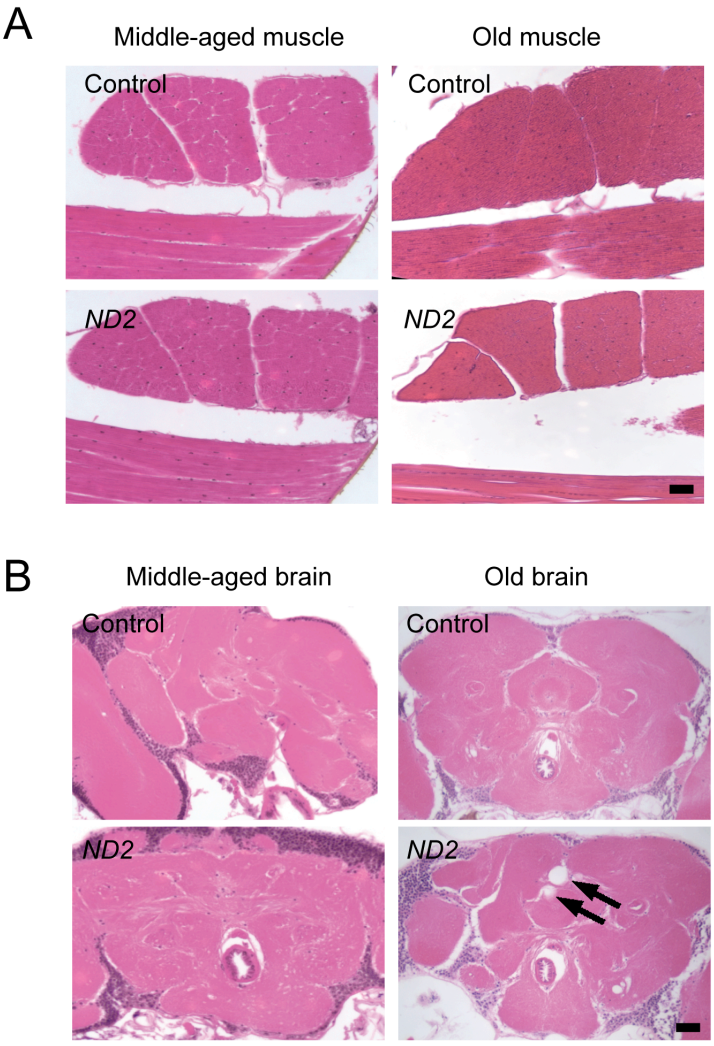
A
Middle-aged muscle
Old muscle
Control
Control
ND2
ND2
B
Middle-aged brain
Old brain
Control
Control
ND2
ND2
C
Vacuole area in old brains (μm)
14
12
10
8
6
4
2
0
***
w1118
ND2

Figure 2.3. *ND2* mutants exhibit progressive neurodegeneration, but lack muscle pathology (A) Thoracic muscle integrity was analyzed by coronal sectioning of the thorax of middle-aged (26-day-old) or old (42-day-old) *ND2* mutant and controls. Representative images of hematoxylin and eosin stained thoracic muscle sections are depicted. Scale bars represent 200 mm. (B) Brain integrity was analyzed by coronal sectioning of the heads of middle-aged or old *ND2* mutants and controls. Representative images of hematoxylin and eosin stained coronal brain sections are depicted. Arrows demark neurodegenerative vacuoles. Scale bars represent 200 mm. (C) Quantification of vacuole size in the brains of old *ND2* mutant and control animals demonstrates an increase in vacuole size in *ND2* mutants ($p=0.0002$). Vacuoles were rarely detected in the brains of middle-aged *ND2* mutants and were, therefore, not subjected to quantification. Error bars represent standard deviation; n=3 independent histological preparations; ***=$p<0.001$.

vacuoles, which indicate neurodegeneration in flies, were observed in the brains of old *ND2* mutants and were significantly larger than those that occurred in age-matched controls (Fig. 2.3, B and C). These findings suggest that the age-dependent behavioral phenotypes of *ND2* mutants derive from progressive neurodegeneration rather than muscle pathology.

2.3.4 Functional analyses of mitochondria isolated from ND2 mutants

To explore the biochemical mechanisms underlying *ND2* mutant phenotypes, we isolated mitochondria from middle-aged (14-day-old) and old (30 to 35-day-old) *ND2* mutants and controls, and used complex I–specific substrates to measure rotenone-sensitive mitochondrial respiration. We performed these experiments using both limiting and saturating amounts of ADP to measure state 3 and maximal state 3 complex I-dependent respiratory rates, respectively. As previously reported, state 3 and maximal state 3 rates decreased with age in controls flies[129], and *ND2* mutants showed a similar age-related decrease (Fig. 2.4, A). Mitochondria isolated from either middle-aged or old *ND2* mutants showed unimpaired state 3 respiration, but maximal state 3 values were significantly decreased in *ND2* mutants relative to age-matched controls (Fig. 2.4, A and

Table 1). The *ND2*^{del1} mutation thus causes a complex I–dependent respiratory defect specifically under maximally demanding conditions.

The respiratory defect of *ND2* mutants offered the opportunity to investigate the functional role of the ND2 subunit in complex I activity. To test whether ND2 plays a role in the proton pumping activity of complex I, we measured the coupling of proton pumping to ATP production in *ND2* mutants relative to control animals. This coupling is defined as the number of ADP molecules converted to ATP per oxygen atom consumed under state 3 conditions (ADP/O), and is a measure of complex I efficiency. We found a significant decrease in complex I–dependent ADP/O ratios in both middle-aged and old *ND2* mutants. This decrease was not due to a change in the efficiency of ATP production by complex V, nor a proton leak in the mitochondrial membrane, as *ND2* mutant ADP/O ratios were normal when respiration was dependent on complex II (Table 1 and Fig. 2.4, B). We thus find that the *ND2*^{del1} mutation causes a decrease in complex I efficiency, without an effect on electron flow (state 3 respiration), indicating that the *ND2* subunit is involved in the proton pumping mechanism of complex I.

Because oxidative phosphorylation is dependent on an intact proton gradient across the inner mitochondrial membrane, the decreased efficiency of complex I-dependent ATP production (ADP/O) observed in *ND2* mutants could also be explained by an increased proton leak through this membrane. As noted in the previous paragraph, such a leak should affect the ADP/O ratio when respiration is driven by complex II, which was not the case. To further test this hypothesis we measured the mitochondrial respiratory rate following depletion of ADP (state 4), an indicator of proton leak across the mitochondrial inner membrane. State 4 values from either middle-aged or old

mitochondria were not significantly different between *ND2* mutants and age-matched controls (Fig. 2.4, A and Table 1). Our results thus demonstrate that electron flow through complex I is inefficiently coupled to proton pumping in *ND2* mutants.

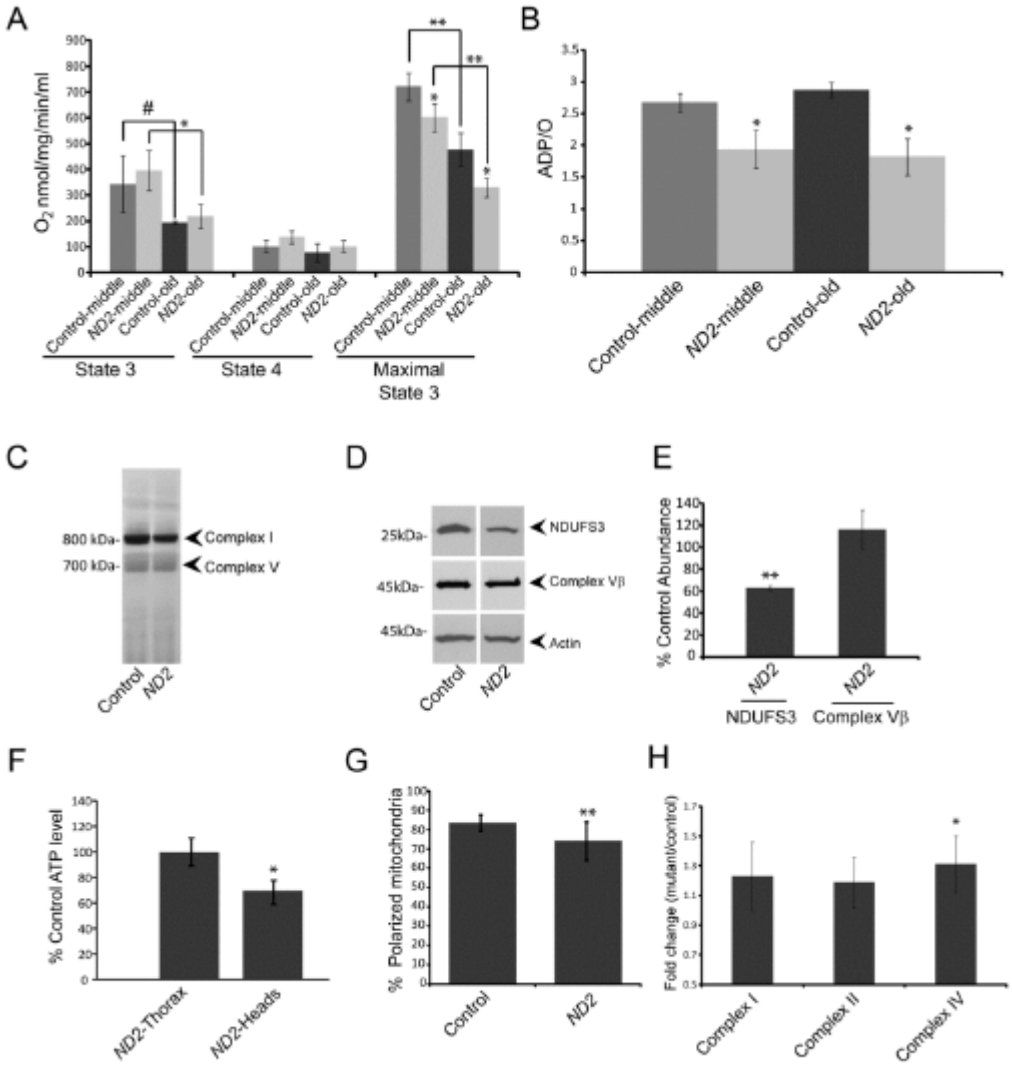

Figure 2.4. *ND2* mutants exhibit decreased mitochondrial function (A) Complex I mitochondrial respiration rates from 14-day-old or 30 to 35-day-old *ND2* mutant or control animals. Both state 3 and maximal state 3 values declined with age within genotypes (p=0.08 and p=0.04 for either genotype middle-aged and old control or *ND2* mutant state 3 values, respectively; p=0.007 and p=0.003 for comparison of middle-aged and old control or *ND2* mutant maximal state 3 values, respectively). State 4 respiration was similar under all conditions tested. No differences were found for state 3 values between control and *ND2* mutants at either middle- or old age. Maximal state 3 values were decreased in both middle-aged and old *ND2* mutants when compared to age-matched controls (p=0.04 for both middle-aged and old animals).

Error bars represent standard deviations; n=3 independent mitochondrial preparations; **=p<0.01; *=p<0.05; #=p<0.1). (B) Oxidative phosphorylation efficiency (ADP/O) is decreased in *ND2* mutants relative to controls at both middle and old ages (p=0.02 and p=0.01, respectively). Error bars represent standard deviations; n=3 independent mitochondrial preparations; *=p<0.05**.** (C) Blue native gel/Complex I In-gel activity analysis of mitochondria isolated from middle-aged *ND2* mutant and control animals reveals similar levels of complex V in both genotypes, but decreased fully assembled complex I in *ND2*. (D) Western blot of protein from middle-aged *ND2* mutant and control flies reveals a decrease in the complex I subunit NDUFS3, with no decrease in the Complex Vβ subunit. (E) Quantification of NDUFS3 in *ND2* relative to controls (n=3 independent tissue extracts; p=0.003) and Complex Vβ (n=3 independent tissue extracts; p=0.46) levels normalized to actin, and expressed as the % of control values. Error bars represent standard error of the mean; **=p<0.01. (F) ATP levels in heads of old *ND2* mutants, and displayed relative to controls values (p=0.05). Error bars represent standard error of the mean; n=3 groups of 5 individuals; *=p≤0.05 for a one-tailed t-test. (G) The fraction of cells with polarized mitochondria (% Polarized mitochondria) measured from neurons isolated from old *ND2* mutants is shown compared to age-matched controls (p=0.004). Error bars represent standard deviation; n=3 independent mitochondrial preparations; **=p<0.01. (H) State 3 respiratory rates from *ND2* and age-matched control mitochondria, utilizing Complex I-, II- and IV-specific substrates. Data from middle-aged and old animals were combined and expressed as the fold change relative to control values. Complex IV-mediated oxygen consumption demonstrated a significant increase relative to control mitochondria (p=0.02); n=6 independent mitochondrial preparations for Complex I; n=4 independent mitochondrial preparations for Complex II; n=5 independent mitochondrial preparations for Complex IV; Error bars represent standard error of the mean, *=p<0.05.

While the decrease in ADP/O in *ND2* mutants indicates that ND2 is required for the efficient coupling of electron transfer to proton pumping, it does not explain the decrease in the maximal state 3 oxygen consumption rate of complex I of *ND2* mutants. One possible explanation for this decrease is a reduction in complex I abundance. To test this model we examined mitochondria isolated from *ND2* mutant and control animals on blue native gels. Blue native gel analysis indicated that the abundance of fully assembled complex I was decreased in *ND2* mutants relative to controls, without an accompanying decrease in complex V abundance (Fig. 2.4, C). Western blot analysis also revealed a decrease in the complex I subunit NDUFS3 in *ND2* mutants, but little to no change in the abundance of the β-subunit of complex V relative to age-matched controls (Fig. 2.4, D and E). Our findings indicate that ND2 is required for both the efficient coupling of electron transport to proton pumping, and the structural integrity of complex I, and that these deficits underlie the pathogenesis of this model of complex I deficiency.

Genotype	Age	Measurement	Consumption Rate (O_2/mg/min) or ratio	Standard Deviation	P value
Control	14	State 3	344.7	±108.9	0.50
***ND2*^{del1}**	14	State 3	396	±58.4	
Control	14	State 4	108.8	±21.2	0.32
***ND2*^{del1}**	14	State 4	130	±25.4	
Control	14	Max. State 3	721	±54.2	0.04
***ND2*^{del1}**	14	Max. State 3	602	±53.6	
Control	14	ADP/O	2.7	±0.15	0.02
***ND2*^{del1}**	14	ADP/O	1.9	±0.1	
Control	14	CII	168.1	±7.7	0.19
***ND2*^{del1}**	14	CII	219.3	±24.8	
Control	14	CII: ADP/O	1.7	±0.13	0.42
***ND2*^{del1}**	14	CII: ADP/O	1.6	±0.12	
Control	14	CIV	1705	±398	0.39
***ND2*^{del1}**	14	CIV	2185	±793	
Control	35	State 3	193.5	±21.3	0.45
***ND2*^{del1}**	35	State 3	218	±46	
Control	35	State 4	78.4	±39.4	0.39
***ND2*^{del1}**	35	State 4	102.7	±22.6	
Control	35	Max. State 3	477.9	±101	0.04
***ND2*^{del1}**	35	Max.State3	330.5	±35.35	
Control	35	ADP/O	2.9	±0.12	0.01
***ND2*^{del1}**	35	ADP/O	1.8	±0.28	

Table 2.1. Oxygen consumption rates and respiratory ratios Oxygen consumption measurements in middle-aged or old mitochondria isolated from *ND2* mutants or aged matched control animals. Respiratory rates (State 3, Max. State 3, State 4, CII) are expressed in units of O_2 consumed nmol/min/mg (n=3 independent mitochondrial preparations). ADP/O ratios are unit-free (n=3 independent mitochondrial preparations). The corresponding standard deviations and p-values for each measurement are indicated.

The decreased maximal state 3 activity and ADP/O of *ND2* mutants suggested that the mutants might have reduced ATP synthesis and mitochondrial membrane potential. To test these possibilities, we compared ATP levels in the thoraces and heads of old (30- to 42-day-old) *ND2* mutants and control animals, and measured mitochondrial membrane potential in dissociated neurons from old (33- to 38-day-old) *ND2* mutants and controls. We detected a decrease in ATP abundance in *ND2* mutants that was specific to heads (Fig. 2.4, F), and a decrease in the fraction of cells with polarized mitochondria in the brains of old *ND2* mutants relative to controls (Fig. 2.4, G). These findings suggest that

the *ND2*^{del1} mutation affects the proton pumping activity of complex I, which reduces the proton gradient available for ATP generation, leading to energy deficiency in the brains of *ND2* mutants.

Previous work has demonstrated compensatory upregulation of complex II or complex IV respiratory capacity in response to complex I deficiency[38,40]. To test for similar compensatory effects in *ND2* mutants we measured complex II- and complex IV-dependent respiration in middle-aged (14-day-old) animals. We did not observe a significant change in complex II-dependent state 3 respiratory rates between *ND2* mutants and controls (Table 2.1). However, there was a consistent increase in complex IV-dependent respiratory rates in *ND2* mutants relative to control animals, but this increase did not reach significance, due to day-to-day variability (Table 2.1). To reduce this variability, we calculated the ratio of mutant to control respiratory rate using pooled data from middle-aged (14-day-old) and old (30-35-day-old) animals. Analysis of complex I-, II- and IV-dependent respiration under these criteria revealed a significant upregulation of complex IV-dependent respiration in *ND2* mutants (Fig. 2.4, H), indicating that compensatory upregulation of complex IV is initiated in response to complex I dysfunction in *ND2* mutants.

In summary, our biochemical work reveals that ND2 is required both for the proton pumping activity and structural integrity of complex I. Our data support a model in which decreased complex I activity results in an energy deficiency that causes the neurodegenerative and behavioral phenotypes associated with this model of mitochondrial disease.

2.4 Discussion

We have characterized a *Drosophila* model of complex I deficiency caused by a mutation in the mitochondrial-encoded respiratory chain complex I subunit *ND2* that exhibits phenotypes paralleling those of mitochondrial encephalopathies. In addition, we provide evidence supporting a model in which the ND2 subunit functions in maintaining the proton pumping activity and structural integrity of complex I. We propose that decreased complex I activity leads to progressive energy deficiency and neurodegeneration in our model.

While the function of complex I is clear, our understanding of the relative functional contributions of many of its ~45 subunits remains incomplete. In particular, the ND2 subunit has been hypothesized to play a role in proton pumping based on its homology to the bacterial complex I NuoN subunit[118], but no biochemical corroboration of this model has been previously described. Our results argue that the $ND2^{del1}$ mutation causes a slippage of proton transport though complex I, as well as a decrease in the abundance of fully formed complex I. The finding that complex I activity and abundance are also reduced in a Leigh syndrome patient harboring an ND2 mutation[29] strongly suggests that the biological role of ND2 is evolutionarily conserved. However, this case report did not examine respiratory chain oxygen consumption or mitochondrial membrane potential, and therefore made no statements regarding the role of ND2 in proton pumping.

A number of hypotheses have been proposed to explain the pathological consequences of complex I deficiency, including energy deficits and increased oxidative stress [40,130]. While these models are not mutually exclusive, our data support a model in

which decreased ATP levels in the head plays a major role in the onset of *ND2* mutant phenotypes. However, the progressive nature of the *ND2* phenotypes, including the energy deficiency of *ND2* mutants requires further explanation. Because complex I activity declines with age in *Drosophila*, one possible explanation for the progressive phenotypes of *ND2* mutants is that energy deficiency does not occur until a critical threshold of complex I activity is crossed. This threshold may never be attained in WT flies, but could occur in *ND2* mutants because they begin life with a lower level of complex I activity. Alternatively, the induction of complex IV–dependent respiration observed in *ND2* mutants may be transient. Such transient induction of mitochondrial compensation in response to respiratory chain deficiency has been observed in previous work[131]. Future studies will be required to distinguish these models, to determine the importance of complex IV upregulation in *ND2* mutants and the role if any of oxidative stress

In summary, our work suggests a central role for ND2 in the proton pumping mechanism of complex I, and provides a genetically tractable animal model of complex I deficiency. This model should prove a valuable tool in which to further explore the pathological mechanisms underlying human mitochondrial disease.

2.5 Materials and Methods

Drosophila strains and maintenance: All *Drosophila* strains were maintained on standard cornmeal/molasses medium at 25°C with a 12-hour light-dark cycle. The $ND2^{del1}$ stock was obtained from the laboratory of Dr. Patrick O'Farrell (University of California, San Francisco)[120]. The isogenic w^{1118} stock was obtained from the Bloomington *Drosophila*

Stock Center at Indiana University. To control for differences in nuclear genetic background, we outcrossed *ND2* mutants to the w^{1118} strain. F_1 offspring derived from crossing *ND2* mutant females to w^{1118} males were used as the experimental group, given that they inherit mtDNA from the *ND2* mutant strain; F_1 offspring derived from crossing *ND2* mutant males to w^{1118} females were used as the wild-type control group, given that they inherit mtDNA from the w^{1118} strain.

*ND2 structural predictions***:** Primary sequence alignment of ND2 was produced using the Bioedit software ClustalW multiple sequence alignment function (Ibis Biosciences, Carlsbad, CA). The secondary structure analysis of ND2 was performed using the protein prediction server PSIPRED[132] and the transmembrane topology program MEMSAT-SVM[133] (Department of Computer Science, University College, London, UK).

*Mechanical stress induced paralysis***:** Flies were assayed for bang sensitivity using a modification of a previously published protocol[123]. Briefly, flies were vortexed for 10 seconds in inverted glass vials containing cotton stoppers, and the time required for each individual animal to right itself was recorded.

*Heat induced paralysis***:** Flies were assayed for heat-induced paralysis by placing groups of 5-10 animals into pre-warmed vials maintained at 39°C. The time for the flies to become completely paralyzed was recorded. After exposure to 39°C for 6 minutes the animals were then placed in new room temperature vials (~20°C), and the recovery time of *ND2* mutants from paralysis recorded.

Lifespan: Lifespan assays using vials containing populations of 12-20 flies were transferred to new vials every two days throughout the assay period. At least 60 flies were monitored for each experiment. For sex specific lifespan assays, *ND2* mutant males and females or gender- and age-matched control flies were separated within 1 day of eclosion, and the assay conducted as described above.

*Flight***:** Flight assays were performed as previously described[127,128]. Briefly, an acetate sheet was divided into five parts, coated with vacuum grease, and inserted into a 1 L graduated cylinder. Flies were gently tapped into a funnel at the top of the cylinder, and became stuck to the vacuum grease where they alighted. The acetate sheet was removed, and the number of flies in each section was counted. Flies that alighted in a higher section of the acetate sheet received a correspondingly higher value in scoring. The number of flies alighting in the top section was summed and multiplied by four, the number of flies alighting in the second highest section was summed and multiplied by three, and so on. Finally, the weighted sum for the entire group of flies was determined and normalized to four times the total number of flies used in the assay (the maximum possible score), and this normalized value was reported as the flight index. Flies that alighted at the top of the cylinder received a flight index score of 1, whereas flies that fell to the bottom of the cylinder received a flight index score of 0. At least six groups of 11-20 flies per genotype were tested.

Tissue preparation and sectioning: Flies were anesthetized, mounted in fixing collars and placed in Carnoy's fixation solution (10% acetic acid; 30% chloroform; 60% absolute ethanol) for 3.5 hours. Fixed flies were then placed in 95% ethanol twice for 30 minutes each, in 100% ethanol for 45 minutes, then in methylbenzoate overnight. Flies were then incubated in a 1:1 mixture of methylbenzoate:paraffin for 1 hour at 60°C, transferred to 100% liquid paraffin and incubated at 60°C for 30 minutes, then transferred to fresh 100% liquid paraffin four times for 15-30 minutes each. The flies were then transferred to 100% liquid paraffin in a plastic mold, placed at 60°C for 15 minutes, and the paraffin was allowed to harden at room temperature. Five µm coronal histological sections were cut on a Shandon Finesse 325 Microtome, and processed for hematoxylin and eosin staining. Images were collected on a Nikon Optiphot-2 using a 20x objective. Vacuole size was quantified in ImageJ[134] by converting pixel values into micrometers. Only vacuoles present in at least two consecutive sections were quantified to avoid artifacts derived from tissue sectioning.

*Mitochondrial Preparations***:** Mitochondria were obtained from 0.25-0.5 g of flies by adapting a previously published protocol[129]. Flies were chilled on ice, and then homogenized on ice using a Potter/Elvehjem homogenizer with 10 manual strokes in 20 mL of homogenization buffer (200 mM mannitol, 70 mM sucrose, 5 mM MOPS, 2 mM EDTA; 0.4% defatted BSA; pH 7.4), avoiding shearing. The homogenate was then filtered through cotton gauze, and spun at 300 x g for 4 minutes at 4°C. The supernatant was then filtered through gauze and spun at 10,000 x g for 10 minutes at 4°C. The pellet was resuspended in 10 ml of resuspension buffer (200 mM mannitol, 70 mM sucrose, 5

mM MOPS, 2 mM EDTA; pH 7.4) and spun at 10,000 x g for 10 minutes at 4°C. The mitochondrial pellet was then resuspended in 10-50 µl of final buffer (200 mM mannitol, 70 mM sucrose, 5 mM MOPS; pH 7.4), to a final concentration of ~50 µg protein/µL. 150-300 µg of mitochondria were used for oxidative phosphorylation assays and 250 µg for blue native gel analysis. All reagents for mitochondrial preps were obtained from Sigma (St. Louis, MO).

*Oxidative Phosphorylation Assays***:** Oxygen consumption of isolated mitochondria was monitored using a Clark-type electrode (Oxytherm with analysis software Oxyg32, Hansatech Instruments, Pentney, Norfolk, Great Britain) by an adaptation of Kayser et al 2001[135]. Briefly, 150-300 µg of purified mitochondria were stirred in 500 µL of assay buffer (100 mM KCl, 50 mM MOPS, 1 mM EGTA, 5mM potassium phosphate, 1 mg/ml defatted BSA; pH 7.4) at 30°C. Ten mM malate and 20 mM pyruvate were added as complex I specific electron donor substrates, 20 mM succinate was added as a Complex II specific electron donor substrate or 25 mM TMPD and 250 mM ascorbate pH 7.0 were added as Complex IV specific electron donor substrates. A low dose of ADP (90.7 nmol) was added to determine state 3 mitochondrial respiration rates, and following depletion of ADP, ensuing state 4 respiration rates. A saturating dose of ADP (1 µmol) was used to assess maximal complex I-dependent electron transport capacity under phosphorylating conditions (maximal state 3). Saturating amounts of TMPD/ascobate were used to measure Complex IV activity. ADP/O was defined as the number of ADP molecules phosphorylated per oxygen atom reduced to water, and ADP/O was calculated by dividing the amount of ADP added (90.7 nmol) by the amount of oxygen consumed

between the time of ADP addition and the onset of state 4. Fold change (mutant/control) of complex-specific respiratory rates depicted in Figure 2.4H were calculated from the combined data from both middle-aged and old *ND2* mutants relative to aged matched controls, and utilized basal state 3 measurements for both complex I and complex II.

*ATP determination***:** Heads or thoraces were sectioned from five flies and homogenized in 6 M guanidine HCl (Sigma); 10 mM TRIS (Sigma) pH 7.3 as previously described[120]. ATP content was measured using an ATP determination kit (Molecular Probes, Eugene, OR). Protein abundance was measured using a Bradford protein assay, and ATP abundance was normalized to total protein abundance as previously described[120].

*Mitochondrial Membrane Potential***:** Measurement of neural mitochondrial membrane potential from flies was conducted as previously described[136], except that dissections of animals were performed in supplemented DME/Ham's F-12 High Glucose media lacking phenol red (Sigma), and all incubation steps were carried out at 25°C. In addition, 10 nM TMRE was utilized throughout the protocol. The % of cells harboring polarized mitochondria was determined using FloJo software (Treestar Inc.), and defined as the % of cells exhibiting relative TMRE fluorescence above 10^3 arbitrary fluorescence units, as previously experimentally determined[136]. All flow cytometry measurements were performed on a Becton-Dickson LSR II flow cytometer.

*Blue Native Gel Electrophoresis and In-gel Activity Staining***:** Assays were carried out using mitochondrial preparations from flies as previously described[137,138]. All reagents were purchased from Sigma.

*Western blots***:** Flies were flash frozen in liquid nitrogen and homogenized with a pestle in 2x RIPA buffer (150mM NaCl; 1% NP-40; 0.1% SDS; 50mM TRIS pH 8.0; 0.5% DOC). Homogenates were centrifuged at 21,000 x g for 5 minutes, and the supernatant subjected to Western blot processing and analysis. Blots were labeled with monoclonal antibodies to actin (Millipore #MAB1501) diluted 1/25,000, the β-subunit of ATP Synthase (Invitrogen #A21351) diluted 1/1,500 or the NDUFS3 subunit of complex I (Abcam #17D95) diluted 1/800. All reagents were purchased from Sigma unless otherwise noted. Western blot band intensities were quantified using Image J gel analysis tools, and the intensities were expressed as the % of control values following normalization to actin[134].

Statistics: Unless otherwise stated statistical significance tests were calculated using two-tailed Student's t-test.

2.6 Notes

Author Contributions: J.L.B., L.S.I., P.G.M., M.M.S., and L.J.P. designed research; J.L.B., L.S.I., W.S., and E.B.K. performed research; J.L.B., L.S.I., W.S., E.B.K., P.G.M., M.M.S., and L.J.P. analyzed data; J.L.B., L.S.I., M.M.S., P.G.M. and L.J.P. wrote the paper.

Acknowledgements: This work was supported by a Parkinson Society Canada Research Fellowship (to J.L.B.), and a subsequent Canadian Institute of Health Research Fellowship (to J.L.B), National Institute of Neurological Disorders and Stroke Fellowship F31NS071857 (to L.S.I.), National Institute of Health grant 1RO1GM086394 (to L.P.) and a grant from the Muscular Dystrophy Association (to L.P.). LSI was also supported on the Genetic Approaches to Aging Training Grant T32AG000057 (to Peter Rabinovitch). WS was supported by a NW Mitochondrial Guild Postdoctoral Fellowship.

3 Oxidative Stress is Not a Major Contributor to Somatic Mitochondrial DNA Mutations

This chapter is in press for publication: Leslie S. Itsara, Scott R. Kennedy, Edward J. Fox, Selina Yu, Joshua J. Hewitt, Monica Sanchez-Contreras, Fernando Cardozo-Pelaez, Leo J. Pallanck. *PLoS Genet*. 2014.

3.1 Summary

The accumulation of somatic mitochondrial DNA (mtDNA) mutations is implicated in aging and common diseases of the elderly, including cancer and neurodegenerative disease. However, the mechanisms that influence the frequency of somatic mtDNA mutations are poorly understood. To develop a simple invertebrate model system to address this matter, we used the Random Mutation Capture (RMC) assay to characterize the age-dependent frequency and distribution of mtDNA mutations in the fruit fly *Drosophila melanogaster*. Because oxidative stress is a major suspect in the age-dependent accumulation of somatic mtDNA mutations, we also used the RMC assay to explore the influence of oxidative stress on the somatic mtDNA mutation frequency. We found that many of the features associated with mtDNA mutations in vertebrates are conserved in *Drosophila*, including a comparable somatic mtDNA mutation frequency (~10^{-5}), an increased frequency of mtDNA mutations with age, and a prevalence of transition mutations. Only a small fraction of the mtDNA mutations detected in young or old animals were G:C to T:A transversions, a signature of oxidative damage, and loss-of-function mutations in the mitochondrial superoxide dismutase, *Sod2*,

had no detectable influence on the somatic mtDNA mutation frequency. Moreover, a loss-of-function mutation in *Ogg1*, which encodes a DNA repair enzyme that removes oxidatively damaged deoxyguanosine residues (8-hydroxy-2'-deoxyguanosine), did not significantly influence the somatic mtDNA mutation frequency of *Sod2* mutants. Together, these findings indicate that oxidative stress is not a major cause of somatic mtDNA mutations. Our data instead suggests that somatic mtDNA mutations arise primarily from errors that occur during mtDNA replication. Further studies using *Drosophila* should aid in the identification of factors that influence the frequency of somatic mtDNA mutations.

3.2 Introduction

Mitochondria play crucial cellular roles in energy production, Ca^{2+} buffering, metabolite synthesis, and programmed cell death in metazoans[2–4]. While most mitochondrial proteins are encoded in the nuclear genome, mitochondria also contain a compact genome that generally encodes 37 genes[139]. Germline mutations that disrupt the functions of mitochondrial DNA (mtDNA) encoded genes cause a number of devastating familial syndromes[140]. mtDNA mutations also occur in somatic tissues, and the accumulation of somatic mtDNA mutations is implicated in aging and common diseases of the elderly, including cancer, diabetes, and neurodegenerative disease[19,59,60,140]. Because there are multiple copies of mtDNA in any given cell, when mtDNA mutations occur, they frequently coexist with wild-type (WT) mtDNA, a condition known as heteroplasmy. For reasons that are not presently understood, many mtDNA mutations expand clonally within a cell, such that a single somatic mtDNA mutation can ultimately

represent a large fraction of the mtDNA within a given cell or tissue[86]. Although the ratio of mutated to WT mtDNA is believed to play a critical pathological role in diseases associated with mtDNA mutations[50], the molecular mechanisms that influence this ratio are poorly understood.

The frequency of somatic mtDNA mutations can exceed the mutation frequency of the nuclear genome by several orders of magnitude[50]. Multiple factors have been proposed to account for this high mutation frequency. Because mitochondria are the major cellular source of DNA-damaging reactive oxygen species (ROS), it is believed that ROS-mediated damage is an important contributor to somatic mtDNA mutations. Indeed, Harman proposed in the 1970s that ROS damage to mtDNA causes mtDNA mutations that result in production of dysfunctional respiratory chain components, which in turn produce increased amounts of ROS, thus leading to a vicious cycle responsible for aging[76]. Another possible source of the high mtDNA mutation frequency is mtDNA replication errors. Unlike the nuclear genome, which does not replicate in postmitotic tissues, mtDNA replicates throughout life in postmitotic tissues[50], and this ongoing replication can potentially lead to the accumulation of replication errors. Finally, the relative lack of particular DNA repair pathways and protective histones in mitochondria has also been suggested as a source of the high frequency of mtDNA mutations[141]. However, the relative contributions of these and other possible causes of the age-dependent accumulation of somatic mtDNA mutations remain unclear.

Recent work in *Drosophila melanogaster* has contributed greatly to our understanding of mitochondrial quality control[142,143], so we sought to use *Drosophila* as a simple, genetically tractable model system to explore the factors that influence somatic

mtDNA mutations. Although much is known about the frequency and distribution of somatic mtDNA mutations in vertebrates[50], these matters are largely unexplored in invertebrates. Only three previous studies have attempted to test whether somatic mtDNA mutations accumulate in *Drosophila*, and these studies have yielded contradictory findings[144–146]. While technical issues likely explain these discordant findings, a limitation of all three studies is the lack of quantitative estimates of the somatic mtDNA mutation frequency, including the somatic mtDNA point mutation frequency. Thus, we used an approach that would enable us to address these issues in *Drosophila.*

To explore the distribution, frequency, and causes of somatic mtDNA mutations in *Drosophila*, we used the Random Mutation Capture (RMC) assay[110,147]. We found that the somatic mtDNA mutation frequencies in fly tissues are similar to those reported in vertebrates, and that their frequencies increase with age. However, the specific types of mtDNA mutation detected, and the results of gene perturbations targeting oxidative stress and repair pathways, indicate that oxidative stress is not a major contributor to the somatic mtDNA mutation frequency. Instead, our findings suggest that somatic mtDNA mutations arise primarily from errors that occur during DNA replication.

3.3 Results

3.3.1 *mtDNA replication occurs in somatic tissues of Drosophila*

Previous work has shown that mtDNA synthesis occurs in mitochondria isolated from adult flies[148] and that mtDNA replication intermediates can be detected in adult *Drosophila* tissues[149], suggesting that mtDNA replication occurs in the somatic tissues of adult *Drosophila*. Given that DNA replication is essential to the formation of point

mutations we performed an additional experiment to verify that mtDNA replication occurs in somatic tissues of *Drosophila* adults. We fed adult flies 5-bromo-2'-deoxyuridine (BrdU) and used Southwestern blot analysis and immunofluorescence confocal microscopy to test whether this thymidine analog was incorporated into mtDNA. After 72 hours of exposure to BrdU, DNA was isolated from *Drosophila* heads, digested with BglII, then subjected to Southwestern blot analysis using antiserum against BrdU. Because the *Drosophila* mitochondrial genome is 19.5 kb in size and contains only one BglII site, BrdU labeling should yield a single 19.5 kb band. Consistent with this prediction, our analysis revealed a single 19.5 kb band, indicating BrdU incorporation into mtDNA (Figure S1A). To further validate this finding, we used immunohistochemistry and confocal microscopy to test whether BrdU immunofluorescence colocalizes with mitochondria in the *Drosophila* thoracic ganglion. After feeding adult flies BrdU for 72 hours, the thoracic ganglion was dissected and stained with MitoTracker Deep Red to detect mitochondria and then incubated with an antibody against BrdU. Confocal microscopy revealed anti-BrdU immunofluorescence that colocalized with MitoTracker Deep Red fluorescence in BrdU-labeled animals, but not in unlabeled controls (Figure S1B). The finding that only a subset of mitochondria stained positively for BrdU is consistent with previous work indicating that mtDNA replication occurs at a low rate in the nervous system compared to other tissues[91]. While we cannot rule out the possibility that some mitochondrial BrdU labeling is due to repair of mtDNA, our data together with previous work supports the occurrence of mtDNA replication in the adult somatic tissues of *Drosophila*[148,149].

3.3.2 Multiple TaqI sites are suitable for detecting mutations in Drosophila mtDNA

A major challenge in detecting somatic mtDNA mutations is that they arise independently in different cells, such that any single mtDNA mutation typically lacks sufficient abundance within a tissue to be reliably detected by direct sequencing[113,150]. Thus, we chose to use the Random Mutation Capture (RMC) assay to quantify the mtDNA mutation frequency in *Drosophila* because this assay can detect sequence variants at a detection limit of 10^{-8} [147]. The RMC assay measures the frequency at which a particular *TaqI* restriction site in mtDNA is eliminated through mutation. The RMC assay is a qPCR-based assay that uses two PCR primer sets. One primer set is used to amplify a portion of the mtDNA that contains a single *TaqI* restriction site (the test primers); the other primer set is used to amplify a portion of mtDNA that lacks a *TaqI* restriction site (the control primers). These primer sets are then used in qPCR reactions with *TaqI*-digested mtDNA to estimate the total number of mtDNA molecules present in the sample (determined by the qPCR reaction containing the control primer set) and the number of mtDNA molecules bearing mutations that eliminate the *TaqI* site (determined by the qPCR reaction containing the test primer set). In addition to the exquisite sensitivity with which RMC can detect mtDNA mutations, another advantage of this method is that WT molecules are eliminated by *TaqI* digestion prior to PCR amplification, and thus PCR amplification errors do not confound the mtDNA mutation frequency estimate. Previous work indicates that the majority of mtDNA mutations detected with this method are single base pair substitutions; however, small deletions and insertions can also be detected[46].

The *D. melanogaster* mtDNA sequence contains 33 *TaqI* sites (Figure 3.1). Because the mutability of these sites could vary, we sought to measure the mtDNA mutation frequency at multiple *TaqI* sites (Figure 3.1, Table S1). Four *TaqI* sites were excluded from analysis because the extreme AT-richness of the flanking sequence precluded primer design. Another 13 *TaqI* sites were excluded because their proximity to one or more adjacent *TaqI* sites did not allow for the design of primer sets that amplify only a single *TaqI* site. We designed primer pairs to the flanking sequences of the remaining 16 *TaqI* sites and used them in experiments aimed at qPCR primer optimization (see Materials and Methods). Only 4 out of these 16 primer sets had optimum amplification profiles (Table S1). These 4 primer sets amplified *TaqI* sites in three different genes, and we used three of these test primer sets (corresponding to three different genes) for our studies. The three *TaqI* sites interrogated in our study are located in *mt:Cyt-b* (Complex III subunit), *mt:CoI* (Complex IV subunit), and *mt:tRNA:Arg* (Figure 3.1, Table S1). The control primer pair anneals to sequences in the *mt:CoIII* gene (Complex IV subunit) (Table S1).

3.3.3 Somatic mtDNA mutations accumulate with age in Drosophila

To explore the frequency and distribution of somatic mtDNA mutations in *Drosophila*, we used an isogenic fly line (w^{1118}) to control for the possible influence of nuclear genetic background on the mtDNA mutation frequency in comparisons between cohorts. We isolated mtDNA separately from the heads and thoraces of adult flies, which contain primarily nervous tissue and muscle tissue, respectively so that the somatic mtDNA mutation frequency could be compared in these tissues. The abdomen was

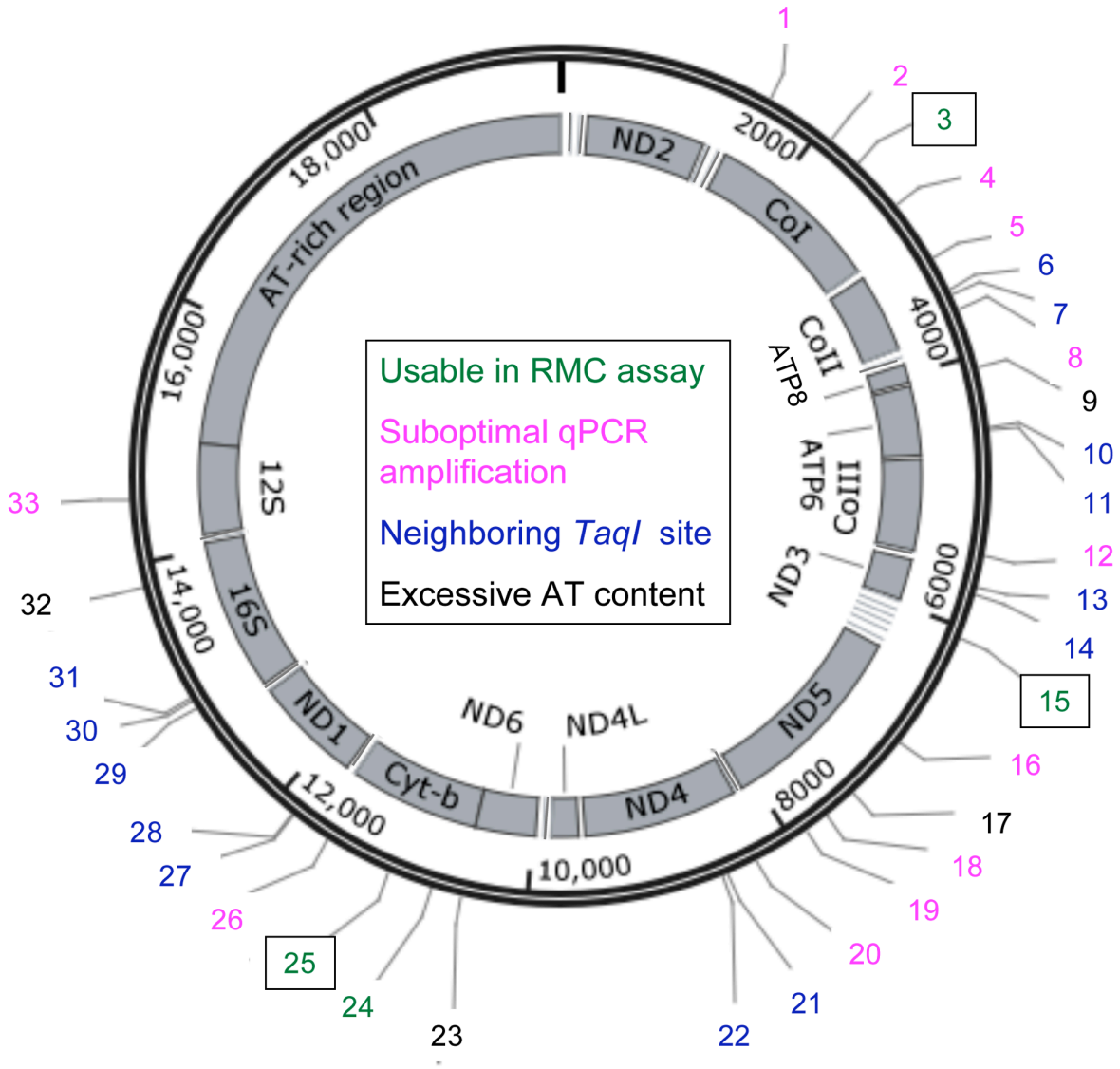

Figure 3.1. The locations of *TaqI* sites in *Drosophila* mtDNA.
Schematic depiction of the *Drosophila melanogaster* mitochondrial genome. Numbers (1-33) indicate the different *TaqI* sites, color coded according to their utility for RMC analysis as indicated. Boxed numbers indicate the *TaqI* sites used for RMC analysis in our work. tRNA genes are represented by horizontal lines adjacent to other mitochondrial genes.

excluded from analysis because mtDNA replication in the female germline might confound our analysis of the somatic mtDNA mutation frequency.

RMC analysis of mtDNA isolated from the heads and thoraces of 1- to 3-day-old flies (hereafter termed "young" animals; Figure S2B, Table S2, Table S3) revealed a

similar mtDNA mutation frequency between the three *TaqI* sites within the same tissue for either young heads or thoraces (Figure S2). Therefore, we pooled the data from the three *TaqI* sites to achieve greater statistical power, and detected a small but significant increase in the mtDNA mutation frequency in young thoraces relative to heads (Figure 3.2A). The mtDNA mutation frequency in heads and thoraces (~10^{-5}) was similar to the mtDNA mutation frequency reported in vertebrates[46,151], and variation in the mtDNA mutation frequency between tissues has also been reported in vertebrates[46,151].

We next asked whether the frequency of somatic mtDNA mutations increases with age in *Drosophila*. Prior to measuring the mtDNA mutation frequency in older flies, we performed a lifespan analysis on the w^{1118} strain to identify a suitable age range for RMC experiments (Figure S2A). We used flies aged between 40 and 66 days (hereafter termed "old" animals) for our studies. As in young tissues, the mutation frequency was similar between *TaqI* sites within the same tissue for either old heads or thoraces (Figure S2C, S2D, Table S2, Table S3**)**. Using pooled data from *TaqI* sites, RMC analysis revealed a significant increase in mtDNA mutation frequency with age in both heads and thoraces (Figure 3.2B, C). As in young animals, the mtDNA mutation frequency was higher in thoraces than in heads from old animals (Figure 3.2D). In contrast to previous work in mice showing an exponential increase in the frequency of mtDNA mutations with age[46], our data fit best to a model of linear increase in the mutation frequency with age (Figure S3). However, this discrepancy might simply reflect the dramatic increase in mtDNA mutation frequency that occurs in mice near the end of life when only 10% of the population is still alive[46]. In our study, the oldest flies examined were at an age in which 25% of the population was still alive.

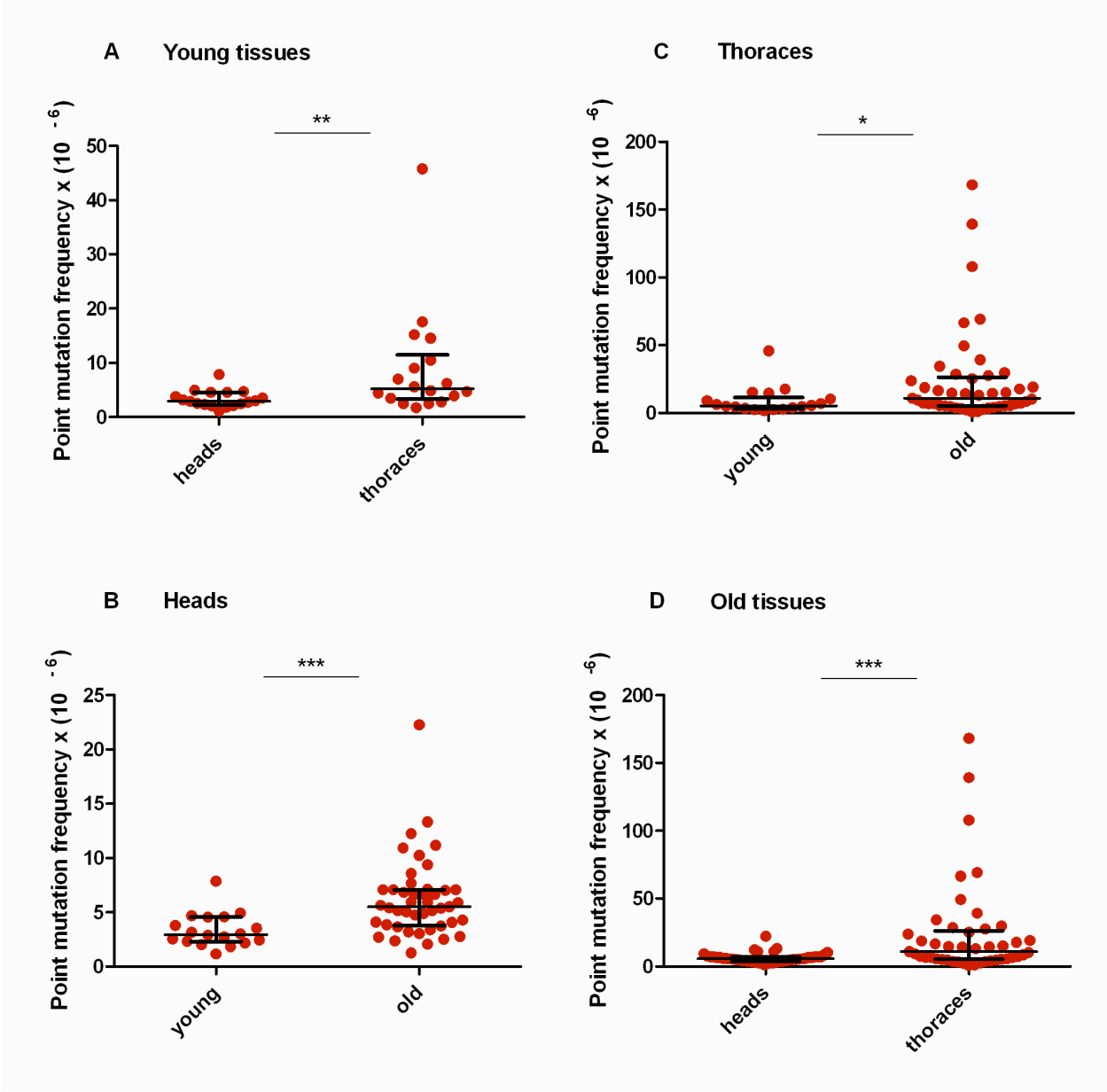

Figure 3.2. Mitochondrial DNA mutation frequency increases with age and is greater in thoraces than in heads.
(A) The mtDNA mutation frequency is greater in young thoraces than in young heads (**$p < 0.01$). **(B)** The mtDNA mutation frequency is greater in old heads than in young heads (***$p < 0.001$) **(C)** and is greater in old thoraces than in young thoraces (*$p < 0.05$). **(D)** The mtDNA mutation frequency is greater in old thoraces than in old heads (**$p < 0.001$). Horizontal bars represent the median mutation frequency, and error bars indicate the interquartile range. Significance was tested using Mann-Whitney unpaired U tests.

Upon closer inspection of our data, it appeared that much of the age-dependent increase in the mtDNA mutation frequency was caused by outlier samples with high

mtDNA mutation frequencies (Figure 3.2). Because mtDNA mutations expand clonally in humans, we hypothesized that these outlier samples represent rare events in which a mutation within the *TaqI* site occurred early in development, and then clonally expanded in just one of the 100 flies in the sample. Assuming that a single fly fully accounts for the mtDNA mutation frequency in the outlier sample with the highest mtDNA mutation frequency, we estimate that the frequency of the clonally expanded mutation within that fly would approach 0.2%. A prediction of the hypothesis that outlier samples with high mtDNA mutation frequencies are a consequence of a single fly with an abundant clonally expanded mutation is that these samples should have a single predominating mutation type. By contrast, samples with an mtDNA mutation frequency nearer to the mean (non-outliers) would be more likely to contain a mixture of different mutation types that are contributed by multiple individuals in the population.

To test the hypothesis that outlier samples with high mtDNA mutation frequencies represent clonal expansion events, we compared the distribution of mutations in outlier and non-outlier samples by cloning and sequencing *TaqI* resistant DNA from these samples (Figure S4). We defined outlier samples as those that lie outside the 95% confidence interval of the mean for a given group. Our analysis revealed a trend towards an increased frequency of the predominating mutation in outlier samples, with the frequency greatest in the head and thorax samples with the highest mutation frequencies. However, this difference did not reach statistical significance ($p = 0.09$, Student's t-test). Thus, our data suggests that clonal expansion may be the explanation for the high mutation frequency in outlier samples; however, it does not allow us to rule out other explanations for outlier samples, including simple chance deviations from the mean.

3.3.4 Oxidative stress is only a minor contributor to somatic mtDNA mutations

Mitochondria are major producers of superoxide anion[152], which can damage DNA[73] and is implicated in the age-dependent accumulation of somatic mtDNA mutations[76,153,154]. To test whether superoxide and other ROS are a major cause of somatic mtDNA mutations in *Drosophila*, we performed several experiments. First, we analyzed the mtDNA mutation spectrum using data obtained from cloning and sequencing RMC processed samples. Superoxide anion reacts with deoxyguanosine to produce 8-hydroxy-2'-deoxyguanosine (8-oxo-dG)[155], which results in G:C to T:A transversions following DNA replication[73]. Thus, if oxidative stress is a major cause of somatic mtDNA mutations, there should be a preponderance of G:C to T:A transversion mutations in our samples. However, G:C to T:A transversions represented less than 10% of the mutations detected, regardless of the age of animals (Figure 3.3). Moreover, the frequency of G:C to T:A transversions did not increase appreciably with age (5% in young flies and 8% in old flies), and thus are not a major contributor to the increase in mtDNA mutation frequency with age. The most common mutation type detected in our samples was G:C to A:T transitions (80% of mutations in young flies and 86% in old flies). Further analysis revealed that the G:C to A:T transition mutations exhibited a strand bias, whereby G to A transitions occur more frequently on the major strand (the coding strand for the majority of mitochondrial genes) in both young and old tissues (Figure S5). Because strand asymmetric mutation accumulation has been postulated to reflect different mutation susceptibilities of the leading and lagging strands during DNA

replication[156], our findings suggest that somatic mtDNA mutations occur primarily during mtDNA replication in *Drosophila*.

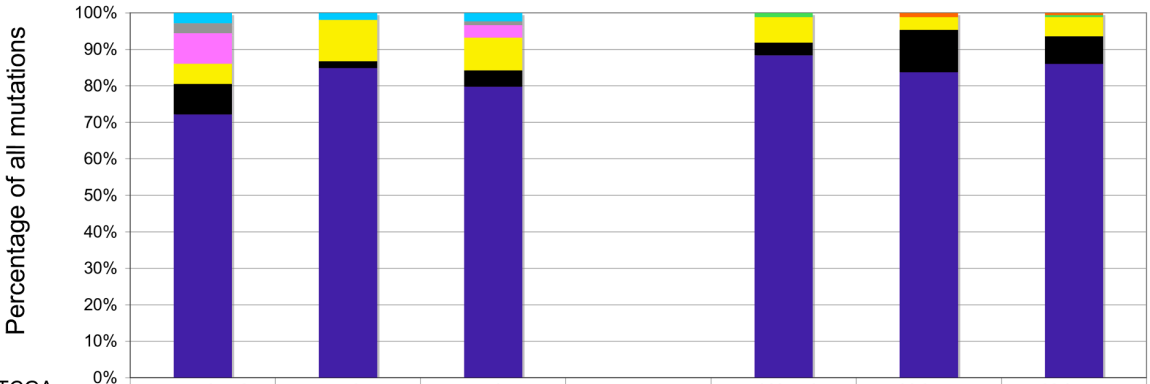

TaqI - TCGA	young head	young thorax	young tissues		old head	old thorax	old tissues
deletion	0% (0)	0% (0)	0% (0)		0% (0)	1% (1)	0.5% (1)
G:C to T:A; T:A to C:G *	0% (0)	0% (0)	0% (0)		1% (1)	0% (0)	0.5% (1)
G:C to C:G; T:A to C:G *	3% (1)	2% (1)	2% (2)		0% (0)	0% (0)	0% (0)
T:A to G:C	3% (1)	0% (0)	1% (1)		0% (0)	0% (0)	0% (0)
T:A to A:T	8% (3)	0% (0)	3% (3)		0% (0)	0% (0)	0% (0)
G:C to C:G	6% (2)	11% (6)	9% (8)		7% (6)	3% (3)	5% (9)
G:C to T:A	8% (3)	2% (1)	5% (4)		4% (3)	12% (10)	8% (13)
G:C to A:T	72% (26)	85% (45)	80% (71)		88% (76)	84% (72)	86% (148)

Figure 3.3. GC:TA transversions account for only a small percentage of mtDNA mutations. The percentage and total number (in parentheses) of each type of mutation identified at *TaqI* sites in young and old animals. Results depict data obtained separately from heads and thoraces and also combined. The wild-type *TaqI* sequence (TCGA) is shown for reference. * = Two mutations identified within a single cloned *TaqI* site.

Biochemical studies indicate that 8-oxo-dG lesions block DNA replication, which may result in mtDNA depletion[157]. Depletion of mtDNA caused by 8-oxo-dG lesions could, therefore, possibly explain the finding that G:C to T:A transversion mutations did not increase appreciably with age. To address this hypothesis, we analyzed mtDNA copy number in fly heads using qPCR. We found no difference in mtDNA copy number relative to nuclear DNA between young and old flies (Figure S6). Therefore, mtDNA depletion does not account for the relative lack of an age-related increase in G:C to T:A mutation frequency.

To further explore the influence of oxidative stress on somatic mtDNA mutations in *Drosophila*, we tested whether flies deficient in the oxidative stress response pathway accumulate somatic mtDNA mutations at a higher rate. Superoxide anion is primarily detoxified in mitochondria by manganese superoxide dismutase 2 (Sod2). While null alleles of the *Drosophila Sod2* gene exist, *Sod2* null homozygotes survive for only a few hours as adults[158]. To circumvent this limitation, we generated transheterozygous flies that bear the $Sod2^{n283}$ null mutation in combination with a hypomorphic mutation of the *Sod2* gene ($Sod2^{wk}$). Studies of $Sod2^{n283}/Sod2^{wk}$ transheterozygotes (hereafter referred to as *Sod2* mutants) have shown that these mutants exhibit increased oxidative stress, but are viable for nearly 50 days as adults[159].

Before conducting RMC analysis on *Sod2* mutants, we verified that they would be suitable for our studies by performing a lifespan analysis (Figure 3.4A). We found that the median lifespan of *Sod2* mutants was 41 days and that both the median and the maximum lifespan of *Sod2* mutants were shortened by ~30% relative to our isogenic w^{1118} strain. We measured the somatic mtDNA mutation frequency in 40- to 42-day-old *Sod2* mutants. Because our data indicate that the somatic mtDNA mutation pattern is similar in heads and thoraces and the *Sod2* gene is ubiquitously expressed[160], we examined the mutation frequency in *Sod2* mutants using only heads. Surprisingly, we detected no increase in the mtDNA mutation frequency at any of the individual *TaqI* sites analyzed in 40- to 42-day-old *Sod2* mutants relative to age-matched control animals (Figure S7). Pooled data from all three *TaqI* sites also failed to reveal a difference in the

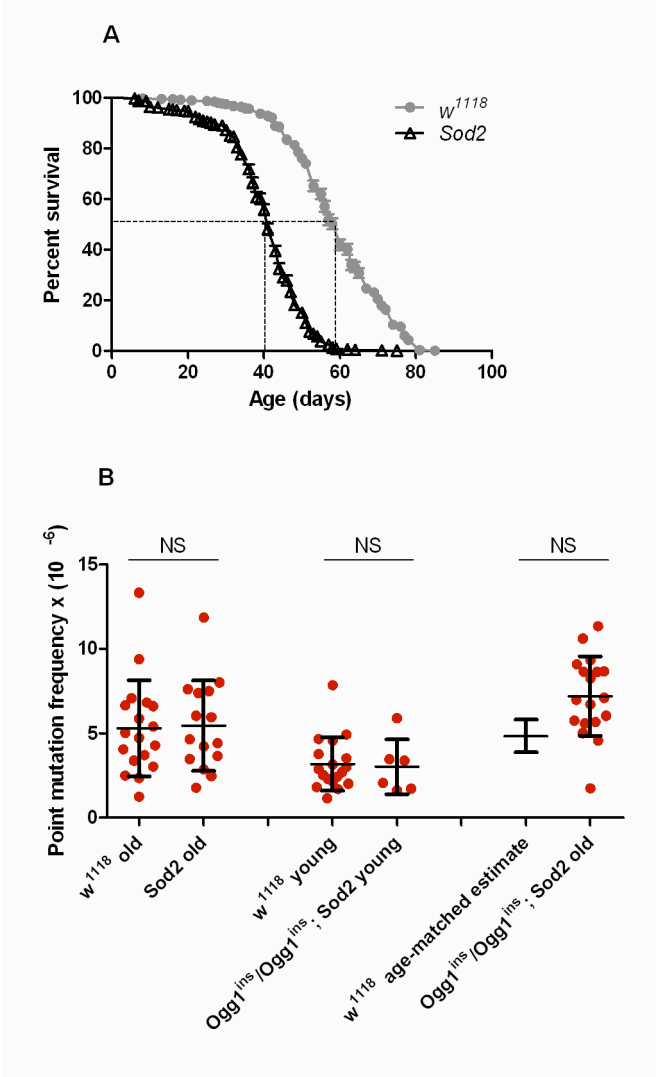

Figure 3.4. Oxidative stress response pathway mutants do not have an increased mtDNA mutation frequency.
(A) Lifespan of w^{1118} and *Sod2* mutant flies. The median lifespan (indicated by dashed lines) was 60 days for w^{1118} flies and 41 days for *Sod2* mutants. **(B)** The mutation frequency using pooled data from all three *TaqI* sites in old *Sod2* mutants (39- to 41-day-old), young $Ogg1^{ins}/Ogg1^{ins}$; *Sod2* double mutants (1- to 3-day-old), old $Ogg1^{ins}/Ogg1^{ins}$; *Sod2* double mutants (26- to 28- day-old), and age-matched w^{1118} controls. The 26- to 28- day-old control estimate was obtained from linear regression of the age-dependent w^{1118} mutation frequency. Horizontal bars represent the median mutation frequency, and error bars indicate the interquartile range. There was no significant difference in mutation frequency between mutants and age-matched controls (Mann-Whitney unpaired U tests).

mutation frequency between *Sod2* mutants and controls (Figure 3.4B, Table S2, Table S3). These findings provide further support for the conclusion that oxidative stress does not contribute significantly to the somatic mtDNA mutation frequency.

A caveat of our findings with *Sod2* mutants is that efficient repair of oxidatively damaged bases might account for the lack of effect of Sod2 deficiency on the mtDNA mutation frequency. Previous work indicates that the 8-oxo-dG lesions formed by superoxide anion attack on mtDNA are primarily removed by a mitochondrially localized 8-oxoguanine glycosylase[155,161]. Studies in *Drosophila* indicate that there are two genes, *dOgg1* (referred to as *Ogg1*) and *Ribosomal protein S3* (*RpS3*) that encode 8-oxoguanine glycosylase activity[162]. However, only the Ogg1 protein sequence bears significant homology to the human Ogg1 protein, and only Ogg1 appears to contain an N-terminal mitochondrial targeting sequence (Figure 3.5A). These findings suggest that Ogg1 is primarily responsible for the repair of mitochondrial 8-oxo-dG lesions in *Drosophila*.

To test the hypothesis that efficient repair of 8-oxo-dG lesions explains the lack of increased mutation frequency in *Sod2* mutants, we inactivated Ogg1 in an *Sod2* mutant background. A search of FlyBase revealed an *Ogg1* allele ($Ogg1^{f08013}$; hereafter referred to as $Ogg1^{ins}$) caused by a *piggyBac* transposable element insertion located 78 bp upstream of the translation start site in the *Ogg1* gene, as well as a large deletion (*Df(1)BSC627*) that removes the Ogg1 gene[163] (Figure 3.5B). We prepared protein lysates from $Ogg1^{ins}$ heterozygotes ($Ogg1^{ins}$/+), $Ogg1^{ins}$ homozygotes ($Ogg1^{ins}/Ogg1^{ins}$), and $Ogg1^{ins}$ hemizygotes ($Ogg1^{ins}$/*Df(1)BSC627*) and used them to assay 8-oxo-dG DNA repair activity. We found that $Ogg1^{ins}$ homozygotes and hemizygotes had reduced DNA repair activity relative to the heterozygous control (Figure 3.5C). The magnitude of this defect was greater in extracts from $Ogg1^{ins}$ hemizygotes relative to $Ogg1^{ins}$ homozygotes, indicating that the $Ogg1^{ins}$ mutation represents a hypomorphic loss-of-function allele of the *Ogg1* gene.

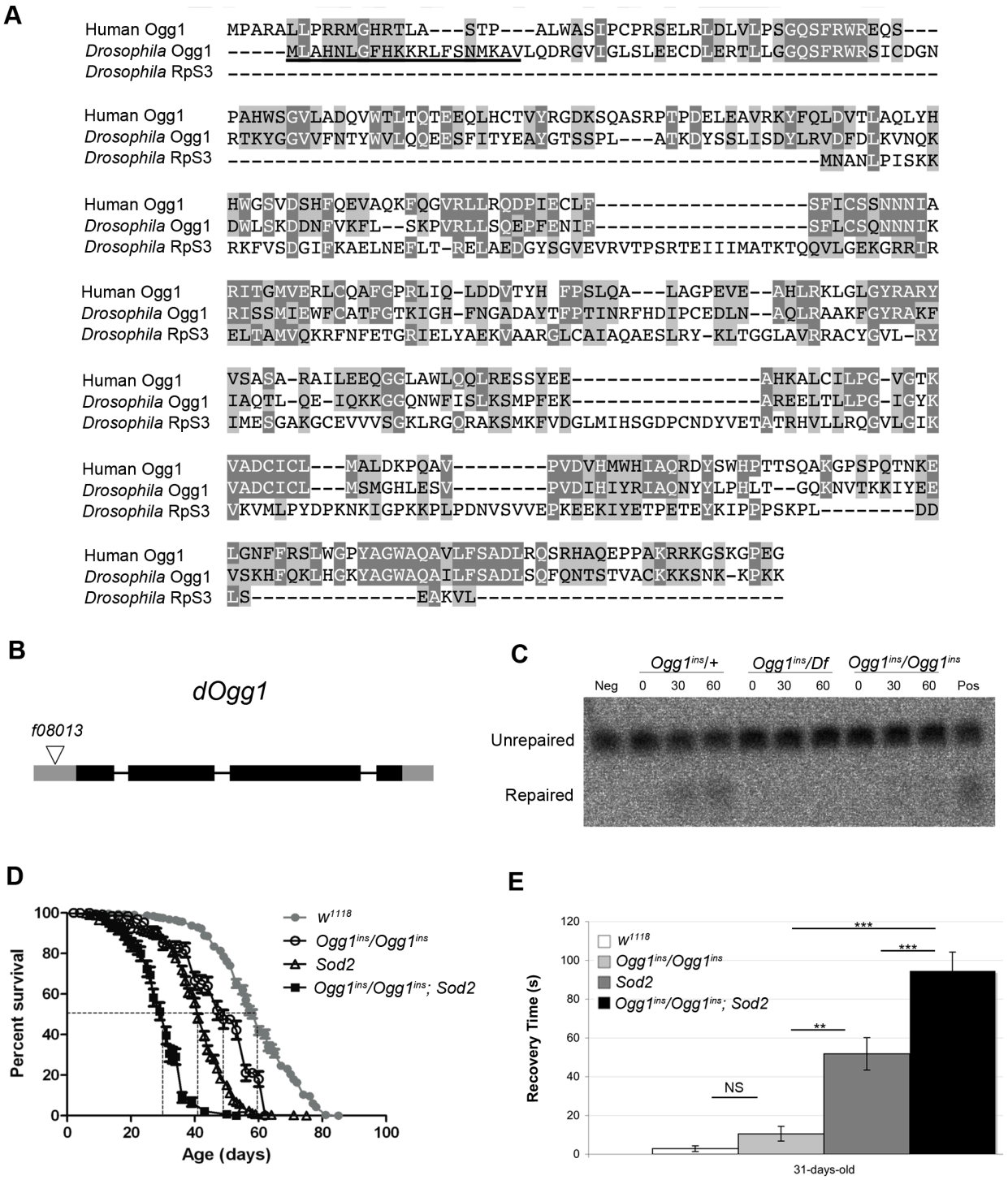

Figure 3.5. An *Ogg1* mutation diminishes Ogg1 activity and interacts genetically with *Sod2*.
(A) Amino acid sequence alignment of human Ogg1 with *Drosophila* Ogg1 and RpS3. Dark shading denotes amino acid identities; light shading denotes amino acid similarities. The putative N-terminal mitochondrial targeting sequence of *Drosophila* Ogg1 is underlined. **(B)** The *Ogg1* gene comprises four exons, designated by rectangles, and the coding sequence is indicated with dark gray shading. The $Ogg1^{f08013}$ *piggyBac* insertion (designated by a triangle) is located 78 base pairs upstream of the *Ogg1*

translation start site. **(C)** 8-oxo-dG repair activity was assayed by monitoring cleavage of a ^{32}P-labeled synthetic probe containing 8-oxo-dG, using protein extracts from flies of the indicated genotypes (Df = the *Df(1)BSC627* deletion that removes *Ogg1*; ins = the *Ogg1^{f08013} piggyBac* insertion). Results of the assay are shown following 0, 30, and 60 minutes of incubation. Neg = No protein; Pos = Mouse brain protein extract. **(D)** Lifespan of *w^{1118}*, *Ogg1^{ins}/Ogg1^{ins}*, *Sod2*, and *Ogg1^{ins}/Ogg1^{ins}*; *Sod2* double mutant flies**.** The median lifespan (indicated by dashed lines) was 60 days for *w^{1118}*, 49 days for *Ogg1^{ins}* mutants, 41 days for *Sod2* mutants, and 31 days for *Ogg1^{ins}*; *Sod2* double mutants. All lifespan curves are statistically different from one another using log rank tests ($p < 0.001$). **(E)** *w^{1118}*, *Ogg1^{ins}/Ogg1^{ins}*, *Sod2*, and *Ogg1^{ins}/Ogg1^{ins}*; *Sod2* double mutant flies were subjected to a mechanical stress sensitivity test at 31 days. Values represent mean time (seconds) of recovery from mechanical stress, and error bars represent standard error of the mean. Significance was determined using one-way ANOVA followed by Tukey's post hoc tests (**p < 0.01; ***p < 0.001).

To test whether *Ogg1* activity masks a somatic mtDNA mutator phenotype of *Sod2* mutants, we constructed and analyzed *Ogg1^{ins}/Ogg1^{ins}; Sod2* double mutants. Behavioral studies of the double mutants revealed that the *Ogg1^{ins}* mutation reduced lifespan and enhanced stress-induced seizure (bang-sensitive) phenotypes of *Sod2* mutants (Figure 3.5D, E), suggesting that these genes act in a common pathway. To test whether these genetic interactions reflect an increased mtDNA mutation frequency in the double mutants, we measured the mtDNA mutation frequency in the heads of young (1- to 3-day-old) and old (26- to 28-day-old) *Ogg1^{ins}/Ogg1^{ins}; Sod2* double mutants. We used 26- to 28-day-old animals as our "old" sample, because this is near the median lifespan of the double mutants (Figure 3.5D). The mtDNA mutation frequency at the corresponding age in *w^{1118}* controls was obtained using linear regression (Figure S3A). To increase our ability to detect small differences, we pooled data from all three *TaqI* sites analyzed. Despite this measure, we were unable to detect a difference in somatic mtDNA mutation frequency between young double mutants and age-matched controls (Figure 3.4B). While there was a trend towards an increase in somatic mtDNA mutations in old double mutants, this difference did not reach significance ($p = 0.08$). Together, our findings

indicate that oxidative stress is not a major contributor to the somatic mtDNA mutation frequency in *Drosophila.*

3.4 Discussion

The accumulation of somatic mtDNA mutations is thought to contribute to aging and common age-related diseases, including cancer and Parkinson's disease. The causes of somatic mtDNA mutations are poorly understood, as are the factors that influence their cellular frequency following their occurrence. Given the powerful genetic tools available in *Drosophila* for studying fundamental biological processes, we explored the utility of this model system to investigate the mechanisms that influence the frequency of somatic mtDNA mutations. We show that features associated with mtDNA mutations in vertebrates are conserved in *Drosophila*, including the somatic mtDNA mutation frequency, an increased frequency of somatic mtDNA mutations with age, a prevalence of G:C to A:T transition mutations, and possibly, clonal expansion of somatic mtDNA mutations. These findings indicate that *Drosophila* will serve as a valuable model system in which to examine the mechanisms influencing somatic mtDNA mutation frequency.

Although oxidative stress is commonly cited as a major contributor to somatic mtDNA mutations[154], our work does not support this idea. The fraction of G:C to T:A transversion mutations, a consequence of 8-oxo-dG lesions, is small in young flies and does not increase appreciably with age. These findings parallel recent results in mice and humans showing a similarly low occurrence of G:C to T:A transversion mutations in samples from both young and old individuals[46,49,81]. Furthermore, we found that mutations in genes that oppose superoxide-induced DNA damage do not detectably

influence the mtDNA point mutation frequency. However, because the total number of somatic mtDNA mutations increases with age but the percentage of G:C to T:A transversions remained nearly constant, our data do leave open the possibility that oxidative stress is a minor contributor to the increased burden of somatic mtDNA mutations with age. Moreover, while our studies indicate that superoxide is not a major cause of mtDNA point mutations, further work will be required to determine whether superoxide contributes to the frequency of mtDNA deletions, and to assess the influence of other forms of ROS, such as hydroxyl radicals, on mtDNA mutation frequency.

How can we reconcile our current findings with the body of work supporting a role of ROS in mtDNA mutations? Such work includes direct sequencing of mtDNA[164,165], and a study showing that catalase expression in mouse mitochondria reduced the frequency of mtDNA mutations[78]. One possible explanation for at least some of the conflicts involving sequencing is that PCR amplification of DNA that contains 8-oxo-dG lesions results in G:C to T:A transversion mutations during the amplification process. Sequencing of material containing amplification-induced mutations could thus result in an overestimation of the true G:C to T:A transversion frequency. Further compounding this potential problem is the finding that oxidative modification of mtDNA can occur during mtDNA isolation[166]. By contrast, the RMC assay is immune to this type of artifact because *TaqI* is capable of digesting oxidized DNA, and thereby removes oxidized molecules prior to mutation detection by qPCR[46,147]. Given that the study involving catalase ovexpression also used RMC to monitor mtDNA mutation frequency, we cannot presently offer an explanation for this conflict. However, it is important to emphasize that the findings from studies of catalase overexpression do not necessarily

represent a direct conflict with our current conclusion because our findings leave open the possibility that ROS makes a small contribution to the mtDNA mutation frequency. Nevertheless, further studies will be required to explain the sizeable magnitude of the effect of catalase overexpression on the mtDNA mutation frequency, given the small contribution of ROS to mtDNA mutations suggested by our work.

If oxidative stress accounts for only a small fraction of the somatic mtDNA mutation burden, what then is the major source of these mutations? Previous work has shown that expression of a proofreading-deficient form of mtDNA polymerase (Pol-γ) causes primarily G:C to A:T transition mutations[167]. This finding raises the possibility that Pol-γ misincorporation errors are responsible for the G:C to A:T mutations that account for the majority of the somatic mtDNA mutations detected in our work. However, while Pol-γ replication errors may account for some of the G:C to A:T transition mutations that occur in somatic tissues, this model is difficult to reconcile with the finding that most of these mutations accumulate in a strand asymmetric fashion. Instead, we propose that most of the G:C to A:T transition mutations that occur in somatic tissues arise because of differing sensitivities of the leading and lagging strands to mutagenesis during mtDNA replication. In *Drosophila*, the mtDNA minor strand is replicated in a continuous fashion (the leading strand) and the major strand is replicated in a discontinuous fashion (the lagging strand)[168–170]. During leading strand synthesis, the template for the lagging strand (the minor strand) is transiently single-stranded, and thus more susceptible to DNA damage than the template for the leading strand (the major strand). One type of DNA damage that is compatible with our findings is spontaneous deamination of cytosine[80,171,172], the rate of which increases several orders of magnitude

in single-stranded DNA[156]. Selective cytosine deamination on the minor strand during leading strand synthesis would offer an explanation for the preponderance of C to T mutations that we detect on the minor strand (equivalent to G to A mutations on the major strand). While transcription can also lead to asymmetric accumulation of mutations on the non-transcribed strand[173–175], the pattern of mutational accumulation observed in our work is inconsistent with a transcriptional origin because most of the C to T mutations occur on the transcribed strand. The strand asymmetric mutational bias detected in our study is consistent with previous findings in aging human brain[49] and in the *Drosophila* germline[176], suggesting that spontaneous cytosine deamination on the lagging strand template during replication is a conserved mechanism of mtDNA mutation accumulation.

Another important question that is raised by our findings is why *Ogg1* mutations enhance *Sod2* mutant phenotypes if the double mutants do not have a significantly higher mtDNA mutation frequency than control flies. While we believe that ROS-mediated damage to proteins and/or lipids[158,159] is the primary explanation for the shortened lifespan and bang sensitivity of *Sod2* mutants, the genetic interaction between the *Sod2* and *Ogg1* mutations cannot readily be explained by an increase in protein or lipid damage in the double mutants because there is no evidence that Ogg1 is involved in the repair of damaged proteins or lipids. However, recent studies show that several other factors involved in base excision repair also function in apoptosis and transcriptional regulation[177,178]. Thus, one possibility is that Ogg1 has a function other than DNA repair, and that the loss of this function is responsible for the genetic interaction with Sod2. Alternatively, Ogg1 may also play a role in nuclear DNA repair, and the genetic

interaction between *Ogg1* and *Sod2* may reflect inefficient repair of oxidatively damaged nuclear DNA. Finally, the genetic interaction between *Ogg1* and *Sod2* may reflect an increase in the somatic mtDNA mutation frequency that was below the detection limit of our assay. Although we did not observe a statistically significant increase in the mtDNA mutation frequency in the *Ogg1; Sod2* double mutants, there was a clear trend in this direction. Future studies will be required to distinguish between these possibilities.

In conclusion, our study sheds additional light on the genesis of mtDNA mutations, and also indicates that *Drosophila* is a tractable genetic model system with which to study the mechanisms that influence the frequency of mtDNA mutations. Little is known of the cellular factors that influence heteroplasmy, clonal expansion, and the inheritance of mtDNA mutations. The use of *Drosophila* should facilitate rapid advancement in our understanding of mtDNA mutations and their roles in aging and disease.

3.5 Materials and Methods

Fly strains and maintenance: Flies were maintained on standard cornmeal-molasses food (70% cornmeal, 10.5% molasses, 2.5% yeast, and 1% agar) at 25°C. The w^{1118} isogenic fly strain, *Ogg1 PiggyBac* element insertion ($Ogg1^{f08013}$) strain, and *Ogg1* deletion (Df(1)BSC627) strain were obtained from the Bloomington *Drosophila* Stock Center. The $Sod2^{n283}$ and $Sod2^{wk}$ mutants have been described previously[158,159].

Behavioral analysis: Lifespan analysis: One- to two-day-old flies were placed in vials in groups of up to 20 flies. Every 2-3 days flies were transferred to fresh vials and the

number of deaths was recorded. Each lifespan trial was repeated at least three times, with a minimum of 100 flies per genotype analyzed. Survivorship was plotted as a function of time (in days) using GraphPad Prism software version 5.04 (GraphPad Software, Inc., La Jolla, CA). Survival curves were compared between genotypes using the log-rank test to determine significance.

Bang sensitivity analysis: Flies were tested for sensitivity to mechanical stress using a modified version of a published procedure[123]. Briefly, one- to two-day-old flies were placed into vials in groups of 2 and aged to 31 days. Fly vials were inverted and vortexed on the maximum setting for ten seconds, and the time required for flies to recover from paralysis and/or seizures was recorded. A minimum of 20 flies was tested per genotype.

5-bromo-2'-deoxyuridine (BrdU) labeling and analysis: One-day-old flies were collected, starved for 24 hours, and then transferred to vials lined with Whatman filter paper (GE Healthcare, Pittsburg, PA). Flies were fed BrdU by adding a solution of 1 mg/mL BrdU (Sigma-Aldrich, St. Louis, MO) in 5% sucrose and 5% yeast directly to the filter paper. Fresh BrdU containing solution was added to the filter paper twice a day for three days. Following BrdU labeling, tissues were collected for Southwestern blot analysis or confocal microscopy.

Southwestern analysis: Flies were flash frozen in liquid nitrogen and vortexed for 10 to 15 seconds to dissociate body parts. One hundred fly heads were collected and homogenized in 300 μL buffer (10 mM Tris-HCl pH 8.0, 150 mM NaCl, 20 mM EDTA,

1% SDS) in a 1.5-mL Eppendorf tube using a plastic pestle. RNase A (Applied Biosystems, Foster City, CA) was added to a final concentration of 10 μg/mL and incubated at 37°C for 30 minutes. Following RNase A treatment, proteinase K (Qiagen, Valencia, CA) was added to a final concentration of 200 μg/mL and incubated either overnight at 37°C or for three hours at 56°C. An equal volume of cold phenol/chloroform/isoamyl alcohol (25:24:1; Fisher, Pittsburgh, PA) was then added, and the samples were inverted ten times, mixed, and centrifuged at 15,800 x *g* for 10 minutes. The aqueous phase containing the DNA was collected and the phenol/chloroform/isoamyl alcohol extraction was repeated once, followed by a single extraction with chloroform. The DNA was then precipitated with 3M sodium acetate pH 5.2 and isopropanol and centrifuged at 15,800 x *g* for 25 minutes at 4°C. The DNA pellet was resuspended in 10 mM Tris-HCl and 0.1 mM EDTA (pH 8.0), and 3 μg of DNA was immediately digested with BglII (New England Biolabs, Beverly, MA) for at least 16 hours at 37°C. The digested DNA was then subjected to Southern blot analysis using nylon membranes (Millipore Corp, Billerica, MA). DNA crosslinking to membranes was performed using a UV Stratalinker 1800 on the auto crosslink setting (Agilent Technologies, Santa Clara, CA). The membrane was blocked for 1 hour in 5% milk in PBS at 25°C, then incubated with antiserum to BrdU (Abcam #92837, Cambridge, MA) at a 1:1000 dilution overnight. Membranes were then washed in 0.1% Tween in PBS, followed by incubation with HRP-conjugated anti-chicken secondary antibody (Sigma-Aldrich #A9046, St. Louis, MO) at a 1:80,000 dilution. Western Blotting Substrate (Fisher, Pittsburgh, PA) was used to detect peroxidase signal.

Immunohistochemistry and confocal microscopy: BrdU-labeled tissues were prepared for confocal microscopy by dissecting the thoracic ganglion in cold PBS using a dissecting microscope. The thoracic ganglion was stained with 25 nM MitoTracker Deep Red for 25 minutes (Invitrogen, Carlsbad, CA), rinsed with 0.1% Triton X-100 in PBS (wash buffer), and fixed for 30 minutes in 4% paraformaldehyde (Ted Pella Inc., Redding, CA) in PBS at 4°C. After rinsing in wash buffer, the thoracic ganglion was incubated in 1 M HCl for 30 minutes at 25°C, then blocked in 0.1% Triton X-100 with 10% heat-inactivated FBS in PBS (blocking buffer) for 1 hour at 25°C. Primary antibody to BrdU (Abcam #Ab6326, Cambridge, MA) was then added at 1:100 dilution and incubated overnight at 4°C. After washing with wash buffer, Alexa Fluor 488 goat anti-rat IgG (Molecular Probes #A11006, Eugene, OR) was added to blocking buffer at 1:10,000 dilution and incubated for 2 hours at 25°C. Stained thoracic ganglia were washed with wash buffer, mounted in Fluoromount (Sigma-Aldrich, St. Louis, MO), and imaged using an Olympus FV-1000 with a 100x lens and 2-4x digital zoom.

Random Mutation Capture Assay:

qPCR primer design and validation: TaqI test primers were designed to flank *TaqI* sites and amplify products sized between 95 and 250 bp using NCBI's Primer-BLAST program (Primer3)[179] (Primer-Blast, National Center for Biotechnology Information, National Library of Medicine, Bethesda, MD). The Primer-BLAST algorithm was also used to optimize primer specificity by testing for mis-priming to related nuclear and mitochondrial sequences. There are four known *Drosophila* mitochondrial pseudogenes that reside in the nuclear DNA[180], and these sequences were excluded from primer design

to ensure that our primers were specific for mitochondrial sequences. Control primers were designed in the same manner as test primers but do not flank a *TaqI* site. Because the *Drosophila* mtDNA has a high A:T content, control primers were sought at mtDNA sequences with a relatively high G:C content.

We validated the efficiency of control and test primer pairs by measuring the cycle threshold (Ct; the cycle number at which the signal rises above background) using a four-fold dilution series of undigested mtDNA, and plotting Ct vs. dilution (Table S1). Theory predicts that product abundance doubles at each cycle of PCR amplification, so the slope of Ct vs. dilution should be 2. Primer pairs that deviated by 15% or more from a slope value of 2 were discarded. Only test and control primers that yielded slope values within 5% of one another were used in our analyses (Table S1). Finally, we sequenced the PCR product produced by each primer pair that passed our quality control thresholds to ensure that only the correct target was amplified.

DNA isolation: One- to three-day-old flies were collected and transferred to fresh food every 2-3 days until they reached the ages chosen for RMC analysis. Flies were then flash frozen in liquid nitrogen in groups of 100 and vortexed for 10 to 15 seconds to dissociate body parts. Heads were collected, and the thorax was sectioned from the abdomen using a razor blade. Groups of 100 heads or thoraces were then processed to isolate DNA as described above (Southwestern analysis). The DNA pellet was resuspended in 10 mM Tris-HCl and 0.1 mM EDTA (pH 8.0), and was then used for *TaqI* digestion or frozen at -80°C until use.

TaqI digestion: The methods for the RMC assay are described in detail in reference[110]. Briefly, each sample of ~10 μg of DNA was treated with 100 U of *TaqI* restriction enzyme (New England Biolabs, Beverly, MA) and incubated at 65°C. An additional 100 U were added every hour for a total of 10 hours to promote complete DNA digestion.

qPCR experiments: qPCR experiments were carried out on an MJ Research DNA Engine Opticon 2 System (Hercules, CA) using Power SYBR Green PCR Master Mix (Agilent, Wilmington, DE). The PCR cycle consisted of an initial denaturing step at 95°C for 10 minutes, followed by 45 cycles of denaturing at 95°C for 30 seconds, annealing at 60°C for 1 min, and extension at 72°C for 15 sec. After the 45 cycles of PCR, a final extension step was performed at 72°C for 1 min. Melting curves were performed on all PCR products and analyzed using the Bio-Rad Opticon Monitor II software to ensure that primers amplified a single product.

Mutation quantification: To quantify the mutation frequency, we first used the Bio-Rad Opticon Monitor II software to determine the Ct values of the control primers ($Ct_{control}$), representing total mtDNA molecules, and the Ct values of the test primers (Ct_{test}), representing mutant mtDNA molecules. The ratio of mutant to WT mtDNA molecules was then calculated from the difference in Ct values using the following equation: Point mutation frequency = Mutant molecules/WT molecules = $1/2^{\Delta Ct} \times 4$, where $\Delta Ct = Ct_{control} - Ct_{test}$. This value is multiplied by a factor of 4 because mutations at any of the four bases in the *TaqI* restriction site would prevent digestion. Following qPCR amplifcation, the amplification products were either sequenced or digested with *TaqI* and subjected to densitometry to estimate the percentage of contaminating WT molecules that

remained. This percentage was then used to adjust the mtDNA mutation calculation to account for contaminating WT mtDNA.

Clonal expansion: To test for clonal expansion, we cloned DNA from eight individual samples, performed Sanger sequencing on at least 10 colonies per sample, and quantified the percentage of each type of mutation detected. Data was collected from the *TaqI* sites located in the *mt:Cyt-b* or *mt:CoI* genes. Additionally, we compared the total amount of mtDNA and total number of mtDNA copies in outlier and non-outliers samples. This analysis revealed that neither of these parameters differed between outliers and non-outliers (Table S4).

DNA copy number: Total DNA was isolated as described above (Random Mutation Capture Assay: DNA isolation) from the heads of young and old flies and used as template in qPCR. qPCR settings were as described above (Random Mutation Capture Assay: qPCR experiments). Relative copy number of mtDNA to nuclear DNA was determined using control mtDNA primers against *mt:CoIII* (see Table S1) and nuclear DNA primers against *β-Tubulin*[181].

Ogg1 repair of 8-oxo-dG: Ogg1 activity was assayed using fly head homogenates as previously described[182]. Briefly, the heads from 15-18 anesthetized flies, aged 1 to 3 days, were collected on ice using a razor blade and homogenized in 20 mM Tris-HCl (pH 8.0), 1 mM EDTA, 1 mM DTT, 0.5 mM spermine, 0.5 mM spermidine, protease inhibitor, and 50% glycerol. A 1:10 volume of 2.5 M KCl was added to this homogenate

and mixed at 4°C for 30 minutes. Samples were then centrifuged at 15,800 x *g* for 30 minutes and the supernatant was collected and frozen at -80°C until use in the 8-oxo-dG repair assay. Ogg1 activity was measured at 37°C using 30 μg of protein extract and a ^{32}P-labeled synthetic probe containing 8-oxo-dG for the indicated times. The reaction was stopped by placing the solution on ice and adding 20 μl of loading buffer containing 90% formamide, 10mM of NaOH, and Blue/Orange Loading Dye (Promega Corp., Madison, WI). The solution was then heated at 95°C for 3 min and placed on ice. The samples were loaded onto a polyacrylamide gel (20%) in 7 M urea and 1× TBE running buffer and run at 400 mV for 2 h. An FLA-3000 Series Fuji Film Fluorescent Image Analyzer was used to obtain images from the gel. All reagents used in this analysis were obtained from Sigma-Aldrich unless indicated otherwise (St. Louis, MO).

Sequence algorithms: Clustal Omega (Cambridge, UK) was used to align human Ogg1 and *Drosophila* Ogg1 and RpS3 sequences[183,184], and MitoPROT (Munich, Germany) was used to identify N-terminal mitochondrial targeting sequences in *Drosophila* Ogg1[185]. Snap Gene software was used to create the *Drosophila* mtDNA map with *TaqI* sites (GSL Biotech LLC, Chicago, IL)

Statistics: Significance was determined using Mann-Whitney unpaired U-tests to compare mtDNA mutation frequencies; log-rank test to compare survival curves for lifespan analyses; a one-way ANOVA followed by Tukey's post hoc test for bang-sensitive experiments; a two-tailed Student's t-test for mtDNA copy number comparison,

and Pearson's correlation coefficient for linear correlation of mtDNA mutation frequency with age.

3.6 Notes

Author contributions

LSI and LJP conceived and designed the experiments; LSI, SRK, EJF, SY, JJH, and MSC performed the experiments; LSI and LJP analyzed the data; SRK, EJF, and FCP contributed reagents/materials/analysis tools; LSI and LJP wrote the paper.

Acknowledgements

This research was supported by a National Institute of Neurological Disorders and Stroke fellowship (F31NS071857) to LSI, and by grants from the National Institute of General Medicine (1RO1GM086394; 1RO1GM104990), the Muscular Dystrophy Association (www.mda.org), and the Nathan Shock Center of Excellence in Basic Biology of Aging (AG013280) to LJP. Work carried out in the laboratory of Lawrence A. Loeb was supported by a National Cancer Institute grant (P01CA07785) to Raymond J. Monnat, and a National Institute on Aging grant (P01AG001751) to Peter Rabinovitch. Finally, support from a training grant from the National Institute on Aging (T32AG000057) was provided to LSI and SRK. The funders had no role in study design, data collection and analysis, decision to publish, or preparation of the manuscript.

4 Detection of Mitochondrial DNA Mutations Using Duplex Sequencing

4.1 Summary

Mitochondrial DNA mutations cause encephalomyopathies and are implicated in aging and age-related diseases. The molecular factors that influence mutation frequencies are not well understood. Therefore, the goal of the studies outlined in this chapter is to establish a high-throughput method to analyze mutation frequencies in flies to study factors that influence heteroplasmy. We utilized a newly developed next-generation sequencing approach with ultra-sensitive detection ability, Duplex Sequencing (DS). Applying this technique, we determined the mutation frequency in head tissue from young control flies to be ~2-8x10^{-6}, which is similar to values we obtained by the Random Mutation Capture Assay method. Our current and future plans include using DS to analyze mitochondrial quality control (mtQC) factors that may influence heteroplasmy in *Drosophila*.

4.2 Introduction

4.2.1 Using Drosophila as a model

We utilize *Drosophila* as a simple invertebrate model to test the effect of the mtQC machinery on mtDNA mutations for several reasons. The mtQC genes in vertebrates, which include *PINK1*, *parkin*, mitochondrial dynamics and autophagy genes have similarly functioning homologs in *Drosophila*. Also, flies lacking *PINK1* and *parkin* exhibit phenotypes resembling patients with Parkinson's disease, including a reduced life span and locomotor defects[128,186,187]; whereas, mouse models that lack *PINK1* or *parkin*

show very mild phenotypes. In addition *PINK1* and *parkin* fly mutants display degeneration of flight muscle, germ line, and dopamine neurons, and mitochondrial enlargement with disrupted cristae accompany defects in all of these tissues[128,186,187]. Subsequent studies in *Drosophila* led to the finding that *PINK1* and *parkin* promote mitochondrial fragmentation, leading to the hypothesis that *PINK1* and *parkin* promote mitophagy[103], which was later tested and proven in mammalian tissue culture[99]. Finally, *in vivo* studies in flies corroborated the *in vitro* mammalian tissue culture studies supporting the role of *PINK1* and *parkin* in mitophagy[188]. In sum several studies on *PINK1* and *parkin* support flies as an ideal model to study the influence of the mtQC on mtDNA mutations.

4.2.2 Methods to measure the frequency of mtDNA mutations

Sequencing methods are the most commonly used techniques to measure and detect mtDNA mutations. While classic Sanger sequencing is useful for some applications, it is limited in revealing sequence differences in heterogeneous populations because Sanger sequencing yields the average genotype of a collection of sequences[189]. Unlike Sanger sequencing, next-generation sequencing provides separate sequences of individual DNA fragments. However, it is limited in detecting variants present below 1% due to sequencing errors along with other errors generated during library preparation and image analysis[114]. While sequencing errors do not restrict the use of next-gen sequencing for some applications, it is not ideal for detecting mtDNA mutations, which can be as rare as 1 in one million nucleotides.

To circumvent the limitations of Sanger and next-gen sequencing, techniques have been developed including ultra-deep sequencing[190] and single molecule sequencing[189]. The benefit of ultra-deep sequencing is that high (>10,000) coverage, or the number of reads representing a certain sequence, enables detection of mutations that are present as low as 1/10,000 in theory. However, in practice inherent errors created during next-gen sequencing may reduce sensitivity by up to 100 fold[190]. Another drawback of ultra-deep sequencing is that early round PCR errors or amplification across DNA damage during library preparation do not appear to be sequencing errors as they exist at high frequency and thus cannot be distinguished from true mutations. A separate method with an advantage over traditional sequencing methods is single molecule sequencing, which produces multiple reads from the same parent molecule. Read alignment identifies true mutations as they are present at the same location in every read while random sequencing errors occur only at some positions in a fraction of reads. While this method can detect high levels of heteroplasmy, the polymerase has an extremely high error rate, decreasing the sensitivity to as low as 30%[191]. While these methods improve the sensitivity of standard sequencing approaches, they are still insufficient to measure low levels of heteroplasmy.

A recently developed method, Duplex Sequencing (DS)[114] utilizes single molecule sequencing and can distinguish artifactual errors from true mutations by using molecular tagging of double-stranded DNA. Because complementary information exists in duplex DNA, sequencing errors are identified by comparing sequencing reads from one strand of a DNA molecule to its complement. False mutations that result from sequencing across DNA damage exist only on a single strand of the duplex, while true

mutations are present on both strands of DNA. DS has the ability to identify rare variants in heterogeneous genetic populations and can detect mutations as low as $1/10^{10}$ [114].

We utilize DS to measure mtDNA mutations in *Drosophila*, and transitioned away from using the Random Mutation Capture Assay (RMC) because DS is more sensitive at detecting mutations and provides a significantly greater amount of mutation data per sample. In this Chapter, I describe the development of and methods for using DS on *Drosophila* mtDNA. Additionally, I show results from DS that corroborate the mtDNA mutation frequencies we obtained using the RMC assay.

4.3 Results

We developed Duplex Sequencing methods to measure mtDNA mutations in *Drosophila* using w^{1118} control flies and four sequencing runs. For the first run, we sequenced total DNA (nuclear and mtDNA) from whole flies. Because the nuclear genome represents roughly 99% of total DNA and because DNA from gut bacteria were also present in the sequencing library, less than 1% of the reads were mitochondrial, which was an insufficient amount to determine a mutation frequency. For the second sequencing run, we performed mtDNA enrichment using whole flies to eliminate nuclear contamination. However, because gut bacteria in the fly abdomen co-fractionates with mitochondria, we also enriched for a common microbe, *Pseudomonas sp*. Only ~1% of the reads were from *Drosophila* mtDNA, which was also an insufficient amount of data to determine a mutation frequency. For the third sequencing run, we sought to eliminate the *Pseudomonas sp*. Contamination by utilizing only head tissue and then performing mtDNA enrichment. However, the w^{1118} strain we were using was infected with the

common intracellular *Drosophila* endosymbiont, *Wolbachia*. While the majority of the reads mapped to *Wolbachia* (>70%), we obtained enough sequencing data to determine the mutation frequency for head tissue from 1 day-old flies to be ~ $2.0x10^{-6}$, which is comparable to the range of values we obtained using RMC for similarly aged tissue.

For the last sequencing run, we utilized 1 day-old fly heads from a w^{1118} strain free of *Wolbachia*. We obtained sufficient data to determine the mutation frequency in young fly heads to be 8.2×10^{-6}, a value similar to what we obtained using the RMC assay (Tables 4.1-2). In addition we obtained mutation frequencies for short (1-4 nucleotides) insertions and deletions (indels). We are the first to report the frequency of mtDNA indels in *Drosophila* as the frequency of insertions was 3.51×10^{-6}, and the frequency of deletions was 1.95×10^{-6} (Table 4.3). While the point mutation frequency we determined using DS is similar to that using RMC, DS does not precisely recapitulate the mutation spectrum we observe using RMC (Table 4.4). One possible explanation for the difference is that RMC provides mutation information for only four base pairs within the *TaqI* site, and these base pairs may not be completely representative of the entire genome. Another explanation is that RMC reports every mutation counted, while DS does not include repeated mutations that have undergone clonal expansion. Finally, mutation spectra information using DS was acquired from only a single run on $1/8^{th}$ of a sequencing lane; whereas, complete mutation spectra from DS is usually obtained from 3-5 samples run on 1/3 of a sequencing lane. Additional experiments are in progress to increase the *Drosophila* samples and total number of base pairs interrogated using DS, which will provide more accurate mutation spectra. In sum, DS corroborates the point mutation frequency we obtained for RMC on head tissue from young w^{11118} flies and will

be used to study the role of the mtQC machinery on heteroplasmy along with mtDNA deletions in *Drosophila*.

Nucleotide	Nucleotides sequenced
A's	986500
T's	985415
C's	330987
G's	259990
Total	2562892

Table 4.1. Number of sequenced mtDNA nucleotides.
The number of each nucleotide and total nucleotides sequenced is listed.

Point Mutation Type	Mutation Frequency	Positive 95% confidence interval	Negative 95% confidence interval
A to T	4.05e-06	1.04e-05	1.58e-06
A to C	0.00e+00	3.89e-06	4.24e-22
A to G	0.00e+00	3.89e-06	4.24e-22
T to A	4.06e-06	1.04e-05	1.58e-06
T to C	0.00e+00	3.90e-06	0.00e+00
T to G	1.01e-06	5.75e-06	1.79e-07
C to A	6.04e-06	2.20e-05	1.66e-06
C to T	9.06e-06	2.67e-05	3.08e-06
C to G	3.02e-06	1.71e-05	5.33e-07
G to A	1.54e-05	3.96e-05	5.98e-06
G to T	7.69e-06	2.81e-05	2.11e-06
G to C	0.00e+00	1.48e-05	0.00e+00
Total	**8.19e-06**	**1.25e-05**	**5.36e-06**

Table 4.2. mtDNA point mutation frequencies.
The mutation frequency and 95% confidence intervals are listed for each type of point mutation.

Insertion or deletion size	# of observed indels	Mutation Frequency	Positive 95% confidence interval	Negative 95% confidence interval
+1 insertion	8	3.12e-06	6.16e-06	1.58e-06
+2 insertion	1	3.90e-07	2.21e-06	6.89e-08
+3 insertion	0	0.00e+00	1.50e-06	-1.06e-22
+4 insertion	0	0.00e+00	1.50e-06	-1.06e-22
Total insertions	**9**	**3.51e-06**	**6.67e-06**	**1.85e-06**
-1 deletion	5	1.95e-06	4.57e-06	8.33e-07
-2 deletion	0	0.00e+00	1.50e-06	-1.06e-22
-3 deletion	0	0.00e+00	1.50e-06	-1.06e-22
-4 deletion	0	0.00e+00	1.50e-06	-1.06e-22
Total deletions	**5**	**1.95e-06**	**4.57e-06**	**8.33e-07**

Table 4.3. Insertion and deletion counts and frequencies.
The count of insertion or deletion (indel) observations, the mutation frequency, and 95% confidence intervals are listed for each type of indel.

Point Mutation	DS	RMC
A to T	4	0
A to C	0	0
A to G	0	0
T to A	4	3
T to C	0	0
T to G	1	1
C to A	2	0
C to T	3	0
C to G	1	0
G to A	4	26
G to T	2	3
G to C	0	2
deletions	5	0

Table 4.4. Mutation spectra obtained using DS and RMC.
The count is given for each type of mutation observed.

4.4 Discussion

We adapt DS to use on *Drosophila* mtDNA as a sensitive and high-throughput method to measure mtDNA mutations and to study factors that influence heteroplasmy. While the majority of the experiments thus far involved troubleshooting methods to enrich for mtDNA, we obtained results that validate the point mutation frequency we obtained using the Random Mutation Capture Assay in young control fly heads. In the following paragraphs, I describe technical issues to consider when using DS on *Drosophila* mtDNA and also current and future experiments using DS to analyze the role of mtQC system components on mtDNA mutations.

There are several technical issues to consider when using DS on *Drosophila* mtDNA. One of these issues involves the presence of microbes when isolating mtDNA because *Drosophlia* gut bacteria and intra-cellular endosymbionts co-fractionate with mitochondria and can represent a major DNA sequencing contaminant. For example, *Pseudomonas sp*. is a prevalent in the fly microbiome and *Wolbachia* is a common

endosymbiont. To circumvent this problem, it is necessary to separate the abdomen containing the majority of gut bacteria and to use fly strains free of *Wolbachia* infection. Moreover, bacteria specific primers may be used to test a strain or tissue sample prior to mtDNA preparation. Another way to eliminate contaminating bacterial genomes prior to sequencing is to use a kit that specifically captures *Drosophila* mtDNA sequences prior to library preparation. Additional benefits of a capture kit include not requiring the nuclear elimination step and drastically reducing the amount of mtDNA required for sequencing library preparation. Without a capture kit, mtDNA preparations require ~2000 fly heads, and while it is not difficult to obtain this number of young control flies, it would prove difficult to collect and age that amount of certain mutant genotypes. In sum future use with the capture kit will simplify DS and the study of the mtQC system on heteroplasmy.

To determine if *PINK1*, *parkin*, and other members of the mtQC influence heteroplasmy, transgenic approaches along with DS will be used. Specifically, the loss of *PINK1* or *parkin* can be studied by using aged flies with null mutations in these genes and comparing the somatic mutation frequency to age-matched control flies. A complimentary experiment is to test the effect of overexpression of *PINK1* and *parkin* on mtDNA mutations. However, because the normal basal frequency of mtDNA mutations may be too low for *PINK1* or *parkin* to detect, the use of a mutator will be used to increase the background mutation load. Our collaborators in Richard Youle's lab at NIH have shown that a transgenic line expressing a proofreading-deficient version of the *Drosophila* mtDNA polymerase (Pol-γ) rescues the recessive lethal phenotype caused by a loss-of function mutation in the *Drosophila pol-γ* gene and causes an increase in

somatic mtDNA mutations. Using DS, one may analyze the effect of overexpressing (or loss of) *PINK1* or *parkin* in the Pol-γ mutator background by comparing the somatic mtDNA mutation frequency to flies expressing only the Pol-γ mutator. Together these studies would address whether the mtQC system influences somatic mtDNA mutations.

In addition to studying the effect of the mtQC system on somatic mtDNA mutations, studies will also be performed to determine the influence on germline mutations. Several studies support the removal of mtDNA mutations in the female germline. For example, female mice with a heteroplasmic mtDNA mutation produce offspring with reduced heteroplasmy compared to the mother, and heteroplasmy levels decrease further with subsequent litters[107]. Additional evidence to support selection against germline mtDNA mutations derives from studies in mice expressing a proof-reading deficient form of Pol-γ. These studies found selection against non-synonymous changes in protein encoding genes[108]. While evidence of selective mechanisms that remove germline mutations exists, the factors that mediate this process are unknown. We hypothesize that the mtQC machinery may play a role in this process because mtQC proteins selectively recognize damaged mitochondria. Additionally, if *PINK1* and Parkin possess a general role of reducing heteroplasmy, it may be most important in the female germline to ensure the integrity of the mitochondrial genome. Studies similar to those outlined in the preceding paragraph may be performed to address this question by interrogating mtDNA from the female germline and/or mtDNA from the progeny of females with genetically altered mtQC genes. Understanding factors that influence mtDNA heteroplasmy will potentially impact understanding and treatment of

mitochondrial diseases, including inherited encephalopathies, aging, and Parkinson's disease.

4.5 Materials and Methods

The following methods were adapted from a protocol written by Dr. Scott R. Kennedy, a collaborator.

Duplex Sequencing

Mitochondrial DNA Isolation: The subcellular mitochondrial fraction was obtained from ~2000 fly heads using the following steps. Four groups of ~500 flies were collected in 50mL conical tubes, flash frozen in liquid nitrogen, and vortexed on maximum speed for thirty seconds to dislodge fly heads from the thoracic-abdominal sections. Flash freezing and vortexing was repeated a second time. Fly heads were separated from other body parts using a series of sieves, and then heads were collected into a dounce homogenizer using a paint brush. Ten mL of homogenization medium (0.32 M sucrose, 1mM EDTA, 10mM Tris-HCl pH 7.8) was added to the homogenizer, and four to five dounce strokes were used to homogenize the tissue. The homogenate was then transferred to a 15 mL centrifuge tube and spun at 1000xg for 20 minutes at 4°C. The supernatant was transferred to a fresh 15 mL tube and spun for 15 minutes at 1000xg at 4°C, and this step was repeated until the nuclear pellet was <1-2mm in height. The final supernatant was then divided into 8 separate 1.5mL eppendorf tubes and spun at 15,800xg for 30 minutes at 4°C to obtain the crude mitochondrial fraction. The mitochondrial pellets were washed in homogenization medium and combined into 2 separate 1.5mL eppendorf tubes. The

supernatant was removed and mitochondrial fractions were either stored at -80°C or immediately processed.

The mitochondrial fractions were then treated with DNaseI to reduce nuclear DNA contamination by resuspending mitochondrial pellets in 1mL DNaseI buffer (0.3M sucrose, 10mM $MgCl_2$, 0.15% (wt/vol) BSA, 20mM Tris-HCl, pH 7.5) containing 30U of DNaseI and RNase A (10ug/mL) and incubated at 37°C for two hours. The homogenate was then centrifuged at 15,800xg for 30 minutes at 4°C, and the supernatant was discarded. The mitochondrial pellets were washed in 1mL of DNase buffer and centrifuged at 15,800xg for 30 minutes at 4°C, and this washing step was repeated for a total of two washes. The mitochondrial pellets were then stored at -80°C until further use or immediately processed.

Mitochondrial DNA was obtained from the pellets using phenol-chloroform extraction by resuspending the mitochondrial pellet in 500uL of lysis buffer (10mM Tris pH 8.0, 150 mM NaCl, 20 mM EDTA, 1% SDS) with 200 ug/mL Proteinase K and 10 ug/mL RNase. The lysis reaction progressed for between 60 and 120 minutes at 56°C until the lysate was clear. An equal volume of phenol-chloroform-isoamyl alcohol (25:24:1) was added, and the contents were mixed by inverting the tubes ten times and followed by brief vortexing. The tubes were then centrifuged at 15,800xg for 10 minutes at 4°C. The top aqueous layer was transferred to a fresh tube and an equal volume of phenol-chloroform-isoamyl alcohol (25:24:1) was added. The contents of the tubes were mixed and centrifuged at 15,800xg for 10 minutes at 4°C and the aqueous phase was transferred to a fresh tube. An equal volume of chloroform was added, and the tubes were centrifuged and spun at 15,800xg for 10 minutes at 4°C. The aqueous layer was

transferred to a new tube and 3M sodium acetate (pH 5.2) was added at a 1:15 dilution along with an equal volume (~300uL) of ice cold 100% ethanol. The mtDNA pellet was obtained by spinning at 15,800xg for 15 minutes at 4°C, and the pellet was then washed in 1mL of 70% ethanol and centrifuged again at 15,800xg for 15 minutes at 4°C. The mtDNA pellet was resuspended in 50uL of nuclease free water for 1 hour at 25°C and then moved to 4°C overnight. A 1:30 dilution of mtDNA was performed to test for nuclear DNA contamination using qPCR as described in Materials and Methods of Chapter 3 (DNA copy number). The mtDNA concentration was determined using a Qubit spectrophotometer, and ~1ug of mtDNA was used to prepare each sequencing library.

Mitochondrial DNA library preparation: DNA was sheared using a Covaris system (Covaris, Wolburn, MA) by filling the water bath reservoir to the 12.5 mark with deionized water. The water was chilled to 4°C and degassed for at least 45 minutes. Samples were then loaded into a Covaris microtube, and the total volume was increased to 130 μL using $T_{low}E$ buffer (10 mM Tris pH 7.4, 0.1 mM EDTA, pH 8.0). Shearing produced 200-300bp fragments using the following setting: Duty Cycle: 10%, Intensity: 5, Cycles/Burst: 200, Time: 20sec x 6, Temp 4-7°C.

The sheared DNA sample was purified by splitting the sheared DNA into two tubes and then adding a 2x volume of Agencourt AMPure XP beads (Beckman Coulter, Brea, CA) that were warmed to 25°C to each tube. The beads are not exchanged during the entire library preparation to prevent DNA loss. The DNA-bead mixture was mixed well by pipetting and then incubated for 5 minutes at 25°C. The tubes were then placed onto an Invitrogen side magnet plate (Life Technologies, Grand Island, NY) for 2

minutes to separate the DNA-bound beads from solution, and then the supernatant was aspirated and discarded. The beads were washed with 200 μL of fresh 70% ethanol and incubated for 30 seconds at room temperature. The tubes were placed on a side magnet plate and the ethanol was aspirated and discarded. The washing step was repeated for a total of two washes. The beads were then dried for 5 minutes at 25°C. The plate was then removed from the plate magnet and the two tubes of beads were collected into one tube using 40 μL of water.

The ends of sheared DNA were repaired using an NEB Next End Repair Kit (New England BioLabs, Ipswich, MA) in a 50 uL total reaction volume, and the reaction was carried out on a thermocycler for 30 minutes at 20°C. After the end repair reaction was complete, 1.5 volumes of PEG solution (20% PEG8000/2.5M NaCl) was added to the well and incubated for 5 minutes at 25°C to promote DNA re-binding of DNA onto the beads,. The sample was placed on the plate magnet for 3 minutes to separate the DNA-bound beads from the solution. The solution was aspirated, and the beads were washed for a total of two times with 70% ethanol. The beads were then dried for 5 minutes at 25°C. The plate was then removed from the plate magnet and 40 μL of water was used to resuspend the beads.

The end-repaired DNA was T-tailed using NEB Klenow exo$^-$ enzyme, NEB buffer #2, and 10mM dTTP in a total reaction volume of 50 μL. The reaction was carried out on a thermocycler for 60 minutes at 37°C. After T-tailing, 1.5 volumes of PEG solution was added to the tubes and incubated for 5 minutes at 25°C. The sample was then placed on the magnet plate for 3 minutes to separate the beads from solution. The solution was aspirated, and the beads were washed for a total of two times with 70%

ethanol. The beads were then dried for 5 minutes at 25°C. The sample was then removed from the plate magnet and 37 μL of water was used to resuspend the beads. Then, the DNA concentration was quantified and length of fragments determined by loading a mixture of 2 μL of DNA and 2 μL of high sensitivity buffer (Agilent, Santa Clara, CA) into a ScreenTape that was analyzed by a TapeStation (Agilent, Santa Clara, CA).

Adaptors compatible with Duplex Sequencing were then ligated to the DNA using a 50:1 adapter:DNA molar ratio and a T4 Ultrapure Ligase Kit (Enzymatics, Beverly, MA), in a total reaction volume of 50 μL. The ligation reaction was carried out in a thermocycler at 25°C for 15 minutes. The adapter-ligated DNA was then purified to remove adapter dimers by adding 0.6 volumes of PEG solution. Lower volumes of PEG select against small DNA products, such as DNA adapter dimers. The solution was mixed well by pipetting and incubated for 5 minutes at 25°C. The samples were placed on the plate magnet for two minutes to separate beads from solution. The solution was aspirated, and the beads were washed for a total of two times with 70% ethanol. The beads were then dried for five minutes at 25°C. The samples were removed from the magnet plate and 30 μL of $T_{low}E$ was used to resuspend the beads. A TapeStation was used to quantify DNA library and check for presence of adapter dimers.

The libraries were amplified using a KAPA HiFi PCR kit (Kapa Biosystems, Woburn, MA) and 5 μL of 7.5 pM DNA in a 50 μL PCR reaction volume (5x buffer, 10mM dNTPs, 20uM primer 1 (mws), 20 uM primer 2, DNA, Kappa HiFi polymerase, 12.5x SYBR). The following qPCR reaction cycle was used: 95°C for 4 minutes, cycle conditions of 98°C for 20 seconds, 60°C for 20 seconds, and 72°C for 15 seconds. The samples are removed ~1 cycle prior to saturation of amplification curve. To obtain an

optimal number of duplicates, the samples had a Ct of ~10-11 and were removed at cycle ~18-20. While 5 μL of 7.5 pM DNA provides an adequate number of duplicates, an alternative approach was to create a 5x dilution series and choose the dilution meeting the given criteria.

The samples were then purified by adding 0.7 volumes of Ampure beads and incubated for 5 minutes at 25°C. The sample was then placed onto a plate magnet for 2 minutes to separate the beads from solution. The solution was aspirated, and the beads were washed for a total of two times with 70% ethanol. The beads were dried for 5 minutes at 25°C, and 22 μL of $T_{low}E$ were used to resuspend the beads. A Tape Station was then used to determine the final concentration of the DNA library. Additional washes were performed if adapter dimers were present. Each DNA sequencing lane could be divided to allow for multiplex sequencing of samples, and a total of 19 fM of DNA was used for each sequencing lane.

Sequencing and Analysis: Sequencing was performed on an Illumina HiSeq 2500, using a short 30-hour run, which produced 125 bp paired-end reads. Each sample occupied between 1/6 and 1/3 of a sequencing lane, yielded between 75-100 gigabytes of data. Analyses were performed using a pipeline and in-house scripts written by Scott R. Kennedy described elsewhere[114].

PCR Primer Sequences:

DNA was prepared using methods described in the DNA Isolation section of **Chapter 3**. The following primer sequences can be used to test for presence of contaminating

Wolbachia or *Pseudomonas Sp*. Wolbachia primers (F-5' TGGTCCAATAAGTGAGGAAGA; R-5'AAAAATTAAACGCTACTCCA) yield a 500 bp product (designed by Dr. Maulik Patel). The PCR cycle consisted of an initial denaturing step at 95°C for 5 minutes, followed by 30 cycles of denaturing at 95°C for 30 seconds, annealing at 60°C for 1 min, and extension at 72°C for 1 min. PCR cycling was followed by a 10 minute extension step at 72°C. *Pseudomonas* primers (F-5’CGAGCGGATGAAGAGAGCTT; R-5’CGAAACGTTGTCCCCCACTA) yield a 91 bp product. The PCR cycle consisted of an initial denaturing step at 95°C for 5 minutes, followed by 30 cycles of denaturing at 95°C for 30 seconds, annealing at 60°C for 1 min, and extension at 72°C for 1 minute. PCR cycling was followed by a 10 minute extension step at 72°C.

5 Summary and Future Directions

5.1 A Drosophila Model of Complex I Disease

In order to study the pathogenesis of complex I disease due to an mtDNA mutation, we characterized a deletion mutation in *mt:ND2*. We found that *Drosophila ND2* mutants have phenotypes resembling mitochondrial disease, including shortened lifespan, progressive neurodegeneration and decreased complex I abundance. *ND2* mutants also exhibit biochemical defects, including decreased mitochondrial membrane potential and ATP levels, and complex I specific defects, including decreased respiratory chain efficiency (ADP/O) and maximal state 3 respiration. We show that the *ND2* mutation uncouples complex I dependent proton pumping from electron transport and demonstrate a role for ND2 in proton pumping

Drosophila represent an ideal whole-organism model to study progressive mitochondrial diseases for several reasons. Compared to nematodes, flies have a more complex nervous system. Compared to mammalian models, flies have a relatively short lifespan, which enables one to study latent or progressive symptoms with less delay. Additionally, their nuclear genome is relatively small and there are many genetic tools available, which enables an experimenter to practically perform genetic screens. Similarly, compound screens are also possible with less time and cost compared to mammalian studies. Moreover, flies are a valid model for complex I disease in particular because the function of complex I in respiration is conserved with mammals.

Dysfunctional complex I is the most common cause of mitochondrial disease and yet there are no cures or effective treatments[33,192]. While there are other models of

complex I disease, including two mouse models that directly affect complex I (Chapter 1), our model offers unique insight into complex I disease and powerful tools to identify potential therapeutics. Another even simpler model that is commonly used are fibroblasts from patients with complex I disease, which are used to study biochemical aspects of the disease. However fibroblasts have limitations due to the *in vitro* nature of the model. For example, fibroblasts rely on glycolysis and oxidation of glycolytic NADH mediated by glycerophosphate shuttle, which bypasses complex I[193]. Secondly, fibroblasts do not allow the study of particular neurons or myocytes that may be specifically affected or degenerate in certain forms of mitochondrial disease. Therefore, we contribute a unique and *in vivo* model to study various aspects and potential therapeutics for complex I disease.

Current studies in the Pallanck lab include testing whether activation of the PINK1/Parkin pathway can rescue *ND2* mutant phenotypes. Because PINK1 and Parkin turnover damaged mitochondria and because *ND2* mutants show upregulation of complex IV, it was hypothesized that the PINK1/Parkin pathway may be able to selectively remove mitochondria incapable of upregulating complex IV. PINK1 activating compounds are being used to determine if promoting the PINK1/Parkin pathway can restore *ND2* mutant phenotypes, including bang sensitivity and membrane potential. Compounds that activate the PINK1/Parkin pathway could also be used as potential therapeutics to treat heteroplasmic disease by specifically removing dysfunctional mitochondria.

A question raised by the work regards the mechanism of complex IV upregulation. In *ND2* mutants, we find a decrease in maximal complex I-dependent

respiration together with a compensatory upregulation in complex IV-dependent respiration. Consistent with our work, a separate study using fibroblasts from *ND6* mutant mice showed a similar finding[40]. While we do not understand the mechanism of complex IV increase, there is evidence for regulatory roles of respiratory chain subunits. For example, the complex I subunit, *Ndufs4* enhances complex I-dependent respiration through phosphorylation by cAMP dependent PKA[194–196]. *Drosophila ND2* mutants could be used to test whether complex IV can be upregulated in a similar manner and to identify potential regulatory complex IV subunits.

A question unanswered by the study is whether ROS play a role in our disease model. Complex I is a major site of ROS production as electrons released from electron transferring components of complex I, such as FeS clusters, flavin mononucleotide, or the ubiquinone-binding site react with molecular oxygen to produce superoxide anion[152]. Therefore, mutations affecting complex I activity may lead to an increase in ROS by influencing electron-handling at one of these sites. Previous studies of ROS production in other complex I mutants yield conflicting results. For example, fibroblasts from a Leigh syndrome patient with an *Ndufs4* mutation do not exhibit increased ROS while fibroblasts from a leukodystrophy patient with an *Ndufs1* mutation show increased O_2^- and H_2O_2[197]. An explanation for this difference is that Ndufs1 but not Ndufs4 contains FeS clusters that are capable of oxidizing O_2, leading to an increase in ROS when *Ndufs1* is mutated. However, fibroblasts from a mouse model of Leber's hereditary optic neuropathy with a mutation in ND6 also exhibits increased levels of ROS, but ND6 does contain FeS clusters[40]. ND6 could possibly influence electron release from other electron transferring sites, such as flavin mononucleotide or the ubiquinone-binding site. Similarly, ND2 does

not contain FeS clusters, but because electrons could be released from other sites, the contribution of ROS to the pathology in *ND2* mutants should be determined.

Another question that the study raises is how the *mt:ND2* mutation preferentially affects females. Men and women have different risks for various diseases including, migraine, neurodegenerative disease, and cancers[31,198–200]. Some of the sex biases of these diseases can be explained by sex hormones, but differences in hormones cannot readily explain gender biases in certain mitochondrial diseases. Leber's hereditary optic neuropathy (LHON) is a well-studied mitochondrial disease with a clear male sex bias, affecting males 5x more frequently than females[31,201]. Additional factors that increase LHON susceptibility include certain mitochondrial haplotypes[201] and smoking[202]. Studies have sought an X-linked gene that makes males more susceptible to LHON; however, no gene has been identified. *ND2* mutants could address whether mtDNA polymorphisms, other nuclear genes, or environmental factors render females more susceptible to disease phenotypes in our model and could provide clues for gender bias in other mitochondrial and neurodegenerative diseases.

Our studies also raise several questions regarding neurodegeneration in old ND2 brains, including which neuronal type(s) undergoes neurodegeneration and the mechanism of cell death. Human pathogenic *ND2* mutations cause Leigh syndrome and LHON, and patients with Leigh syndrome have characteristic necrotizing lesions of the brain stem, basal ganglia, cerebellum, and thalamus[33] while LHON patients exhibit degeneration of the optic nerve[31]. While *Drosophila* neuroanatomy is not an ideal human model, flies share similar neuronal types that can be used to study the cellular events precipitating neuronal death. Additionally, several features and components of the

intrinsic and extrinsic apoptotic and necrotic pathways are conserved in flies[203]. A separate study of complex I disease caused by knock-out of nuclear-encoded *Ndufs4* implicates extrinsic apoptotic signals followed by necrosis as the cell death mechanism[39]. The authors posit a switch occurs between cell death modes because sufficient ATP levels are required for apoptosis to occur while cell death proceeds by necrosis when ATP levels are depleted [204–206]. There is both a progressive decline in ATP levels and brain integrity in *ND2* mutants indicating that necrosis may also cause cell death in our fly model. The cell death pathway in *ND2* mutants should be addressed, and further studies could lead to therapeutics that prevent these processes in patients with complex I disease.

5.2 The Study of Somatic Mitochondrial DNA Mutations in Drosophila

The age-dependent frequency, distribution, and causes of somatic mtDNA mutations were previously unknown in invertebrates, and the main focus of my thesis addresses these questions. I used a previously developed method to measure mtDNA mutations in *Drosophila*, the Random Mutation Capture (RMC) assay[110], which determines the frequency that a restriction enzyme site is lost due to mutation. Using this assay, I studied the relationships between age and oxidative stress on somatic mtDNA mutations. I found that many of the features associated with mtDNA mutations in vertebrates are also conserved in *Drosophila*, including the mtDNA mutation frequency, the finding that their frequency increases with age, a prevalence of transition mutations, and possibly, clonal expansion of somatic mtDNA mutations. I further demonstrate that the types of mutations that accumulate with age do not correspond to those associated

with oxidative stress but rather to errors that occur during mtDNA replication. Moreover, loss-of-function mutations in genes that encode oxidative stress defense factors, Sod2 and Ogg1 do not detectably influence the somatic mtDNA mutation frequency. Thus, our findings indicate that oxidative stress is a minor contributor to somatic mtDNA mutations and suggest that mtDNA mutations accumulate primarily as a result of errors that are introduced during replication. These studies provide support for *Drosophila* as a valid model to study somatic mtDNA mutations, and current and future studies include using *Drosophila* to explore factors that influence heteroplasmy.

An implication from this work is that reactive oxygen species (ROS) are not an important source of mtDNA mutations as was previously hypothesized. Moreover, our results do not support the vicious cycle theory, which predicts an increase in oxidatively mutated bases over time. For example, we do not detect an appreciable increase in G:C to T:A transversions, a signature of oxidative damage with age. Also, reduction of the gene products, *Sod2* and *Ogg1* in aged flies causes only a slight increase in the mutation frequency. One potential explanation for the minor effect of ROS on mtDNA mutations is that replication of mtDNA in adult invertebrates occurs at a low rate as our mtDNA replication data and studies from C. elegans indicate[207]. However, we believe that while replication may be infrequent, it should occur in sufficient amounts to detect an effect of ROS because we observe other features of mtDNA mutations that rely on replication. In particular we find that mutations increase with age; we observe a strand mutational bias due to the mode of *Drosophila* mtDNA leading strand synthesis, and we likely detect clonal expansion only in aged flies. Other explanations for the small effect of ROS on

mtDNA mutations include the presence of redundant DNA repair pathways in mitochondria or the turnover of mitochondria that harbor mtDNA mutations.

A question our work raises is whether or not clonal expansion occurs in *Drosophila*. Clonal expansion of both point mutations and deletions has been documented in many different human cell types, both mitotic cells, such as buccal and gut epithelial[82–84] and post-mitotic cells, including neurons and myocytes[59,60,64,83]. Our mutation spectrum data support clonal expansion because we observe a trend whereby samples with high mutation frequencies exhibit a high percentage of a single predominant mutation indicative of a clonally expanded mutation. To address whether or not clonal expansion definitely occurs in *Drosophila*, it is necessary to measure the mutation frequency in a small number of cells rather than a tissue homogenate. While clonal expansion can cause a mutation to represent the majority of mtDNA within a cell, the presence of WT molecules in a tissue homogenate can dilute this effect. Because the RMC assay requires a relatively large amount of input DNA (100 fly heads or thoraces), RMC cannot adequately resolve whether clonal expansion occurs in *Drosophila*. However, other methods that utilize few cells or single cells can address this question.

While the RMC assay has the advantage compared to other methods of sensitively detecting mtDNA mutations, it has other restrictions in addition to its limit in detecting clonally expanded mutations. As mentioned in Chapter 1, several of these reasons have driven us to use an alternative method to measure mutations, Duplex Sequencing (DS)[114]. For example, the *TaqI* restriction enzyme site is four base pairs, so the assay can only monitor 4 bp of the entire 19.5 kb *Drosophila* mitochondrial genome, while DS has the potential to interrogate the entire genome. An additional limitation is that RMC relies on

precise quantification of molecules by qPCR, which is less accurate than determining the mutation frequency based on sequencing a known number of bases. Nevertheless, I am confident in the results obtained by RMC as the mutation frequency we obtained has been replicated using both DS (Chapter 4) and a new form of single molecule RMC[208] (communication Jason Bielas). Because DS is not limited by the factors described here, our current and future experiments on mtDNA mutations in flies utilize DS.

There are several unaddressed questions related to mtDNA deletions, including measuring their frequency in *Drosophila* and whether oxidative stress may influence their occurrence. Several studies in flies have reached disparate conclusions regarding the age-dependent accumulation of mtDNA deletions[144–146]. While the difference in the findings is likely due to difference in methodology, no studies have addressed the frequency of mutations in aging flies. We used the RMC assay in our studies to measure point mutations, and it can also be used to detect mtDNA deletions by using assay primers that flank multiple *TaqI* sites[110]. A deletion is counted if the qPCR primers amplify a product after digestion with *TaqI* restriction enzyme as it is more likely that a deletion occurred to remove all of the *TaqI* sites rather than multiple mutations occurring in each *TaqI* site. One drawback of using RMC to detect mtDNA deletions is that the assay primer design requires the experimenter to choose specific sites where deletions are likely to occur. However, DS does not have this requirement and can currently detect small deletions (1-4 base pairs) and larger deletions using either read depth or split-read analysis. For read depth analysis, a decrease in read coverage at a certain region in the genome would indicate a deletion. For split-read analysis, if two ends of a single read map to regions of the mitochondrial genome that are farther apart than the length of the read itself, this

would indicate a deletion. In addition to addressing the age-depending frequency of deletions in *Drosophila*, one could also use genetic or pharmacologic approaches to increase and/or decrease ROS to determine the role of oxidative stress on mtDNA deletions.

A current project in the Pallanck lab addresses one of the original motivating questions of this thesis – does the mitochondrial quality control (mtQC) system influence heteroplasmy? As described in Chapter 1, components of the mtQC system target and degrade depolarized mitochondria through autophagy[99,100]. The existence of a process that can remove damaged mitochondria raises the question of whether the mtQC system can also influence heteroplasmy by selectively eliminating mitochondria the bear a high degree of mtDNA mutations. These studies are described in further detail in the Discussion of **Chapter 4**.

A.1 Supplemental Figures

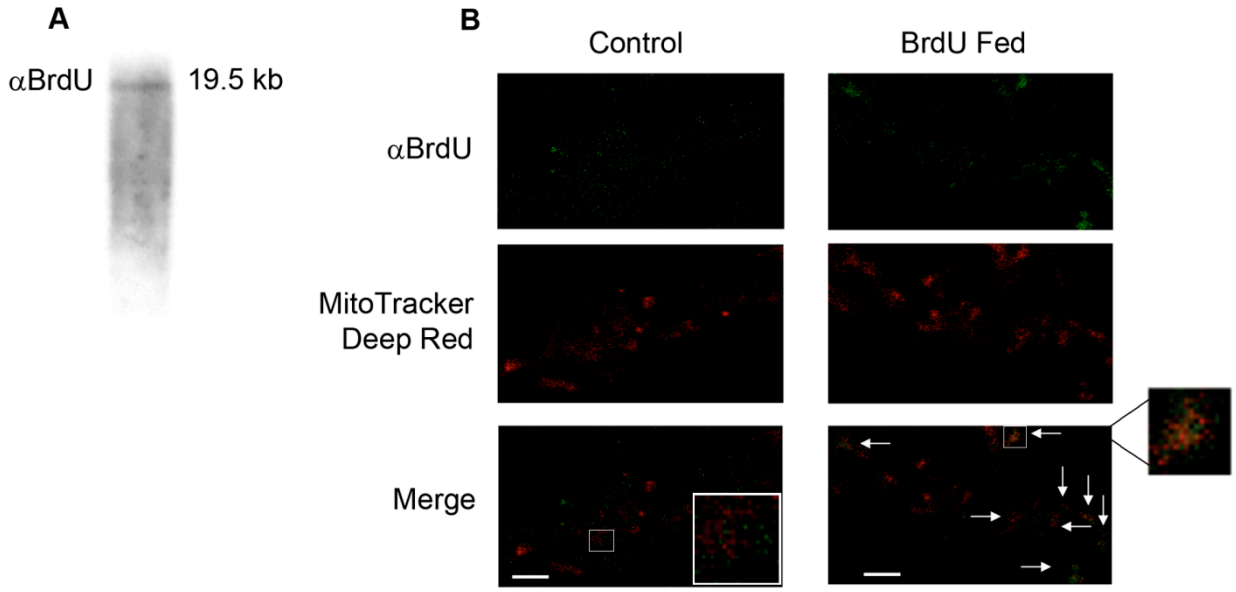

Figure A1. BrdU labeling of mtDNA provides support for mtDNA replication in *Drosophila* somatic tissues.
(A) DNA was isolated from the heads of BrdU-fed flies, digested with BglII, then subjected to Southwestern blot analysis using an anti-BrdU antiserum. A single 19.5kb band was detected in BrdU-fed flies, consistent with the size expected for linearized *Drosophila* mtDNA. **(B)** Thoracic ganglia from BrdU-fed and untreated control flies were labeled with MitoTracker Red and a primary antibody against BrdU (green) and subjected to confocal imaging. While non-specific labeling of BrdU is present in control images, colocalization (yellow) of BrdU with mitochondria (arrows) is present only in BrdU-fed flies. Scale bar = 2 μm.

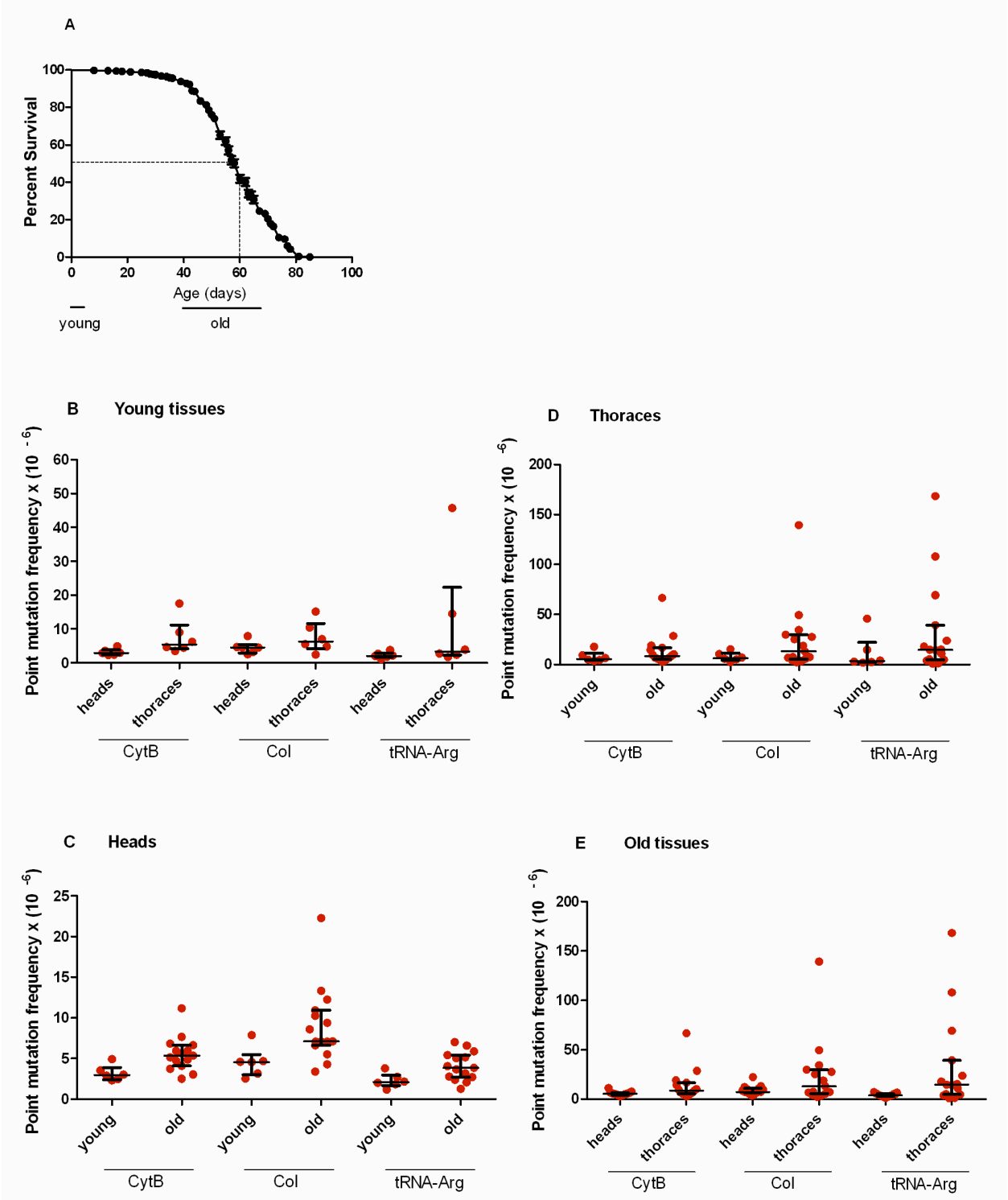

Figure A2. Lifespan analysis and mutation frequencies of an isogenic w^{1118} strain.
(A) The median lifespan of w^{1118} flies was 60 days. Horizontal bars indicate age ranges selected for RMC analysis. The mtDNA mutation frequency at the three *TaqI* sites in **(B)** heads and thoraces of young animals, **(C)** heads of young and old animals, **(D)** thoraces of young and old animals, and **(E)** heads and thoraces of old animals. Horizontal bars represent the median mutation frequency, and error bars indicate the interquartile range.

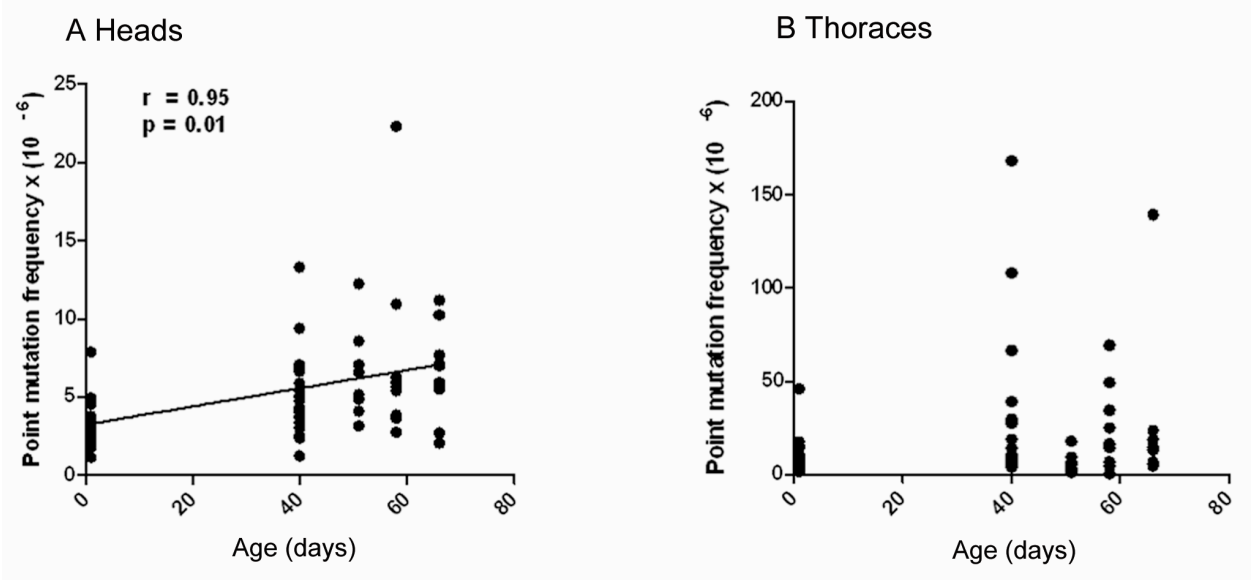

Figure A3. The mtDNA mutation frequency as a function of age.
The point mutation frequency determined from RMC analysis is plotted relative to ages in heads (**A**) and thoraces (**B**). Mutation frequency data from heads fit best to a model of linear increase as a function of age. Data from thoraces could not be reliably fit to any specific model due to the broad fluctuation between samples. Linear correlation was determined using Pearson's correlation coefficient (r).

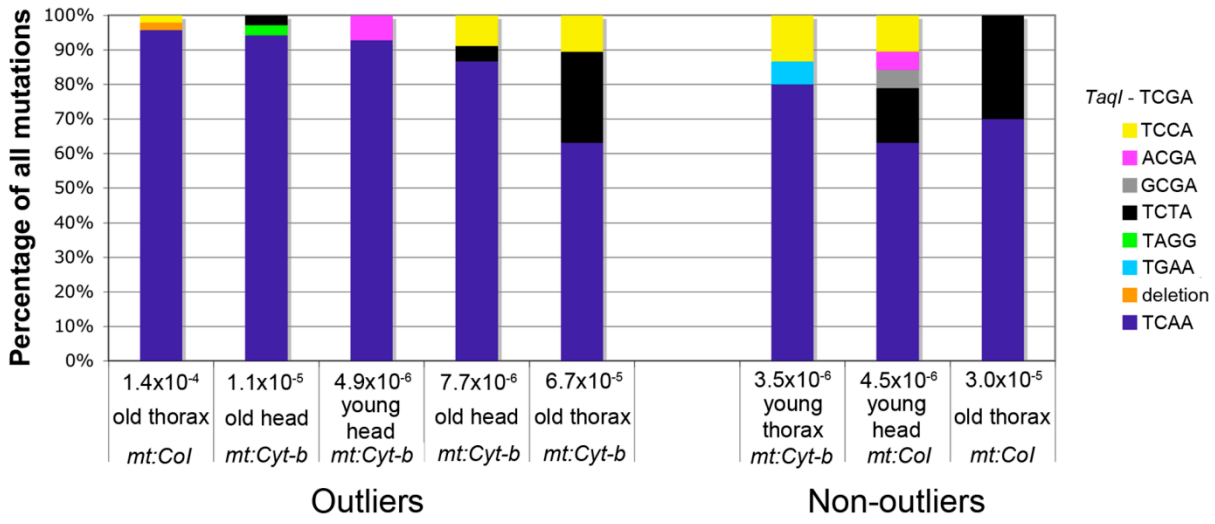

Figure A4. Clonal expansion of mtDNA mutations may explain variance in outlier samples.
Histograms show the relative proportions of the mtDNA mutations detected in outlier and non-outlier samples. The mtDNA mutation frequency, age (young or old), tissue type (head or thorax), and *TaqI* sites (*mt:Cyt-b* or *mt:CoI*) are indicated. The wild-type *TaqI* sequence (TCGA) is shown for reference, and the mutations detected by sequencing are color-coded as indicated. In four out of five outlier samples, a single mutation accounts for > 85% of all mutations detected, while no single mutation exceeded 80% in non-outlier samples.

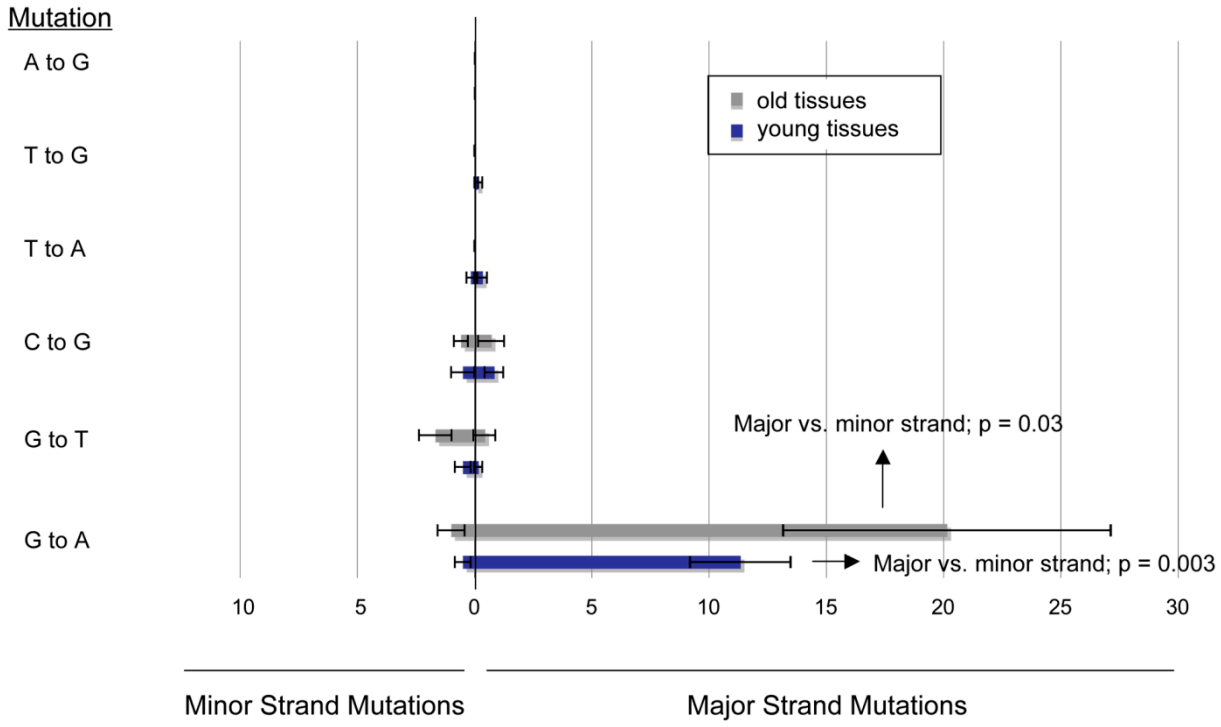

Figure A5. *Drosophila* mtDNA exhibits mutational strand bias.
Horizontal bars indicate the number of mtDNA mutations of the indicated type on the minor and major strands in young (n=6) and old tissues (n=7). G to A transitions are significantly more frequent on the major strand than on the minor strand in young and old tissues. None of the other mutation types exhibited significant strand asymmetry. Significance was determined using a Students t-test, and error bars represent standard error of the mean.

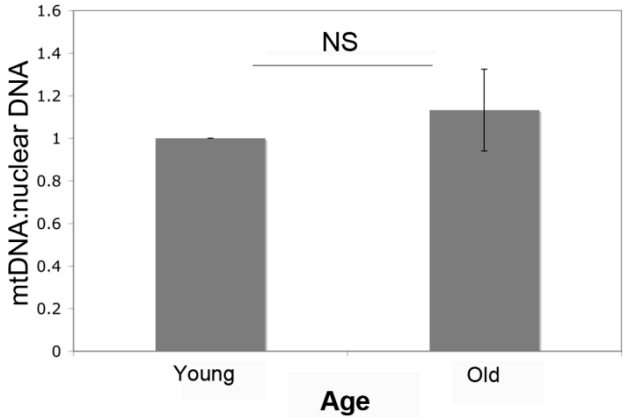

Figure A6. Mitochondrial DNA copy number does not decrease with age.
Total DNA from the heads of young or old w^{1118} flies was subjected to qPCR to determine the mtDNA copy number relative to nuclear DNA. No significant difference in the mtDNA:nuclear DNA ratio was detected between young (n = 4) and old flies (n = 4) (p = 0.3). Significance was determined using a Student's t-test and error bars represent standard deviation.

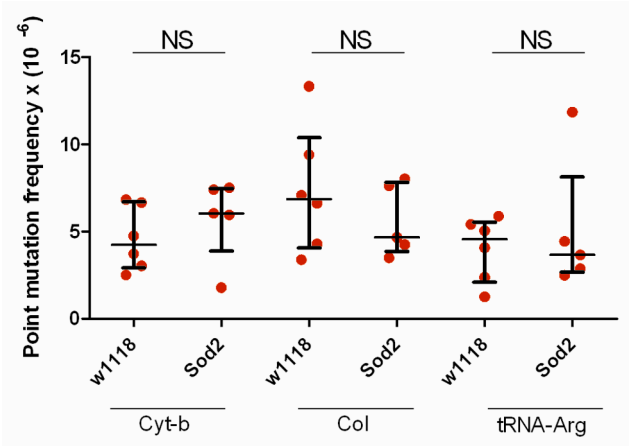

Figure A7. The mutation frequency is not greater in *Sod2* mutants at separate *TaqI* sites.
The mtDNA mutation frequency at the three *TaqI* sites in heads of old *Sod2* mutant and age-matched w^{1118} animals. Horizontal bars represent the median mutation frequency, and error bars indicate the interquartile range. There was no significant difference in mutation frequency between mutants and age-matched controls (Mann-Whitney unpaired U tests).

A.2 Supplemental Tables

TaqI Site and Location	Gene	Comments on *TaqI* Site	*TaqI* Flanking Primer Sequence	Comments on qPCR and Line of Best Fit for Dilution Series
1. 1578	*CoI*	Suboptimal qPCR amplification	5' TGGAGCTTGAGCTGGAATAGTTGGA 3' TCGTGGGAATGCTATATCAGGAGCA	TaqI: y = -2.248x + 27.085 R^2 = 0.9983 Ctrl: y = -2.267x + 35.174 R^2 = 0.9993
2. 2103	*CoI*	Suboptimal qPCR amplification	5' GCAGGGATTTCTTCAATTTTAGGAGCTG 3' GATCTCCTCCTCCCGCTGGGTC	Misprime
3. 2370	***CoI***	Usable in assay	5' GAGCTCATCATATATTTACCGTTGG 3' CAACTCCTGTTAATCCTCCTACTG	**Good** TaqI: y = -2.119x + 33.58 R^2=0.9937 Ctrl: y = -2.214x + 34.76 R^2=0.9959
4. 2778	*CoI*	Suboptimal qPCR amplification	5' GCAGGTTTTATTCACTGATACCCCT 3' CATGTTGTGTAAGCATCTGGGT	Poor TaqI: y = -2.203x + 34.262 R^2 = 0.9966 Ctrl: y = -2.122x + 31.835 R^2 = 0.9966
5. 3238	*CoII*	Suboptimal qPCR amplification	5' TTAGGTTTACAAGATAGAGCTTCTCC 3' AGTAAACGTAAAGAAGGAAGAGCA	Poor No Amplification
6. 3481	*CoII*	Neighboring *TaqI* site		
7. 3532	*CoII*	Neighboring *TaqI* site		
8. 3643	*CoII*	Suboptimal qPCR amplification	5' GCTTTAGGAGTAAAAGTTGACGGTACACC 3' GAGACCAGTACTTGCTTTCAGTCATC	Misprime
9. 4087	*ATP6*	Excessive AT content		
10. 4517	*ATP6*	Neighboring *TaqI* site		
11. 4538	*ATP6*	Neighboring *TaqI* site		
12. 5472	*CoIII*	Suboptimal qPCR amplification	5' GGTTTTGAAGCAGCTGCATGATATTGAC 3' ATTATCCTCCTCATCAGTAAATTGTG	Poor TaqI: y = -2.3623x + 33.75 R^2 = 0.9989 Ctrl: y = -2.362x + 37.32 R^2 = 0.9969

13. 5699	*ND3*	Neighboring *TaqI* site		
14. 5754	*ND3*	Neighboring *TaqI* site	5' CCCCATTTGAATGTGGATTTGAT 3' CCTTGATTTCATTCATGGTATAATCC	Poor No amplification
15. 6084	***tRNA -Arg***	Usable in assay	5' AACTGAATATGAAGCGATTGATTGC 3' CAGTGATATGCCTCTTTTTGGCTTC	**Good** TaqI: y = -2.023x + 32.43 R^2=0.9916 Ctrl: y = -2.122x + 31.83 R^2=0.9966
16. 6943	*ND5*	Suboptimal qPCR amplification	5' CCACGGAGTATAATTCAACTTTCATC 3' CCTTTAACTTCAGCTTGTTTTAACGTATC	Poor No amplification
17. 7435	*ND5*	Excessive AT content		
18. 7696	*ND5*	Suboptimal qPCR amplification	5'GCTGCAGGTAACCAAGAAGAAAAAGGAATC 3'TAGGGTGAGATGGTTTAGGACTTGTTTC	Poor No amplification
19. 7873	*ND5*	Suboptimal qPCR amplification	5' CAAGTCCTAAACCATCTCACCCT 3' TTGAGTGAGAATTAGTTTCTTTAAATTCT	Poor No amplification
20. 8285	*ND4*	Suboptimal qPCR amplification	5' TGAATATTTTCATATCACTAACACCACAA 3' AGTCAGCATGGTAAATTATTTTCTGGA	Poor No amplification
21. 8518	*ND4*	Neighboring *TaqI* site		
22. 8561	*ND4*	Neighboring *TaqI* site		
23. 10479	*ND6*	Excessive AT content		
24. 10710	*Cyt-b*	Usable in assay	5' TGCCAATAATGCTTTAGTAGATTTACCAGC 3' TGCACCGTTAGCATGTAAAGTTCGT	Good TaqI: y = -2.169x + 33.429 R^2 = 0.9798 Ctrl: y = -2.122x + 31.835 R^2 = 0.9966
25. 11028	***Cyt-b***	Usable in assay	5' GTTCAATGATTATGAGGTGGATTTGCTG 3' GGATTATTAGATCCTGTTTGATGAAGG	**Good** TaqI: y = -2.172x + 36.39 R^2=0.9994 Ctrl: y = -2.15x + 35.70 R^2=0.9994
26. 11520	*Cyt-b*	Suboptimal qPCR amplification	5' TGCTTATGCTATTTTACGATCTATTCCA 3' GTCCAATTAATACATAAGGTTCTTCAACTG	Poor TaqI: y = -2.335x + 38.09 R^2 = 0.9404

				Ctrl: y = -2.219x + 33.141 R^2 = 0.9922
27. 11831	*ND1*	Neighboring *TaqI* site		
28. 11846	*ND1*	Neighboring *TaqI* site		
29. 12874	*16S*	Neighboring *TaqI* site		
30. 12929	*16S*	Neighboring *TaqI* site		
31. 12950	*16S*	Neighboring *TaqI* site		
32. 13827	*16S*	Excessive AT content		
33. 14462	*12S*	Suboptimal qPCR amplification	5' CTGATTACAAATTTAAGTAAGGTCCATCG 3' GGCGGTATTTTAGTCTATCTAGAGGAACC	*Poor* *TaqI: y = -2.109x + 35.05* *R^2 = 0.9778* *Ctrl: y = -2.219x + 33.141* *R^2 = 0.9922*
Control Primers 5162-5360	*CoIII*		5' GTTACTGTAACTTGAGCCCACCATAGAC 3' CATGAATTCCGTGGAATCCTGTTGCT	See Test Primers for information

Table A1. RMC test primers and usability in RMC assay.
The 33 *TaqI* sites in *Drosophila* mtDNA are indicated according to their position relative to the first base pair in the mitochondrial genome and the gene in which they reside. The sequences of all primer pairs designed for use in the RMC assay are provided. Test primer pairs flanking *TaqI* sites used in the RMC assay are highlighted in bold, and coloring corresponds to that used in the legend of Figure 3.1. Control primer pair location and sequences are also listed.

w^{1118}

Heads

	Day 1	Day 40	Day 51	Day 58	Day 66
mt:Cyt-b	$4.9x10^{-6}$	$6.8x10^{-6}$	$5.1x10^{-6}$	$5.9x10^{-6}$	$7.7x10^{-6}$
mt:Cyt-b	$2.3x10^{-6}$	$3.0x10^{-6}$	$4.9x10^{-6}$	$5.6x10^{-6}$	$5.9x10^{-6}$
mt:Cyt-b	$3.5x10^{-6}$	$4.7x10^{-6}$	$4.1x10^{-6}$	$5.4x10^{-6}$	$1.1x10^{-5}$
mt:Cyt-b	$2.9x10^{-6}$	$2.5x10^{-6}$			
mt:Cyt-b	$2.4x10^{-6}$	$6.6x10^{-6}$			
mt:Cyt-b	$3.0x10^{-6}$	$3.7x10^{-6}$			
mt:CoI	$7.9x10^{-6}$	$9.4x10^{-6}$	$7.1x10^{-6}$	$1.1x10^{-5}$	$5.5x10^{-6}$
mt:CoI	$4.7x10^{-6}$	$3.4x10^{-6}$	$1.2x10^{-5}$	$7.1x10^{-6}$	$7.1x10^{-6}$
mt:CoI	$4.5x10^{-6}$	$6.6x10^{-6}$	$8.6x10^{-6}$	$2.2x10^{-5}$	$1.0x10^{-5}$
mt:CoI	$4.6x10^{-6}$	$4.3x10^{-6}$			
mt:CoI	$3.1x10^{-6}$	$7.1x10^{-6}$			
mt:CoI	$2.5x10^{-6}$	$1.3x10^{-5}$			
tRNA-Arg	$1.8x10^{-6}$	$5.0x10^{-6}$	$3.2x10^{-6}$	$2.7x10^{-6}$	$2.0x10^{-6}$
tRNA-Arg	$3.8x10^{-6}$	$2.4x10^{-6}$	$6.6x10^{-6}$	$3.8x10^{-6}$	$2.7x10^{-6}$
tRNA-Arg	$2.7x10^{-6}$	$5.4x10^{-6}$	$5.1x10^{-6}$	$3.6x10^{-6}$	$7.0x10^{-6}$
tRNA-Arg	$2.2x10^{-6}$	$1.2x10^{-6}$			
tRNA-Arg	$1.2x10^{-6}$	$5.9x10^{-6}$			
tRNA-Arg	$2.0x10^{-6}$	$4.1x10^{-6}$			

Thoraces

	Day 1	Day 40	Day 51	Day 58	Day 66
mt:Cyt-b	$9.0x10^{-6}$	$6.7x10^{-5}$	$3.6x10^{-6}$	$6.8x10^{-6}$	$5.5x10^{-6}$
mt:Cyt-b	$1.8x10^{-5}$	$2.9x10^{-5}$	$2.6x10^{-6}$	$4.8x10^{-6}$	$6.8x10^{-6}$
mt:Cyt-b	$6.2x10^{-6}$	$5.3x10^{-6}$	$9.4x10^{-6}$	$1.6x10^{-5}$	$1.4x10^{-5}$
mt:Cyt-b	$3.5x10^{-6}$	$8.6x10^{-6}$			
mt:Cyt-b	$4.7x10^{-6}$	$1.0x10^{-5}$			
mt:Cyt-b	$4.4x10^{-6}$	$1.9x10^{-5}$			
mt:CoI	$1.5x10^{-5}$	$2.8x10^{-5}$	$6.7x10^{-6}$	$2.5x10^{-5}$	$1.9x10^{-5}$
mt:CoI	$4.8x10^{-6}$	$3.0x10^{-5}$	$3.3x10^{-6}$	$3.4x10^{-5}$	$1.4x10^{-4}$
mt:CoI	$6.9x10^{-6}$	$5.5x10^{-6}$	$2.3x10^{-6}$	$4.9x10^{-5}$	$1.3x10^{-5}$
mt:CoI	$5.6x10^{-6}$	$4.1x10^{-6}$			
mt:CoI	$1.0x10^{-5}$	$7.2x10^{-6}$			

mt:CoI	$2.5x10^{-6}$	$7.4x10^{-6}$			
tRNA-Arg	$4.6x10^{-5}$	$1.7x10^{-4}$	$5.1x10^{-6}$	$7.7x10^{-7}$	$4.8x10^{-6}$
tRNA-Arg	$3.9x10^{-6}$	$1.1x10^{-4}$	$1.1x10^{-6}$	$1.5x10^{-5}$	$1.5x10^{-5}$
tRNA-Arg	$1.4x10^{-5}$	$3.7x10^{-6}$	$1.8x10^{-5}$	$6.9x10^{-5}$	$2.4x10^{-5}$
tRNA-Arg	$1.7x10^{-6}$	$1.1x10^{-5}$			
tRNA-Arg	$2.4x10^{-6}$	$1.4x10^{-5}$			
tRNA-Arg	$2.8x10^{-6}$	$3.9x10^{-5}$			

Sod2 mutants *Ogg1; Sod2* double mutants

Heads

	Day 40		**Day 1**		**Day 27**
mt:Cyt-b	$6.0x10^{-6}$	***mt:Cyt-b***	$1.7x10^{-6}$	***mt:Cyt-b***	$9.3x10^{-6}$
mt:Cyt-b	$1.8x10^{-6}$	***mt:Cyt-b***	$1.6x10^{-6}$	***mt:Cyt-b***	$1.1x10^{-5}$
mt:Cyt-b	$7.5x10^{-6}$	***mt:CoI***	$3.4x10^{-6}$	***mt:Cyt-b***	$5.8x10^{-6}$
mt:Cyt-b	$7.4x10^{-6}$	***mt:CoI***	$5.9x10^{-6}$	***mt:Cyt-b***	$6.0x10^{-6}$
mt:Cyt-b	$5.9x10^{-6}$	***tRNA-Arg***	$2.1x10^{-6}$	***mt:Cyt-b***	$5.7x10^{-6}$
mt:CoI	$8.0x10^{-6}$	***tRNA-Arg***	$3.5x10^{-6}$	***mt:Cyt-b***	$7.0x10^{-6}$
mt:CoI	$4.2x10^{-6}$			***mt:CoI***	$1.7x10^{-6}$
mt:CoI	$3.5x10^{-6}$			***mt:CoI***	$8.7x10^{-6}$
mt:CoI	$7.6x10^{-6}$			***mt:CoI***	$6.7x10^{-6}$
mt:CoI	$4.6x10^{-6}$			***mt:CoI***	$8.7x10^{-6}$
tRNA-Arg	$1.2x10^{-5}$			***mt:CoI***	$4.6x10^{-6}$
tRNA-Arg	$3.6x10^{-6}$			***mt:CoI***	$7.1x10^{-6}$
tRNA-Arg	$2.9x10^{-6}$			***tRNA-Arg***	$9.1x10^{-6}$
tRNA-Arg	$2.5x10^{-6}$			***tRNA-Arg***	$8.2x10^{-6}$
tRNA-Arg	$4.4x10^{-6}$			***tRNA-Arg***	$1.1x10^{-5}$
				tRNA-Arg	$8.6x10^{-6}$
				tRNA-Arg	$5.6x10^{-6}$
				tRNA-Arg	$5.0x10^{-6}$

Table A2. Mitochondrial DNA mutation frequencies.
The mtDNA mutation frequency for each sample analyzed is listed according to genotype (w^{1118}, *Sod2* single mutants, or $Ogg1^{ins}/Ogg1^{ins}$*; Sod2* double mutants), *TaqI* site (*mt:Cyt-b, mt:CoI,* or *tRNA-Arg*) analyzed, tissue source (heads or thoraces), and age (in days).

w1118				
Age and Section	***TaqI site***	**Biological Replicates**	**Base pairs screened**	**Mutations detected**
Day 1 Head	*Cyt-b*	six	1.20E+08	3.83E+02
	CoI	six	1.18E+08	4.91E+02
	tRNA-Arg	six	1.18E+08	2.58E+02
Day 1 Thorax	*Cyt-b*	six	2.26E+08	1.29E+03
	CoI	six	1.72E+08	1.04E+03
	tRNA-Arg	six	1.69E+08	7.69E+02
Day 40 Head	*Cyt-b*	six	1.11E+08	5.07E+02
	CoI	six	1.11E+08	8.31E+02
	tRNA-Arg	six	1.05E+08	3.99E+02
Day 40 Thorax	*Cyt-b*	six	3.08E+07	3.15E+02
	CoI	six	3.08E+07	2.13E+02
	tRNA-Arg	six	3.08E+07	5.30E+02
Day 51 Head	*Cyt-b*	three	5.86E+07	2.59E+02
	CoI	three	5.86E+07	4.11E+02
	tRNA-Arg	three	3.67E+07	2.41E+02
Day 51 Thorax	*Cyt-b*	three	2.13E+08	7.15E+02
	CoI	three	1.43E+08	6.83E+02
	tRNA-Arg	three	1.48E+08	4.83E+02
Day 58 Head	*Cyt-b*	three	4.87E+07	2.77E+02
	CoI	three	4.87E+07	6.92E+02
	tRNA-Arg	three	4.87E+07	1.74E+02
Day 58 Thorax	*Cyt-b*	three	4.23E+07	3.28E+02
	CoI	three	4.23E+07	1.34E+03
	tRNA-Arg	three	4.23E+07	6.55E+02
Day 66 Head	*Cyt-b*	three	8.07E+07	6.67E+02
	CoI	three	8.29E+07	4.68E+02
	tRNA-Arg	three	8.29E+07	4.29E+02
Day 66 Thorax	*Cyt-b*	three	5.82E+07	4.42E+02
	CoI	three	4.69E+07	1.69E+03
	tRNA-	three	4.64E+07	5.37E+02

	Arg			
Age and Section	***TaqI site***	**Biological Replicates**	**Base pairs screened**	**Mutations detected**
Sod2 mutants				
Day 40 Head	*Cyt-b*	five	1.05E+08	5.10E+02
	CoI	five	8.35E+07	4.35E+02
	tRNA-Arg	five	8.35E+07	4.43E+02
Ogg1; Sod2 double mutants				
Day 1 Head	*Cyt-b*	two	6.35E+07	1.06E+02
	CoI	two	6.35E+07	3.01E+02
	tRNA-Arg	two	6.35E+07	1.79E+02
Day 27 Head	*Cyt-b*	six	1.01E+08	6.77E+02
	CoI	six	1.01E+08	7.39E+02
	tRNA-Arg	six	1.01E+08	9.61E+02

Table A3. Number of base pairs screened and mutations detected.
The number of base pairs screened and the number of mutations detected are indicated for each genotype (w^{1118} flies, *Sod2* single mutants, and $Ogg1^{ins}/Ogg1^{ins}$; *Sod2* double mutants), age (days), tissue source (heads or thoraces), number of independent biological replicates, and *TaqI* site (*mt:Cyt-b, mt:CoI,* or *tRNA-Arg*) analyzed.

	Outliers	Non-outliers	p-value
Total DNA (ug)	9.69	8.53	
Standard deviation	3.32	1.6	0.58
Total mtDNA (# of molecules)	3.75E+08	3.19E+08	
Standard deviation	2.67E+08	2.52E+08	0.81

Table A4. mtDNA abundance is indistinguishable in outlier and non-outliers samples.
Amount of DNA isolated (ug) and total number of mtDNA molecules were determined for outlier and non-outlier samples, and no significant difference was detected. Significance was determined using a Student's t-test (n=5 for outliers and n=3 for non-outliers).

REFERENCES

1. Gray, M. W., Burger, G. & Franz Lang, B. The origin and early evolution of mitochondria. *Genome Biol.* **2,** 1018.1–1018.5 (2001).

2. McBride, H. M., Neuspiel, M. & Wasiak, S. Mitochondria: more than just a powerhouse. *Curr. Biol.* **16,** R551–R560 (2006).

3. Wallace, D. C. Mitochondrial function and cancer. *Nat. Rev. Cancer* 1 (2012). at <message:<20120516125307.ad83pawmookk0gco@correoweb.usc.es>>

4. Wang, C. & Youle, R. J. The role of mitochondria in apoptosis*. *Annu. Rev. Genet.* **43,** 95–118 (2009).

5. Chen, H. & Chan, D. C. Mitochondrial dynamics--fusion, fission, movement, and mitophagy--in neurodegenerative diseases. *Hum. Mol. Genet.* **18,** R169–R176 (2009).

6. Larsen, N. B., Rasmussen, M. & Rasmussen, L. J. Nuclear and mitochondrial DNA repair: similar pathways? *Mitochondrion* **5,** 89–108 (2005).

7. Legros, F., Malka, F., Frachon, P., Lombes, A. & Rojo, M. Organization and dynamics of human mitochondrial DNA. *J. Cell Sci.* **117,** 2653–2662 (2004).

8. García-Rodríguez, L. J. in *Mitochondria, 2nd Ed.* (Biology, L. A. P. and E. A. S. B. T.-M. in C.) **Volume 80,** 809–812 (Academic Press, 2007).

9. Holt, I. J., Harding, A. E. & Morgan-Hughes, J. A. Deletions of muscle mitochondrial DNA in patients with mitochondrial myopathies. *Nature* **331,** 717–719 (1988).

10. Wallace, D. *et al.* Mitochondrial DNA mutation associated with Leber's hereditary optic neuropathy. *Science (80-.).* **242,** 1427–1430 (1988).

11. Montagna, P. *et al.* MELAS syndrome: characteristic migrainous and epileptic features and maternal transmission. *Neurology* **38,** 751–754 (1988).

12. Schapira, A. H. V. Mitochondrial diseases. *Lancet* **379,** 1825–1834 (12AD).

13. Schon, E. a, DiMauro, S. & Hirano, M. Human mitochondrial DNA: roles of inherited and somatic mutations. *Nat. Rev. Genet.* **13,** 878–90 (2012).

14. Tavi, P., Hansson, A., Zhang, S.-J., Larsson, N.-G. & Westerblad, H. Abnormal Ca(2+) release and catecholamine-induced arrhythmias in mitochondrial cardiomyopathy. *Hum. Mol. Genet.* **14,** 1069–1076 (2005).

15. Taylor, R. W. & Turnbull, D. M. Mitochondrial DNA mutations in human disease. *Nat. Rev. Genet.* **6,** 389–402 (2005).

16. Jenuth, J. P., Peterson, A. C., Fu, K. & Shoubridge, E. A. Random genetic drift in the female germline explains the rapid segregation of mammalian mitochondrial DNA. *Nat. Genet.* **14,** 146–151 (1996).

17. Hayashi, J. *et al.* Introduction of disease-related mitochondrial DNA deletions into HeLa cells lacking mitochondrial DNA results in mitochondrial dysfunction. *Proc. Natl. Acad. Sci. U. S. A.* **88,** 10614–8 (1991).

18. Chomyn, a *et al.* MELAS mutation in mtDNA binding site for transcription termination factor causes defects in protein synthesis and in respiration but no change in levels of upstream and downstream mature transcripts. *Proc. Natl. Acad. Sci. U. S. A.* **89,** 4221–5 (1992).

19. Park, C. B. & Larsson, N.-G. Mitochondrial DNA mutations in disease and aging. *J. Cell Biol.* **193,** 809–818 (2011).

20. Carroll, J. *et al.* Bovine complex I is a complex of 45 different subunits. *J. Biol. Chem.* **281,** 32724–32727 (2006).

21. Sazanov, L. A. & Hinchliffe, P. Structure of the hydrophilic domain of respiratory complex I from Thermus thermophilus. *Science* **311,** 1430–1436 (2006).

22. JE, W. *et al.* Sequences of 20 subunits of NADH:ubiquinone oxidoreductase from bovine heart mitochondria. Application of a novel strategy for sequencing proteins using the polymerase chain reaction. *J Mol Biol* **226,** 1051–1072 (1992).

23. Distelmaier, F. *et al.* Mitochondrial complex I deficiency: from organelle dysfunction to clinical disease. *Brain* **132,** 833–842 (2009).

24. Kwong, J. Q., Henning, M. S., Starkov, A. A. & Manfredi, G. The mitochondrial respiratory chain is a modulator of apoptosis. *J. Cell Biol.* **179,** 1163–1177 (2007).

25. Smeitink, J. A. M., Koopman, W. J. H. & Willems, P. H. G. M. Monogenic Mitochondrial Disorders. *N. Engl. J. Med.* **366,** 1132–1141 (2012).

26. Mammucari, C., Patron, M., Granatiero, V. & Rizzuto, R. Molecules and roles of mitochondrial calcium signaling. *Biofactors* **37,** 219–227 (2011).

27. Johns, D. R. & Berman, J. Alternative, simultaneous complex I mitochondrial DNA mutations in Leber's hereditary optic neuropathy. *Biochem. Biophys. Res. Commun.* **174,** 1324–1330 (1991).

28. Schwartz, M. & Vissing, J. Paternal Inheritance of Mitochondrial DNA. *N. Engl. J. Med.* **347,** 576–580 (2002).

29. Ugalde, C. *et al.* Mutated ND2 impairs mitochondrial complex I assembly and leads to Leigh syndrome. *Mol. Genet. Metab.* **90,** 10–14 (2007).

30. Ma, Y.-Y. *et al.* Genetic and biochemical findings in Chinese children with Leigh syndrome. *J. Clin. Neurosci.* **20,** 1591–1594 (2013).

31. Man, P. Y. W., Turnbull, D. M. & Chinnery, P. F. Leber hereditary optic neuropathy. *J. Med. Genet.* **39,** 162–169 (2002).

32. DiMauro, S. & Andreu, A. L. Mutations in mitochondrial DNA as a cause of exercise intolerance. *Ann. Med.* **33,** 472–476 (2001).

33. Finsterer, J. Leigh and Leigh-like syndrome in children and adults. *Pediatr. Neurol.* **39,** 223–235 (2008).

34. Schon, E. A. & Manfredi, G. Neuronal degeneration and mitochondrial dysfunction. *J. Clin. Invest.* **111,** 303–312 (2003).

35. Vahsen, N. *et al.* AIF deficiency compromises oxidative phosphorylation. *EMBO J.* **23,** 4679–4689 (2004).

36. Joza, N. *et al.* Muscle-specific loss of apoptosis-inducing factor leads to mitochondrial dysfunction, skeletal muscle atrophy, and dilated cardiomyopathy. *Mol. Cell. Biol.* **25,** 10261–10272 (2005).

37. Pospisilik, J. A. *et al.* Targeted deletion of AIF decreases mitochondrial oxidative phosphorylation and protects from obesity and diabetes. *Cell* **131,** 476–491 (2007).

38. Kruse, S. E. *et al.* Mice with mitochondrial complex I deficiency develop a fatal encephalomyopathy. *Cell Metab.* **7,** 312–320 (2008).

39. Quintana, A., Kruse, S. E., Kapur, R. P., Sanz, E. & Palmiter, R. D. Complex I deficiency due to loss of Ndufs4 in the brain results in progressive encephalopathy resembling Leigh syndrome. *Proc. Natl. Acad. Sci. U. S. A.* **107,** 10996–11001 (2010).

40. Lin, C. S. *et al.* Mouse mtDNA mutant model of Leber hereditary optic neuropathy. *Proc. Natl. Acad. Sci. U. S. A.* **109,** 20065–70 (2012).

41. Brandon, M., Baldi, P. & Wallace, D. C. Mitochondrial mutations in cancer. *Oncogene* **25,** 4647–62 (2006).

42. Guo, L. J. *et al.* Mitochondrial genome polymorphisms associated with type-2 diabetes or obesity. *Mitochondrion* **5,** 15–33 (2005).

43. Mohlke, K. L. *et al.* Mitochondrial polymorphisms and susceptibility to type 2 diabetes-related traits in Finns. *Hum. Genet.* **118,** 245–254 (2005).

44. Khusnutdinova, E. *et al.* A mitochondrial etiology of neurodegenerative diseases: evidence from Parkinson's disease. *Ann. N. Y. Acad. Sci.* **1147,** 1–20 (2008).

45. Pikó, L., Hougham, A. J. & Bulpitt, K. J. Studies of sequence heterogeneity of mitochondrial DNA from rat and mouse tissues: evidence for an increased frequency of deletions/additions with aging. *Mech. Ageing Dev.* **43,** 279–293 (1988).

46. Vermulst, M. *et al.* Mitochondrial point mutations do not limit the natural lifespan of mice. *Nat. Genet.* **39,** 540–543 (2007).

47. Gadaleta, M. N. *et al.* Mitochondrial DNA copy number and mitochondrial DNA deletion in adult and senescent rats. *Mutat. Res.* **275,** 181–193 (1992).

48. TRIFUNOVIC, A. & KUKAT, A. Somatic mtDNA mutations and aging – Facts and fancies. *Exp. Gerontol.* **44,** 101–105 (2009).

49. Kennedy, S. R., Salk, J. J., Schmitt, M. W. & Loeb, L. a. Ultra-Sensitive Sequencing Reveals an Age-Related Increase in Somatic Mitochondrial Mutations That Are Inconsistent with Oxidative Damage. *PLoS Genet.* **9,** e1003794 (2013).

50. Larsson, N.-G. Somatic mitochondrial DNA mutations in mammalian aging. *Annu. Rev. Biochem.* **79,** 683–706 (2010).

51. Trifunovic, A. *et al.* Premature ageing in mice expressing defective mitochondrial DNA polymerase. *Nature* **429,** 417–423 (2004).

52. Kujoth, G. C. *et al.* Mitochondrial DNA mutations, oxidative stress, and apoptosis in mammalian aging. *Science* **309,** 481–4 (2005).

53. Vermulst, M. *et al.* DNA deletions and clonal mutations drive premature aging in mitochondrial mutator mice. *Nat. Genet.* **40,** 392–394 (2008).

54. Edgar, D. *et al.* Random point mutations with major effects on protein-coding genes are the driving force behind premature aging in mtDNA mutator mice. *Cell Metab.* **10,** 131–138 (2009).

55. Kraytsberg, Y., Simon, D. K., Turnbull, D. M. & Khrapko, K. Do mtDNA deletions drive premature aging in mtDNA mutator mice? *Aging Cell* **8,** 502–506 (2009).

56. Del Bo, R. *et al.* Remarkable infidelity of polymerase gammaA associated with mutations in POLG1 exonuclease domain. *Neurology* **61,** 903–908 (2003).

57. Wanrooij, S. *et al.* Twinkle and POLG defects enhance age-dependent accumulation of mutations in the control region of mtDNA. *Nucleic Acids Res.* **32,** 3053–3064 (2004).

58. Simon, D. K. *et al.* Somatic mitochondrial DNA mutations in cortex and substantia nigra in aging and Parkinson's disease. *Neurobiol. Aging* **25,** 71–81 (2004).

59. Bender, A. *et al.* High levels of mitochondrial DNA deletions in substantia nigra neurons in aging and Parkinson disease. *Nat. Genet.* **38,** 515–517 (2006).

60. Kraytsberg, Y. *et al.* Mitochondrial DNA deletions are abundant and cause functional impairment in aged human substantia nigra neurons. *Nat. Genet.* **38,** 518–520 (2006).

61. Ekstrand, M. I. *et al.* Progressive parkinsonism in mice with respiratory-chain-deficient dopamine neurons. *Proc. Natl. Acad. Sci. U. S. A.* **104,** 1325–1330 (2007).

62. Wang, Y. *et al.* Muscle-specific mutations accumulate with aging in critical human mtDNA control sites for replication. *Proc. Natl. Acad. Sci. U. S. A.* **98,** 4022–4027 (2001).

63. Lin, M. T., Simon, D. K., Ahn, C. H., Kim, L. M. & Beal, M. F. High aggregate burden of somatic mtDNA point mutations in aging and Alzheimer's disease brain. *Hum. Mol. Genet.* **11,** 133–145 (2002).

64. Khrapko, K. *et al.* Cell-by-cell scanning of whole mitochondrial genomes in aged human heart reveals a significant fraction of myocytes with clonally expanded deletions. **27,** 2434–2441 (1999).

65. Corral-Debrinski, M. *et al.* Mitochondrial DNA deletions in human brain: regional variability and increase with advanced age. *Nat. Genet.* **2,** 324–329 (1992).

66. Cortopassi, G. A. & Arnheim, N. Detection of a specific mitochondrial DNA deletion in tissues of older humans. *Nucleic Acids Res.* **18,** 6927–6933 (1990).

67. Schon, E. A. *et al.* A direct repeat is a hotspot for large-scale deletion of human mitochondrial DNA. *Science* **244,** 346–349 (1989).

68. Mita, S. *et al.* Recombination via flanking direct repeats is a major cause of large-scale deletions of human mitochondrial DNA. *Nucleic Acids Res.* **18,** 561–567 (1990).

69. Samuels, D. C., Schon, E. A. & Chinnery, P. F. Two direct repeats cause most human mtDNA deletions. *Trends Genet.* **20,** 393–398 (2004).

70. Chance, B., Sies, H. & Boveris, A. Hydroperoxide metabolism in mammalian organs. *Physiol. Rev.* **59,** 527–605 (1979).

71. Quinlan, C. L., Treberg, J. R., Perevoshchikova, I. V, Orr, A. L. & Martin, D. NIH Public Access. **53,** 1807–1817 (2013).

72. Pryor, W. A. Oxy-Radicals and Related Species: Their Formation, Lifetimes, and Reactions. *Annu. Rev. Physiol.* **48,** 657–667 (1986).

73. De Bont, R. & van Larebeke, N. Endogenous DNA damage in humans: a review of quantitative data. *Mutagenesis* **19,** 169–185 (2004).

74. Wang, D., Kreutzer, D. A. & Essigmann, J. M. Mutagenicity and repair of oxidative DNA damage: insights from studies using defined lesions. *Mutat. Res.* **400,** 99–115 (1998).

75. Mishra, P. C. & Jena, N. R. Formation of ring-opened and rearranged products of guanine: Mechanisms and biological significance. *Free Radic. Biol. Med.* **53,** 81–94 (2012).

76. Harman, D. The biologic clock: the mitochondria? *J. Am. Geriatr. Soc.* **20,** 145–147 (1972).

77. Bandy, B. & Davison, A. J. Mitochondrial mutations may increase oxidative stress: implications for carcinogenesis and aging? *Free Radic. Biol. Med.* **8,** 523–539 (1990).

78. Dai, D.-F. *et al.* Overexpression of catalase targeted to mitochondria attenuates murine cardiac aging. *Circulation* **119,** 2789–2797 (2009).

79. Wei, Y. H., Lu, C. Y., Lee, H. C., Pang, C. Y. & Ma, Y. S. Oxidative damage and mutation to mitochondrial DNA and age-dependent decline of mitochondrial respiratory function. *Ann. N. Y. Acad. Sci.* **854,** 155–170 (1998).

80. Zheng, W., Khrapko, K., Coller, H. A., Thilly, W. G. & Copeland, W. C. Origins of human mitochondrial point mutations as DNA polymerase gamma-mediated errors. *Mutat. Res.* **599,** 11–20 (2006).

81. Ameur, A. *et al.* Ultra-deep sequencing of mouse mitochondrial DNA: mutational patterns and their origins. *PLoS Genet.* **7,** e1002028 (2011).

82. Taylor, R. W. *et al.* Mitochondrial DNA mutations in human colonic crypt stem cells. *J. Clin. Invest.* **112,** 1351–1360 (2003).

83. Nekhaeva, E. *et al.* Clonally expanded mtDNA point mutations are abundant in individual cells of human tissues. **99,** 5521–5526 (2002).

84. Greaves, L. C. *et al.* Mitochondrial DNA mutations are established in human colonic stem cells, and mutated clones expand by crypt fission. *Proc. Natl. Acad. Sci. U. S. A.* **103,** 714–719 (2006).

85. Bogenhagen, D. & Clayton, D. A. Mouse L cell mitochondrial DNA molecules are selected randomly for replication throughout the cell cycle. *Cell* **11,** 719–727 (1977).

86. De Grey, A. D. N. J. How is mutant mitochondrial DNA clonally amplified? Much new evidence, still no answers. *Rejuvenation Res.* **12,** 217–219 (2009).

87. Wallace, D. C. Mitochondrial DNA mutations and neuromuscular disease. *Trends Genet.* **5,** 9–13 (1989).

88. Shadel, G. S. & Clayton, D. A. Mitochondrial DNA maintenance in vertebrates. *Annu. Rev. Biochem.* **66,** 409–435 (1997).

89. De Grey, A. D. A proposed refinement of the mitochondrial free radical theory of aging. *Bioessays* **19,** 161–166 (1997).

90. Elson, J. L., Samuels, D. C., Turnbull, D. M. & Chinnery, P. F. Random intracellular drift explains the clonal expansion of mitochondrial DNA mutations with age. *Am. J. Hum. Genet.* **68,** 802–806 (2001).

91. Gross, N. J., Getz, G. S. & Rabinowitz, M. Apparent Turnover of Mitochondrial Deoxyribonucleic Acid and Mitochondrial Phospholipids in the Tissues of the Rat. *J. Biol. Chem.* **244,** 1552–1562 (1969).

92. Ashrafi, G. & Schwarz, T. L. The pathways of mitophagy for quality control and clearance of mitochondria. *Cell Death Differ.* (2012). doi:10.1038/cdd.2012.81

93. Sato, M. & Sato, K. Degradation of Paternal Mitochondria by Fertilization-Triggered Autophagy in C. elegans Embryos. *Science (80-.).* **334,** 1141–1144 (2011).

94. Hajjar, C. *et al.* Postfertilization Autophagy of Sperm Organelles Prevents Paternal Mitochondrial DNA Transmission. *Science (80-.).* **334,** 1144–1147 (2011).

95. Sandoval, H. *et al.* Essential role for Nix in autophagic maturation of erythroid cells. *Nature* **454,** 232–235 (2008).

96. Kanki, T., Wang, K., Cao, Y., Baba, M. & Klionsky, D. J. Atg32 is a mitochondrial protein that confers selectivity during mitophagy. *Dev. Cell* **17,** 98–109 (2009).

97. Kissová, I., Deffieu, M., Manon, S. & Camougrand, N. Uth1p is involved in the autophagic degradation of mitochondria. *J. Biol. Chem.* **279,** 39068–39074 (2004).

98. Kanki, T. & Klionsky, D. J. Mitophagy in yeast occurs through a selective mechanism. *J. Biol. Chem.* **283,** 32386–32393 (2008).

99. Narendra, D., Tanaka, A., Suen, D.-F. & Youle, R. J. Parkin is recruited selectively to impaired mitochondria and promotes their autophagy. *J. Cell Biol.* **183,** 795–803 (2008).

100. Narendra, D. P. *et al.* PINK1 is selectively stabilized on impaired mitochondria to activate Parkin. *PLoS Biol.* **8,** e1000298 (2010).

101. Kitada, T. *et al.* Mutations in the parkin gene cause autosomal recessive juvenile parkinsonism. *Nature* **392,** 605–608 (1998).

102. Valente, E. M. *et al.* Hereditary early-onset Parkinson's disease caused by mutations in PINK1. *Science* **304,** 1158–1160 (2004).

103. Poole, A. C. *et al.* The PINK1/Parkin pathway regulates mitochondrial morphology. *Proc. Natl. Acad. Sci. U. S. A.* **105,** 1638–1643 (2008).

104. Poole, A. C., Thomas, R. E., Yu, S., Vincow, E. S. & Pallanck, L. The mitochondrial fusion-promoting factor mitofusin is a substrate of the PINK1/parkin pathway. *PLoS One* **5,** e10054 (2010).

105. Ziviani, E., Tao, R. N. & Whitworth, A. J. Drosophila parkin requires PINK1 for mitochondrial translocation and ubiquitinates mitofusin. *Proc. Natl. Acad. Sci. U. S. A.* **107,** 5018–5023 (2010).

106. Chan, N. C. *et al.* Broad activation of the ubiquitin-proteasome system by Parkin is critical for mitophagy. *Hum. Mol. Genet.* **20,** 1726–1737 (2011).

107. Fan, W. *et al.* A mouse model of mitochondrial disease reveals germline selection against severe mtDNA mutations. *Science* **319,** 958–962 (2008).

108. Stewart, J. B. *et al.* Strong purifying selection in transmission of mammalian mitochondrial DNA. *PLoS Biol.* **6,** e10 (2008).

109. Suen, D.-F., Narendra, D. P., Tanaka, A., Manfredi, G. & Youle, R. J. Parkin overexpression selects against a deleterious mtDNA mutation in heteroplasmic cybrid cells. *Proc. Natl. Acad. Sci. U. S. A.* **107,** 11835–11840 (2010).

110. Vermulst, M., Bielas, J. H. & Loeb, L. a. Quantification of random mutations in the mitochondrial genome. *Methods* **46,** 263–268 (2008).

111. Smigrodzki, R., Parks, J. & Parker, W. D. High frequency of mitochondrial complex I mutations in Parkinson's disease and aging. *Neurobiol. Aging* **25,** 1273–1281 (2004).

112. Wilding, C. S. *et al.* Mitochondrial DNA mutations in individuals occupationally exposed to ionizing radiation. *Radiat Res* **165,** 202–207 (2006).

113. Shendure, J. & Ji, H. Next-generation DNA sequencing. *Nat. Biotechnol.* **26,** 1135–1145 (2008).

114. Schmitt, M. W. *et al.* Detection of ultra-rare mutations by next-generation sequencing. **2012,** 1–6 (2012).

115. Efremov, R. G., Baradaran, R. & Sazanov, L. A. The architecture of respiratory complex I. *Nature* **465,** 441–445 (2010).

116. Dieteren, C. E. *et al.* Subunits of mitochondrial complex I exist as part of matrix- and membrane-associated subcomplexes in living cells. *J Biol Chem* **283,** 34753–34761 (2008).

117. Roberts, P. G. & Hirst, J. The deactive form of respiratory complex I from Mammalian mitochondria is a na+/h+ antiporter. *J Biol Chem* **287,** 34743–34751 (2012).

118. Amarneh, B. & Vik, S. B. Mutagenesis of subunit N of the Escherichia coli complex I. Identification of the initiation codon and the sensitivity of mutants to decylubiquinone. *Biochemistry* **42,** 4800–4808 (2003).

119. Triepels, R. H., Van Den Heuvel, L. P., Trijbels, J. M. & Smeitink, J. A. Respiratory chain complex I deficiency. *Am J Med Genet* **106,** 37–45 (2001).

120. Xu, H., DeLuca, S. Z. & O'Farrell, P. H. Manipulating the metazoan mitochondrial genome with targeted restriction enzymes. *Science (80-.).* **321,** 575–577 (2008).

121. Brown, M. D. *et al.* Mitochondrial DNA complex I and III mutations associated with Leber's hereditary optic neuropathy. *Genetics* **130,** 163–173 (1992).

122. Pieczenik, S. R. & Neustadt, J. Mitochondrial dysfunction and molecular pathways of disease. *Exp Mol Pathol* **83,** 84–92 (2007).

123. Ganetzky, B. & Wu, C. F. Indirect Suppression Involving Behavioral Mutants with Altered Nerve Excitability in DROSOPHILA MELANOGASTER. *Genetics* **100,** 597–614 (1982).

124. Fergestad, T., Bostwick, B. & Ganetzky, B. Metabolic disruption in Drosophila bang-sensitive seizure mutants. *Genetics* **173,** 1357–1364 (2006).

125. Celotto, A. M. *et al.* Mitochondrial encephalomyopathy in Drosophila. *J Neurosci* **26,** 810–820 (2006).

126. Chinnery, P. F. Mitochondrial Disorders Overview. (1993).

127. Seymour, B. Genetic dissection of behavior. *Sci. Am.* **229,** 24–37 (1973).

128. Greene, J. C. *et al.* Mitochondrial pathology and apoptotic muscle degeneration in Drosophila parkin mutants. *Proc Natl Acad Sci U S A* **100,** 4078–4083 (2003).

129. Ferguson, M., Mockett, R. J., Shen, Y., Orr, W. C. & Sohal, R. S. Age-associated decline in mitochondrial respiration and electron transport in Drosophila melanogaster. *Biochem J* **390,** 501–511 (2005).

130. Torraco, A., Diaz, F., Vempati, U. D. & Moraes, C. T. Mouse models of oxidative phosphorylation defects: powerful tools to study the pathobiology of mitochondrial diseases. *Biochim Biophys Acta* **1793,** 171–180 (2009).

131. Rolland, S. G. *et al.* Impaired complex IV activity in response to loss of LRPPRC function can be compensated by mitochondrial hyperfusion. *Proc Natl Acad Sci U S A* **110,** E2967–76 (2013).

132. Jones, D. T. Protein secondary structure prediction based on position-specific scoring matrices. *J Mol Biol* **292,** 195–202 (1999).

133. Nugent, T. & Jones, D. T. Transmembrane protein topology prediction using support vector machines. *BMC Bioinformatics* **10,** 159 (2009).

134. Abramoff, M. D., Magalhães, P. J. & Ram, S. J. Image processing with ImageJ. *Biophotonics Int.* **11,** 36–42 (2004).

135. Kayser, E. B., Morgan, P. G., Hoppel, C. L. & Sedensky, M. M. Mitochondrial expression and function of GAS-1 in Caenorhabditis elegans. *J Biol Chem* **276,** 20551–20558 (2001).

136. Burman, J. L., Yu, S., Poole, A. C., Decal, R. B. & Pallanck, L. Analysis of neural subtypes reveals selective mitochondrial dysfunction in dopaminergic neurons from parkin mutants. *Proc Natl Acad Sci U S A* **109,** 10438–10443 (2012).

137. Suthammarak, W., Yang, Y. Y., Morgan, P. G. & Sedensky, M. M. Complex I function is defective in complex IV-deficient Caenorhabditis elegans. *J Biol Chem* **284,** 6425–6435 (2009).

138. Wittig, I., Braun, H. P. & Schagger, H. Blue native PAGE. *Nat Protoc* **1,** 418–428 (2006).

139. Boore, J. L. Animal mitochondrial genomes. *Nucleic Acids Res.* **27,** 1767–1780 (1999).

140. DiMauro, S. & Hirano, M. Mitochondrial encephalomyopathies: an update. *Neuromuscul. Disord.* **15,** 276–286 (2005).

141. Brierley, E. J., Johnson, M. A., Lightowlers, R. N., James, O. F. & Turnbull, D. M. Role of mitochondrial DNA mutations in human aging: implications for the central nervous system and muscle. *Ann Neurol* **43,** 217–223 (1998).

142. Guo, M. What have we learned from Drosophila models of Parkinson's disease? *Prog. Brain Res.* **184,** 3–16 (2010).

143. Chung, J. & Koh, H. PINK1 as a molecular checkpoint in the maintenance of mitochondrial function and integrity. *Mol. Cells* **34,** 7–13 (2012).

144. Calleja, M. *et al.* Mitochondrial DNA remains intact during Drosophila aging, but the levels of mitochondrial transcripts are significantly reduced. *J. Biol. Chem.* **268,** 18891–18897 (1993).

145. Schwarze, S. R., Weindruch, R. & Aiken, J. M. Decreased mitochondrial RNA levels without accumulation of mitochondrial DNA deletions in aging Drosophila melanogaster. *Mutat. Res.* **382,** 99–107 (1998).

146. Yui, R. & Matsuura, E. T. Detection of deletions flanked by short direct repeats in mitochondrial DNA of aging Drosophila. *Mutat. Res.* **594,** 155–161 (2006).

147. Bielas, J. H. & Loeb, L. A. Quantification of random genomic mutations. *Nat. Methods* **2,** 285–290 (2005).

148. Martínez-Azorín, F. *et al.* Over-expression of the catalytic core of mitochondrial DNA (mtDNA) polymerase in the nervous system of Drosophila melanogaster reduces median life span by inducing mtDNA depletion. *J. Neurochem.* **105,** 165–176 (2008).

149. Jõers, P. & Jacobs, H. T. Analysis of replication intermediates indicates that Drosophila melanogaster mitochondrial DNA replicates by a strand-coupled theta mechanism. *PLoS One* **8,** 1–12 (2013).

150. Jones, S. *et al.* Comparative lesion sequencing provides insights into tumor evolution. *Proc. Natl. Acad. Sci. U. S. A.* **105,** 4283–4288 (2008).

151. Khrapko, K. & Vijg, J. Mitochondrial DNA mutations and aging: devils in the details? *Trends Genet.* **25,** 91–98 (2009).

152. Murphy, M. P. How mitochondria produce reactive oxygen species. *Biochem. J.* **417,** 1–13 (2009).

153. HARMAN, D. Aging: a theory based on free radical and radiation chemistry. *J. Gerontol.* **11,** 298–300 (1956).

154. Wallace, D. C. A mitochondrial paradigm for degenerative diseases and ageing. *Novartis Found. Symp.* **235,** 247–266 (2001).

155. Mishra PC, Singh AK, S. S. Interaction of singlet oxygen and superoxide radical anion with guanine and formation of its mutagenic modification 8-oxoguanine. *Int. J. Quantum Chem.* **102,** 282–301 (2005).

156. Frederico, L. A., Kunkel, T. A. & Shaw, B. R. A sensitive genetic assay for the detection of cytosine deamination: determination of rate constants and the activation energy. *Biochemistry* **29,** 2532–2537 (1990).

157. Graziewicz, M. A., Bienstock, R. J. & Copeland, W. C. The DNA polymerase gamma Y955C disease variant associated with PEO and parkinsonism mediates the incorporation and translesion synthesis opposite 7,8-dihydro-8-oxo-2'-deoxyguanosine. *Hum. Mol. Genet.* **16,** 2729–2739 (2007).

158. Duttaroy, A., Paul, A., Kundu, M. & Belton, A. A Sod2 null mutation confers severely reduced adult life span in Drosophila. *Genetics* **165,** 2295–2299 (2003).

159. Paul, A. *et al.* Reduced mitochondrial {SOD} displays mortality characteristics reminiscent of natural aging. *Mech. Ageing Dev.* **128,** 706–716 (2007).

160. Chintapalli, V. R., Wang, J. & Dow, J. A. T. Using FlyAtlas to identify better Drosophila melanogaster models of human disease. *Nat. Genet.* **39,** 715–720 (2007).

161. De Souza-Pinto, N. C. *et al.* Repair of 8-oxodeoxyguanosine lesions in mitochondrial dna depends on the oxoguanine dna glycosylase (OGG1) gene and 8-oxoguanine accumulates in the mitochondrial dna of OGG1-defective mice. *Cancer Res.* **61,** 5378–5381 (2001).

162. Dherin, C., Dizdaroglu, M., Doerflinger, H., Boiteux, S. & Radicella, J. P. Repair of oxidative DNA damage in Drosophila melanogaster: identification and characterization of dOgg1, a second DNA glycosylase activity for 8-

hydroxyguanine and formamidopyrimidines. *Nucleic Acids Res.* **28,** 4583–4592 (2000).

163. McQuilton, P., St Pierre, S. E. & Thurmond, J. FlyBase 101--the basics of navigating FlyBase. *Nucleic Acids Res.* **40,** D706–14 (2012).

164. Wei, Y. H. Oxidative stress and mitochondrial DNA mutations in human aging. *Proc Soc Exp Biol Med* **217,** 53–63 (1998).

165. Ruiz-Pesini, E. *et al.* An enhanced MITOMAP with a global mtDNA mutational phylogeny. *Nucleic Acids Res.* **35,** D823–D828 (2007).

166. Bokov, A., Chaudhuri, A. & Richardson, A. The role of oxidative damage and stress in aging. *Mech Ageing Dev* **125,** 811–826 (2004).

167. Spelbrink, J. N. *et al.* In vivo functional analysis of the human mitochondrial DNA polymerase POLG expressed in cultured human cells. *J. Biol. Chem.* **275,** 24818–24828 (2000).

168. Goddard, J. M. & Wolstenholme, D. R. Origin and direction of replication in mitochondrial DNA molecules from Drosophila melanogaster. *Proc. Natl. Acad. Sci. U. S. A.* **75,** 3886–3890 (1978).

169. Goddard, J. M. & Wolstenholme, D. R. Origin and direction of replication in mitochondrial DNA molecules from the genus Drosophila. *Nucleic Acids Res.* **8,** 741–757 (1980).

170. Saito, S., Tamura, K. & Aotsuka, T. Replication origin of mitochondrial DNA in insects. *Genetics* **171,** 1695–1705 (2005).

171. Wagner, J. R. & Cadet, J. Oxidation reactions of cytosine DNA components by hydroxyl radical and one-electron oxidants in aerated aqueous solutions. *Acc. Chem. Res.* **43,** 564–571 (2010).

172. Kreutzer, D. A. & Essigmann, J. M. Oxidized, deaminated cytosines are a source of C --> T transitions in vivo. *Proc. Natl. Acad. Sci. U. S. A.* **95,** 3578–3582 (1998).

173. A, B. & AS, B. Correlation between transcription and C to T mutations in the non-transcribed DNA strand. *Biol Chem* **379,** 549–551 (1998).

174. Francino, M. P., Chao, L., Riley, M. A. & Ochman, H. Asymmetries generated by transcription-coupled repair in enterobacterial genes. *Science* **272,** 107–109 (1996).

175. MP, F. & H, O. Deamination as the basis of strand-asymmetric evolution in transcribed Escherichia coli sequences. *Mol Biol Evol* **18,** 1147–1150 (2001).

176. Haag-Liautard, C. *et al.* Direct Estimation of the Mitochondrial DNA Mutation Rate in Drosophila melanogaster. *PLoS Biol* **6,** e204 (2008).

177. Bernstein, C., Bernstein, H., Payne, C. M. & Garewal, H. DNA repair/pro-apoptotic dual-role proteins in five major DNA repair pathways: fail-safe protection against carcinogenesis. *Mutat. Res. Mutat. Res.* **511,** 145–178 (2002).

178. De Souza-Pinto, N. C. *et al.* Novel DNA mismatch-repair activity involving YB-1 in human mitochondria. *DNA Repair (Amst).* **8,** 704–719 (2009).

179. Rozen, S. & Skaletsky, H. Primer3 on the WWW for general users and for biologist programmers. *Methods Mol. Biol.* **132,** 365–386 (2000).

180. Griffiths-Jones, S. & Rogers, H. H. Mitochondrial Pseudogenes in the Nuclear Genomes of Drosophila. *PLoS One* **7,** e32593 (2012).

181. Zhang, K. *et al.* The C8ORF38 homologue Sicily is a cytosolic chaperone for a mitochondrial complex I subunit. *J. Cell Biol.* **200,** 807–820 (2013).

182. Cardozo-Pelaez, F., Brooks, P. J., Stedeford, T., Song, S. & Sanchez-Ramos, J. DNA damage, repair, and antioxidant systems in brain regions: a correlative study. *Free Radic Biol Med* **28,** 779–785 (2000).

183. Sievers, F. *et al.* Fast, scalable generation of high-quality protein multiple sequence alignments using Clustal Omega. *Mol. Syst. Biol.* **7,** (2011).

184. Goujon, M. *et al.* A new bioinformatics analysis tools framework at EMBL-EBI. *Nucleic Acids Res.* **38,** W695–W699 (2010).

185. Claros, M. G. & Vincens, P. Computational method to predict mitochondrially imported proteins and their targeting sequences. *Eur. J. Biochem.* **241,** 779–786 (1996).

186. Park, J. *et al.* Mitochondrial dysfunction in Drosophila PINK1 mutants is complemented by parkin. *Nature* **441,** 1157–1161 (2006).

187. Clark, I. E. *et al.* Drosophila pink1 is required for mitochondrial function and interacts genetically with parkin. *Nature* **441,** 1162–1166 (2006).

188. Vincow, E. S. *et al.* The PINK1-Parkin pathway promotes both mitophagy and selective respiratory chain turnover in vivo. *Proc. Natl. Acad. Sci. U. S. A.* **110,** 6400–5 (2013).

189. Gundry, M. & Vijg, J. Direct mutation analysis by high-throughput sequencing: from germline to low-abundant, somatic variants. *Mutat. Res.* **729,** 1–15 (2012).

190. He, Y. *et al.* Heteroplasmic mitochondrial DNA mutations in normal and tumour cells. *Nature* **464,** 610–614 (2010).

191. Ganapathy, G. *et al.* Hybrid error correction and de novo assembly of single-molecule sequencing reads. *Nat. Biotechnol.* **30,** 693–700 (2012).

192. Celotto, A. M., Chiu, W. K., Van Voorhies, W. & Palladino, M. J. Modes of Metabolic Compensation during Mitochondrial Disease Using the Drosophila Model of ATP6 Dysfunction. *PLoS One* **6,** e25823 (2011).

193. Eto, K. *et al.* Role of NADH shuttle system in glucose-induced activation of mitochondrial metabolism and insulin secretion. *Science* **283,** 981–985 (1999).

194. Pearson, R. B. & Kemp, B. E. Protein kinase phosphorylation site sequences and consensus specificity motifs: tabulations. *Methods Enzymol.* **200,** 62–81 (1991).

195. Papa, S., Sardanelli, A. M., Scacco, S. & Technikova-Dobrova, Z. cAMP-dependent protein kinase and phosphoproteins in mammalian mitochondria. An extension of the cAMP-mediated intracellular signal transduction. *FEBS Lett.* **444,** 245–249 (1999).

196. Scacco, S. *et al.* cAMP-dependent phosphorylation of the nuclear encoded 18-kDa (IP) subunit of respiratory complex I and activation of the complex in serum-starved mouse fibroblast cultures. *J. Biol. Chem.* **275,** 17578–17582 (2000).

197. Iuso, A. *et al.* Dysfunctions of cellular oxidative metabolism in patients with mutations in the NDUFS1 and NDUFS4 genes of complex I. *J. Biol. Chem.* **281,** 10374–10380 (2006).

198. Lemos, C. *et al.* Assessing risk factors for migraine: differences in gender transmission. *PLoS One* **7,** e50626 (2012).

199. Simunovic, F., Yi, M., Wang, Y., Stephens, R. & Sonntag, K. C. Evidence for gender-specific transcriptional profiles of nigral dopamine neurons in Parkinson disease. *PLoS One* **5,** e8856 (2010).

200. Harris, J. R., Lippman, M. E., Veronesi, U. & Willett, W. Breast Cancer. *N. Engl. J. Med.* **327,** 319–328 (1992).

201. Tońska, K., Kodroń, A. & Bartnik, E. Genotype-phenotype correlations in Leber hereditary optic neuropathy. *Biochim. Biophys. Acta* **1797,** 1119–23 (2010).

202. Kirkman, M. A. *et al.* Gene-environment interactions in Leber hereditary optic neuropathy. *Brain* **132,** 2317–2326 (2009).

203. Settles, E. W. Flock house virus induces replication-dependent apoptosis by depleting the Drosophila inhibitor-of-apoptosis protein, DIAP1. 1–223 (2008).

204. Ferrari, D., Stepczynska, A., Los, M., Wesselborg, S. & Schulze-Osthoff, K. Differential regulation and ATP requirement for caspase-8 and caspase-3 activation during CD95- and anticancer drug-induced apoptosis. *J. Exp. Med.* **188,** 979–984 (1998).

205. Hartmann, A. *et al.* Caspase-8 is an effector in apoptotic death of dopaminergic neurons in Parkinson's disease, but pathway inhibition results in neuronal necrosis. *J. Neurosci.* **21,** 2247–2255 (2001).

206. Tsujimoto, Y. Apoptosis and necrosis: intracellular ATP level as a determinant for cell death modes. *Cell Death Differ.* **4,** 429–434 (1997).

207. Bratic, I. *et al.* Mitochondrial DNA level, but not active replicase, is essential for Caenorhabditis elegans development. *Nucleic Acids Res.* **37,** 1817–1828 (2009).

208. Taylor, S. D. *et al.* Targeted enrichment of high-resolution digital profiling of mitochondrial DNA deletions in human brain. *Aging Cell* 1–10 (2013). doi:10.1111/acel.12146

VITA

Leslie Sook Itsara was born in Opelika, Alabama in 1985. She grew up in Opelika, AL and graduated from Opelika High School in 2003. She then attended Vanderbilt University from 2003-2007 and graduated *summa cum laude* with a bachelor's degree in Bioloigcal Sciences and Chemistry. In 2007 Leslie began the Molecular and Cellular Biology program at the University of Washington under the mentorship of Dr. Leo Pallanck. In 2014 Leslie graduated with a Doctor of Philosophy in Molecular and Cellular Biology from the University of Washington.